Study of liquid crystal –composite films prepared by Langmuir- Blodgett Technique

A
Thesis
Submitted for the Award
of the Degree of

DOCTOR OF PHILOSOPHY

By

Ramneek Kaur
(Roll No. 901012002)

Under the Supervision of

Dr. K. K. Raina
Distinguished Professor
Materials Research Laboratory
School of Physics and Materials Science
Thapar University
Patiala (Punjab) – 147004, India

October 2015

THAPAR UNIVERSITY, PATIALA

CERTIFICATE

This is to certify that the thesis entitled **"Study of liquid crystal – Composite films prepared by Langmuir- Blodgett Technique"** submitted by **Ramneek Kaur**, for the award of the degree **DOCTOR OF PHILOSOPHY** of THAPAR UNIVERSITY, Patiala, Punjab, India, is a record of the study conducting by her under my supervision and guidance. The subject matter of this dissertation has not been previously published or submitted to any other university for the award of any other degree, diploma, associate ship, fellowship or any other similar title.

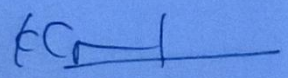

Dr. K.K. Raina
(Supervisor)
Distinguished Professor
School of Physics and Materials Science
Thapar University, Patiala

ACKNOWLEDGEMENT

I would like to express my special appreciation and thanks to my supervisor **Dr. K.K. Raina, Distinguished Professor, School of Physics and Materials Science, Thapar University, Patiala**. This work would not have been possible without his supervision, encouragement and support. Under his guidance, I successfully overcame many difficulties and learned a lot. He always helped me whenever I required. He taught me to improve my presentation skills. He used to motivate for good quality of research work. He viewed my research manuscripts thoroughly. With his help all proposed objectives are fulfilled and results are published in good journals. In spite of his busy schedule, he checked and corrected my compiled work in form of this thesis. I am very thankful for all what he has done for my research work. It has been completed with support and encouragement of numerous peoples including my well wishers, my friends, colleagues and professors from various institutions. I would like to thank all those people who made this thesis possible.

I express my deep gratitude to ***Dr. Puneet Sharma*** and my PhD progress committee members, ***Dr. Manoj K. Sharma (Head SPMS & Prof.), Dr. Kulvir Singh, Dr. D.P. Singh and Dr. H. Bhunia*** for their useful suggestions and comments during my progress report presentations.

My sincere thanks to ***Prof. O.P. Pandey*** (**Dean Research and Sponsored Projects**) for the various encouraging lectures during course work classes.

My special thanks go to **Miss L.K. Brar** for her help and support at many stages of work. I am highly thankful to her for providing training to operate LB and AFM.

I acknowledge ***University Grants Commission, Delhi*** for their financial support as a '***UGC SRF Fellow'*** under **MANF** scheme.

I am also thankful to all **Staff of SPMS**, Thapar University, Patiala for their helping nature throughout my research work.

My special thanks go to my friend ***Mrs. Gurpreet Kaur Bhullar*** for her great sense of co-operation throughout my Ph.D. work. We worked collectively and sort out many issues regarding data analysis.

My sincere thanks to my seniors ***Dr. Pankaj Kumar***, ***Dr. Parveen Malik***, ***Dr. Ravi Shukla***, ***Dr. Parveen Kumar, Dr. Rekha and Dr. Renu*** for their support and encouragement.

I am also thankful to my colleagues **Dr. Rishi Kumar,** ***Mrs. Manju Middha and Miss Deepti*** at the Materials Research Laboratory for maintaining a congenial, competitive lab atmosphere and providing a stimulating fun filled environment.

Last but not least, I place a deep sense of gratitude to ***my parents, my younger sister Dr. Manmeet Kaur Aujla and my Husband, Er. Jatinder Singh Dhaliwal*** for their sincere encouragement, being source of inspiration throughout my research. I have no words to express thanks for their love, care and blessings.

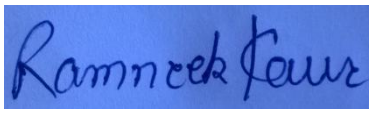

Dated **Ramneek Kaur**

CONTENTS

Chapter 5: Langmuir Blodgett thin film of bent core liquid crystalline molecules

CHAPTER 6 : Conclusions and Future Scope of the Work

List of Figures

Chapter 2

Chapter 3

Chapter 4

Chapter 5

List of Publications
Journal Publications

SCI Journals

1) Kaur R., Bhullar G.K., Raina K K. **Behaviour of an ultrathin ferroelectric liquid crystal Langmuir–Blodgett film at an air–water and air–solid interface.** Liq Cryst. 2012, **39**, 1375.

2) Kaur R., Raina K.K. **Influence of single-wall carbon nanotubes on Langmuir–Blodgett films of ferroelectric liquid crystals as studied by atomic force microscopy.** Liq Cryst. 2014, **41**, 1065.

3) Kaur R., Bhullar G.K., Rao N. V. S., Raina K. K. **Effect of pH on the control of molecular orientation in monolayer of bent core liquid crystals materials by Langmuir-Blodgett method.** Liq Cryst. 2014, **42(1),** 8.

4) Kaur R., Raina K.K. **Effects of nano-particle doping on the Phase transitional behaviour of ferroelectric liquid crystal Langmuir -Blodgett composite films**. Phase Transit Multinat J. 2015, doi.: 10.1080/01411594.2015.1044900.

5) Kaur R., Raina K. K. **Self - assembling effects of nano-particle doping on the mesomorphic behaviour of ferroelectric liquid crystal Langmuir -Blodgett composite films**. Ferroelectrics. 2015 (under review).

6) Kaur R., Raina K.K. **Tuning of band gap of liquid crystal molecules having translation behaviour with doping of nanoparticles.** (under preparation)

Other related Publications

7) Bhullar G.K., Kaur R., Raina K.K. **Hybrid Polyaniline–TiO_2 Nanocomposite Langmuir–Blodgett Thin Films: Self-Assembly and Their Characterization**. J. App. Poly. Sci. 2015, **135(5)**, 1.

8) Bhullar G.K., Kaur R., Raina K. K. **Growth, Morphology and Electrical Characterization of Polyaniline-ZnO Nano-Composite Langmuir Blodgett thin Films.** J. Electron. Mater., 2015. doi: 10.1007/s11664-015-3868-4.

9) Bhullar G.K., Kaur R., Raina K.K. **Electrical Characterization of Polyaniline-ZnO nano composite Langmuir Blodgett thin film by Conductive Atomic Force Microscopy.** MRS Spring Meeting Proceedings 2014, Volume **1668,** doi: 10.1557/opl.2014.834.

Non-SCI Journals

1) Kaur R., Bhullar G.K., Raina K.K. **Surface viscoelastic properties of spread ferroelectric liquid crystal monolayer on air-water interface.** AIP Conf. Proc. 2013, **1536**, 1377.

2) Kaur R., Raina K.K. **Structural study of Langmuir liquid crystal monolayer.** AIP Conf. Proc. 2014, **1591**, 954.

Other related Publications

3) Bhullar G.K., Kaur R., Raina K.K. **Investigations on polyaniline–TiO2 nano-composite Langmuir Blodgett thin films.** AIP Conf. Proc.. 2013, **1536**, 491.

4) Vishalli, Kaur R., Raina K.K., Dharamvir K. **Investigation on single walled carbon nanotube thin films deposited by Langmuir Blodgett method** AIP Conf. Proc.,2015, **1661**, 080033(1-4).

5) Vishalli , Kaur R., Raina K.K., Avasthi D.K., Jeet K., Dharamvir K. **Investigation on optical absorption properties of ion irradiated single walled carbon nanotubes.** AIP Conf. Proc. 2015, 1675, 030037(1-5).

List International/National Conference

International Conferences

[1] "Optical investigation on thin films of ferroelectric liquid crystal deposited by Langmuir Blodgett technique."
Kaur R., Bhullar G.K., Raina K.K. **International Workshop on Soft Matter Chemistry**, RRI Bangalore, (9-11.November.2011), pp86.

[2] "Optical and Morphological Study of Ferroelectric Liquid Crystal Langmuir-Blodgett Films"
Kaur R., Bhullar G.K., Raina K.K. **16th International workshop on physics of semiconductor devices**, IIT Kanpur (19-22. December. 2011), DL P.04.

[3] "Surface viscoelastic properties of spread ferroelectric liquid crystal monolayer on air-water interface.''
Kaur R., Bhullar G.K., Raina K.K. **International Conference on Recent Trends in Applied Physics & Material Science**, Govt. College of Engineering & Technology , Bikaner. (1-2 February. 2013). J-1310, pp 340.

[4] "Isothermal behaviour of Langmuir Monolayer of Liquid Crystal composite at air-water interface."
Kaur R., Bhullar G.K., Raina K.K. **Organic Devices: The future Ahead (ODeFA-2014)**, BARC, Mumbai. (3-6. March. 2014). CP-63.

[5] "Self - assembling effects of nano-particle doping on the mesomorphic behaviour of ferroelectric liquid crystal Langmuir -Blodgett composite films"

Kaur R., Raina K.K. **Challenges in polar self-assembling systems,** Prague, Czech Republic. (June 28 – July 3 2015) (Accepted).

National Conferences

[6] "Formation of polyaniline-ZrO_2 nano-composites using Langmuir - Blodgett technique."

Kaur R., Bhullar G.K., Raina K.K. **National Symposium on Radiation Physics and Nano-materials (NSRPN-11)**, Punjabi University, Patiala (4-5. February. 2011). pp NP7.

[7] "Systems for Langmuir-Blodgett films a unique tool for molecular electronics."
Kaur R., Bhullar G.K., Raina K.K. **National Seminar on Advanced Materials and Devices**, G.V.M. girls college Sonepat (3-4. July 2011). CP59, pp80.

[8] "Phase change study in polymer-ferroelectric liquid crystal composite thin film on air-water interface by Langmuir Blodgett technique."
Kaur R. and Raina K.K. **23rd AGM MRSI 2012**, Thapar University Patiala (13-14. February. 2012). pp156.

[9] "Langmuir monolayer of Bent-Core liquid crystal formed by changing sub phase pH."
Kaur R., Bhullar G.K., Raina K.K. **National conference on Recent trends in material Science research**, NIT Srinagar, (3-5 September, 2012).

[10] "Langmuir monolayer of Bent-Core liquid crystal formed by changing sub phase pH."
Kaur R., Bhullar G.K., Raina K.K. **19th National Conference on Liquid Crystals (NCLC-19)**, Thapar University Patiala, (21-23,.November. 2012) pp. 91.(**Best Poster Prize**).

[11] "Structural study of Langmuir Liquid Crystal Monolayer."
Kaur R, Raina K.K. **58th DAE- Solid State Physics Symposium** at Thapar University Patiala, (17-21.December. 2013). F-197.

[12] "Investigations on ultrathin films of Ferroelectric Liquid Crystal Polymer Composite."
Kaur R., Bhullar G.K., Raina K.K. **National Symposium on Electroceramics-Materials and Devices (NSE-MD-2014)**, GVM Girls College, Sonepat, (21-22 February. 2014). pp CP-46.

PREFACE

We have prepared homogenous Langmuir-Blodgett (LB) films of liquid crystals (LC) and it's composite with nano-particles. Interaction between nano-particles and host LC matrix resulted in phase changes of monolayer. Orientation and ordering of LC at air-water interface have been significantly improved by adding nano-particles into it. It has improved many physical properties of liquid crystal matrix. These LB films have opened up opportunities for understanding of many properties for application point of view. Results are summarized in this dissertation:-

- **Chapter 1** reviews of liquid crystal science and recent development of this subject. It explains about amphiphilic character of molecules which is necessary for LB film formation. Thermotropic liquid crystal posses amphilphicity due to chirality and electronegative functional groups attached with phenyl rings. Both ferroelectric and bent core liquid crystals have both hydrophobic and hydrophilic character in their molecular structure.

  An overview of physical properties of thermo tropic liquid crystals is given on the basis of their molecular arrangement. Amphiphilic character of ferroelectric and bent core liquid crystal molecules make them suitable candidate for the formation of LB films.

- **Chapter 2** provides details about Langmuir Blodgett experimental set up and methodology used for depositing thin films. Characterization was done using Fourier Transform infrared Spectroscopy (FTIR) to confirm complete deposition at substrate, Low Angle X-Ray Diffraction for layer ordering of thin films and Atomic Force Microscopy in non-contact mode for topographical imaging of thin films. Molecular Structures and 3-D models of Ferroelectric Liquid Crystals, Bent Core Liquid Crystals and functionalized nano-particles are given in this chapter.

- **Chapter 3** describes about LB films of a ferroelectric liquid crystal (FLC) and its composite with SWCNTs at air–water interface and deposited onto solid substrates It is concluded that the amphiphilic nature of the FLC played a vital role in the orientation and ordering of the FLC film. The XRD profile of FLC film indicated smectic layering of the FLC molecules, and FTIR spectra confirmed

complete deposition of the FLC films. AFM images show uniform films with average height profile of 2.53 nm.

Langmuir–Blodgett films of ferroelectric liquid crystal (LC) doped with low concentration of octadecylamine functionalized single-wall carbon nanotubes show that the interaction between nanotubes and LC molecules in the monolayer was increased during barrier compression, resulting in increased surface pressure. It is due to π–π stacking of SWCNTs with the FLC molecules. AFM profile of films SWCNT and FLC-SWCNT composite systems infer uniform film deposition on Si substrate. This study of composite film is helpful in alignment of LC molecules with improved properties for various device applications.

- **Chapter 4** contains deposition of LB films of functionalized nano-particles (octadecylamine functionalized AZO and dodecanethiol functionalized Ag) in FLC host matrix. Nano-particles has noticeable effect on monolayer stabilization at air-water interface. It enhances ordering of films. Deposited composite films have been examined under FTIR, Low Angle XRD and AFM. All tools confirm uniform deposition and retaining of smectic layer ordering of FLC at low concentration doping of nano-particles into it. . These kind of LC films having nano-particles patterned in them have various optical and sensor applications.

- **Chapter 5** presents the formation of Langmuir monolayer of bent-core liquid crystals at air–water interface by changing pH of the sub phase on silicon substrate. Atomic force microscopy images showed decreased height profiles with varied sub phase pH= 6, 4, 2 levels. Thus LB technique has provided new insight into monolayer formation of bent-core molecule. So the major requirement of aligning bent core is fulfilled, it provides new innovations in research and technology.

- **Chapter 6** contains summary of the work. It shows that LB technique provide a method to develop ultrathin films. Future scope of work is also proposed here.

CHAPTER -1

Liquid Crystals and Langmuir-Blodgett Technique

Overview

This chapter explains about amphiphilic character of liquid crystal molecules in particular which is necessary for Langmuir-Blodgett (LB) film formation. Thermo-tropic liquid crystal posses amphiphilic character due to chirality and electronegative functional groups attached with phenyl rings. Both ferroelectric and bent core liquid crystals have both hydrophobic and hydrophilic character in their molecular structure.

An overview of physical properties of thermotropic liquid crystals is given on the basis of their molecular arrangement. History of Langmuir Blodgett films is discussed briefly. Langmuir monolayer is formed at air-water interface with constant compression of barriers. Modes of Langmuir monolayer deposition are also discussed.

Introduction

1.1 Amphiphiles

The molecules which have covalently bonded hydrophilic and hydrophobic groups are termed as amphiphilies. Many amphiphiles are found in nature for example long chain fatty acids like stearic acid ($C_{17}H_{35}COOH$), arachidic acid ($CH_3(CH_2)_{18}COOH$), behenic acid($CH_3(CH_2)_{20}COOH$) etc. The carboxyl (-COOH) group of fatty acids is hydrophilic in nature due to presence of oxygen (strong electronegative) element and the long alkyl chains are hydrophobic. Organic molecules which contain a hydrophilic group like -$NHCOCH_3$, -$CONH_2$, -CH_2OH, -CN, -COO-, -CH_2COCH_3, -CH=NOH, -C_6H_4OH etc., and having hydrophobic groups are another examples of amphiphilic molecules [1-3].

When an amphiphilic molecule is placed at water surface, it can undergo two different mechanisms depending upon concentration of the spread materials. At high concentration micellization occurs at the interface. Whereas at low concentration, a stable monolayer is formed at air-water interface as shown in figure 1.1 [4, 5]. Hydrophilic (polar) part of molecule is attracted toward water surface and hydrophobic (non polar) part stay away from water surface. Alignment of molecules at the interface is also dependent upon chemical structure of molecules, temperature of water sub phase, concentration of ions at interface etc. [6].

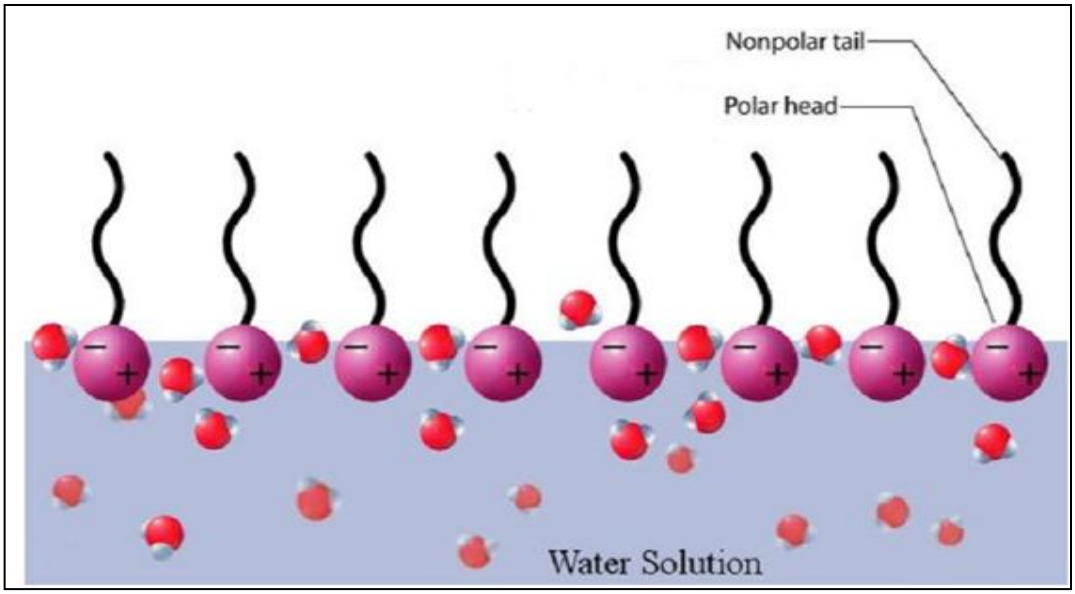

Figure 1.1: It shows alignment of amphiphilic molecules at the air-water interface. Polar groups are hydrophilic and non-polar tails are hydrophobic.

1.2 Liquid Crystals as Soft Matter

Reintzer and Lehmann had discoverd liquid crystals in 1888 [7- 9]. It is a state of matter whose properties are intermediate to liquids and solid crystals [10]. They have high mobility like liquids as well as positional and orientational ordering like crystal. In crystal phase, molecules are highly ordered having long range positional and orientational order (figure 1.2). When temperature is increased LC phase appear having orientational order and partial or no positional order. With further increase in temperature ordering of molecules vanish completely and liquid phase of matter is formed. The materials which exhibit liquid crystalline phases during heating are known as mesogens [11].

Liquid Crystals molecules can be categorized into two different types: **Thermotropic** LC phases and **Lyotropic** LC.

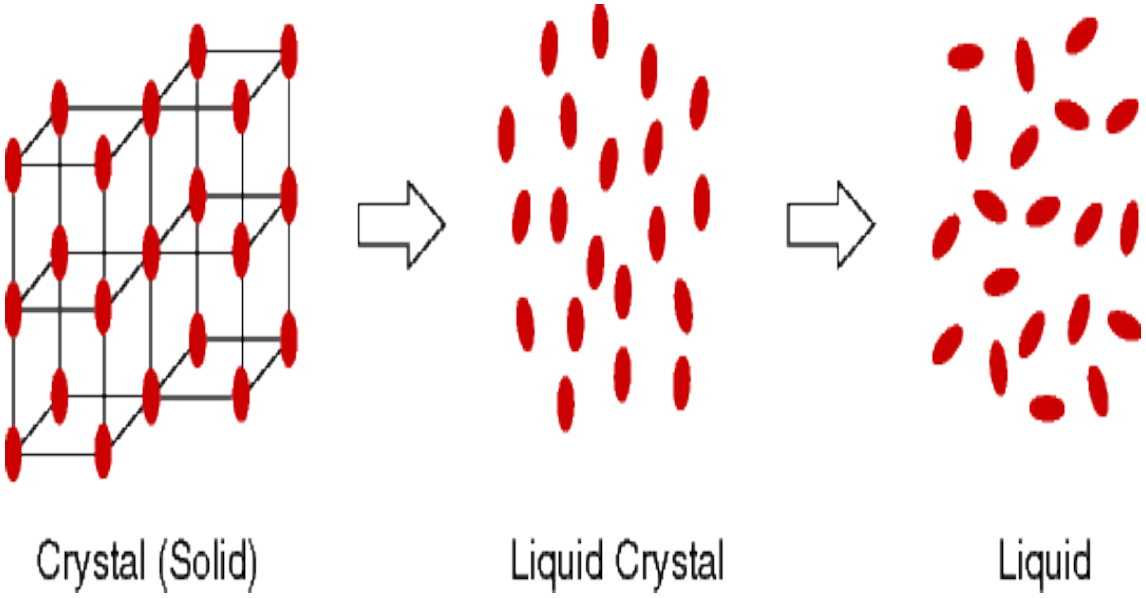

Figure 1.2: It shows organization of molecules in crystals (solid), Liquid Crystals and isotropic liquid phase.

Thermotropic LC phase is observed in certain temperature range, phase transition occurs with increase and decrease of temperature. When temperature is decreased below some certain point solid crystal phase is attained and isotropic liquid phase is formed at higher temperatures [12-14]. These LCs have many applications in electro-optic devices and sensors due to their phase variation with temperature.

Lyotropic LC phases are formed in a solution, with change of concentration of dissolved materials. Molecules forming lyotropic liquid crystals are usually amphiphilic

in nature. With variation of concentration molecules arrange themselves in different structures e.g.: spheres, bilayers, discs etc [15-17].

Depending upon arrangement and orientation of molecules, thermotropic as well as lyotropic liquid crystals are further classified in different phases. Since our present work is focused on ultrathin films of thermotropic liquid crystals. We will discuss detail of LCs of our interest only. Thermotropic LCs has four types: Calamitic (rod shaped), Discotic (disc shaped), Bent Core (banana shape) and LC-polymers. A brief description of calamitic liquid crystals and bent core LC phases is given below:

1.3 Calamitic Liquid Crystals

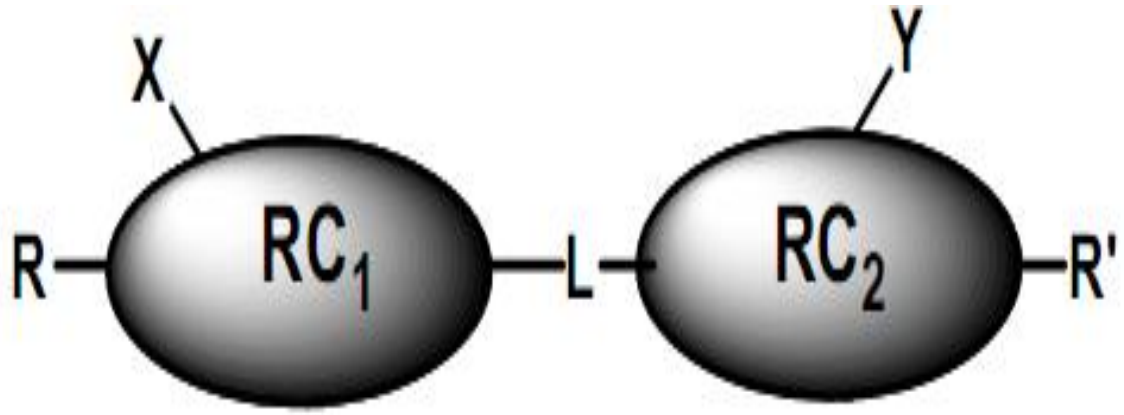

Figure 1.3: Schematic view of molecular structure of Calamitic Liquid Crystals [18].

Calamitic liquid crystal molecules are rod shaped. Their schematic view of molecular structure is shown in figure 1.3. RC_1 and RC_2 are rigid aromatic cores. These cores are attached with flexible chains at ends. These are shown as R and R'. These are generally alkyl or alkoxy chains. L is linking group like -N=N-, -COO-, -CH=N, CH_2-CH_2- etc between rigid cores. X and Y (F, Cl, CN, CH_3 etc.) are lateral substitution attached to cores. They insert special properties to liquid crystalline phase [18].

Depending upon degree of orientational and positional order calamatic LCs are divided in four types **nematic**, **cholesteric**, **smectic** phase and **Ferroelectric Sm C*** phase as shown in figure 1.4.

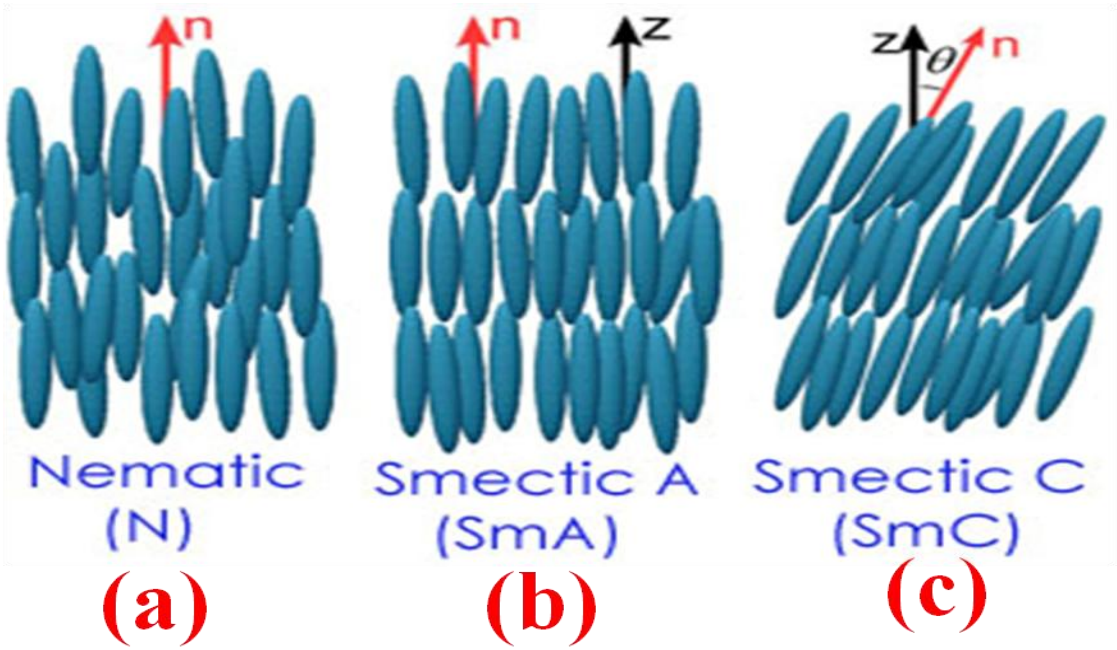

Figure 1.4: It shows schematic representation of molecular organization in (**a**) nematic (N), (**b**) smectic A (SmA) and (**c**) Smectic C(Sm C) phase.

1.3.1 Nematic phase

The nematic phase posses long-range orientational order and no positional order. This is the least ordered phase among calamatic liquid crystal phases. The long axes of the all molecules tend to align along a direction. $\vec{n}$(r) (Represents local orientation of all molecules) is the director. In nematic phase long axis of all molecules is parallel to director. When LC molecules are cooled down from isotropic phase, nematic phase appear with decrease in entropy. Long axes of molecules get orientated along one direction with cooling. The thread like defect patterns of the nematic liquid crystals are observed under the polarizing microscopy [19].

1.3.2 Smectic Phase

Smectic liquid crystals posses both orientational and positional order. They have layered structures with fixed interlayer spacing. In each layer molecules have liquid like arrangement [20]. Long molecular axis of all molecules is in one fixed direction (n). $\vec{z}$ represents layer normal. When director (n) is parallel to layer normal (z), the molecular

arrangement result in formation of Smectic A phase and if n makes an angle (θ) with the layer normal it forms Smectic C phase as shown in figure 1.4.

1.3.3 Cholesteric Phase

Cholesteric LC phase is achieved by doping chiral molecules to nematic mesophase and therefore it is also named as chiral nematic phase. Chiral doping makes them optically active [21]. Cholesteric mesophase was first found in esters of cholesterols [22].

In these systems, neighbouring molecules of each layer are aligned at a slight angle to molecule of another layer. This result in formation of helix with well defined pitch (P) along local director as shown in figure 1.5. Size of pitch is much longer as compared to size of single molecule. Depending on the molecular conformation helical twist can be either right handed or left handed.

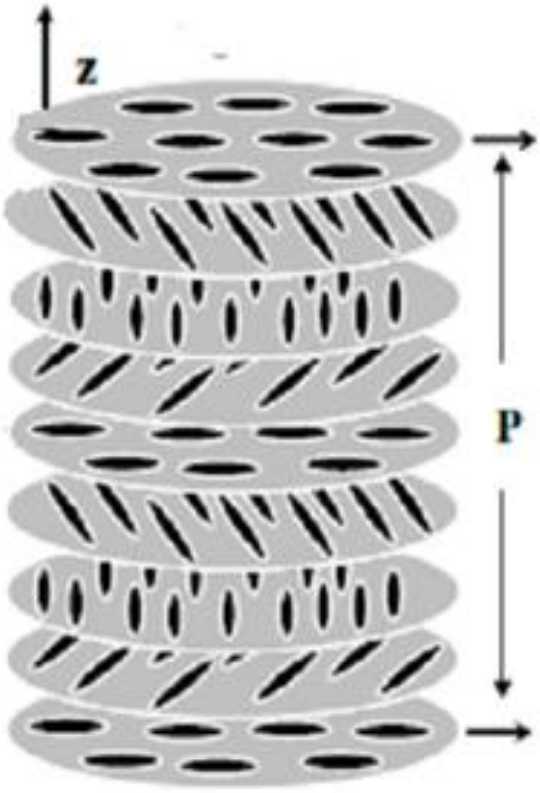

Figure 1.5: It shows Helical structure of the chiral nematic phase (cholesteric phase) [22].

Helical arrangement of molecules in this phase has great importance in developing optical devices. When polarised light is passed through these LCs thier plane gets tilted toward direction of helix. Cholesteric Phase exhibit schlieren and oily streak textures depending upon doping materials and surface conditions [23, 24].

1.3.4 Ferroelectric SmC* Phase

In the smectic C* phase (* indicate a chiral phase), the molecules posses positional ordering in a layered structure similar to smectic C phases, with the molecules making a finite angle with layer normal. When we add chiral materials to Smectic LC or some functionalization group is attached to it results in chiral compound in SmC* phase.

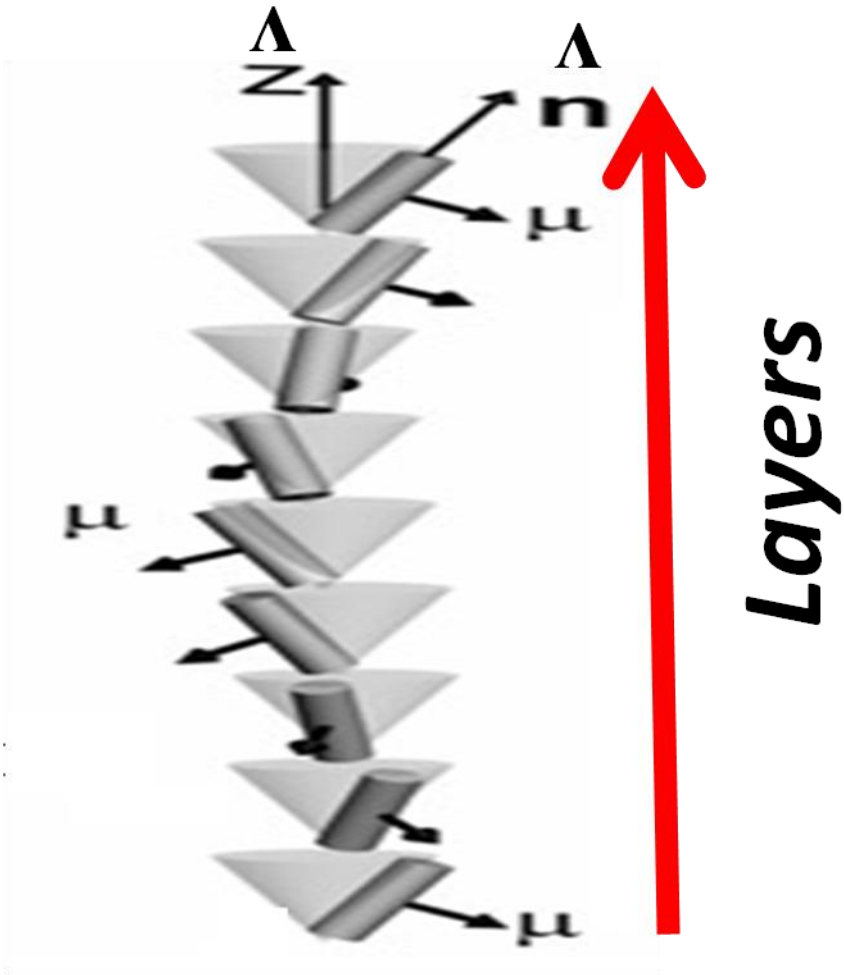

Figure 1.6: Helical structure of SmC* liquid crystals: **n** is director; **z** is twist axis; μ is dipole moment.

$\hat{n}$ shown in figure 1.6 represents long molecular axis of molecules in each layer. Layer normal is represented by $\hat{z}$. It rotates by small angle from one layer to the next. The molecules in SmC* exhibit ferroelectric properties due to presence of dipole moment (μ) having direction perpendicular to layer normal $\hat{z}$.

1.4 Bent Core Liquid Crystals

In the recent past, a new system known as bent-shaped liquid crystals have been discovered.

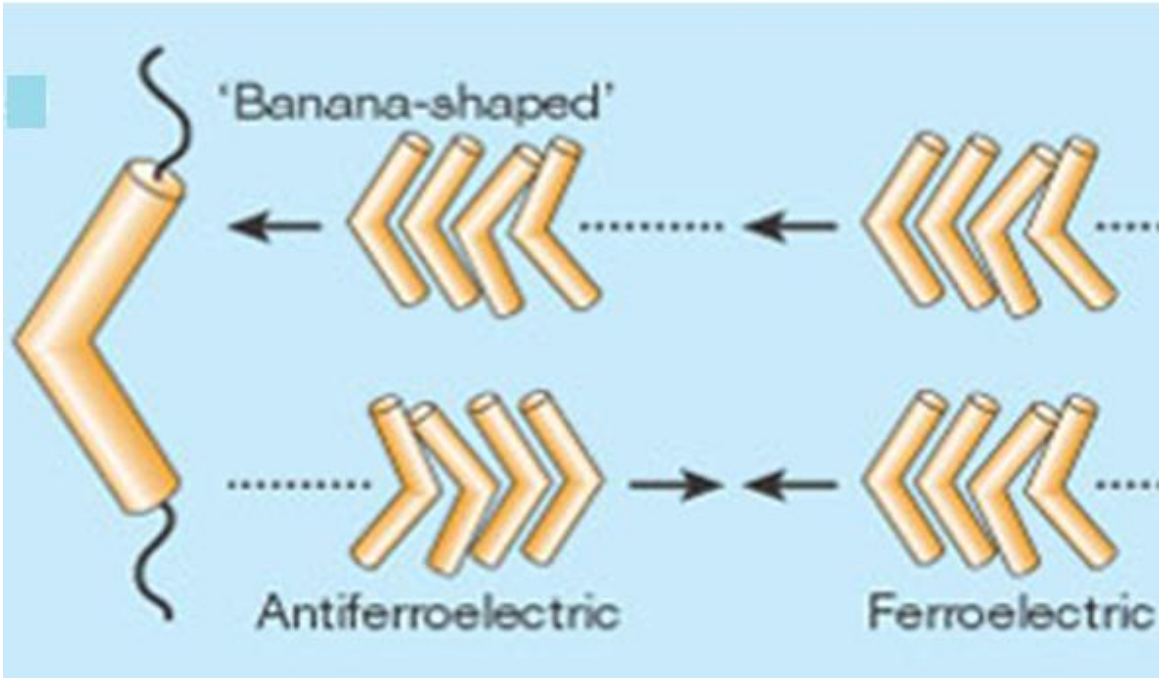

Figure 1.7: Layer ordering of bent core molecules in Anti ferroelectric and ferroelectric phase.

Bent shaped liquid crystal molecules also arrange themselves in layers having positional ordering but their properties are different from smectic phases. They are immiscible in each other [25-32]. They posses ferroelectricity but do not contain any chiral carbon atom. This property appears from bend shape as shown in figure 1.7.

1.5 Structure of bent-core mesogens

Bent core mesogens are not linear in shape like calamatic liquid crystals. They are consist of calamitic liquid crystals attached by varied linking groups (Y, Y'). Linking groups are organic functional groups like methylene, carbonyl, ether and thioether [33-38]. (X, X') are also linking groups with which calamitic rods are connected to central core.

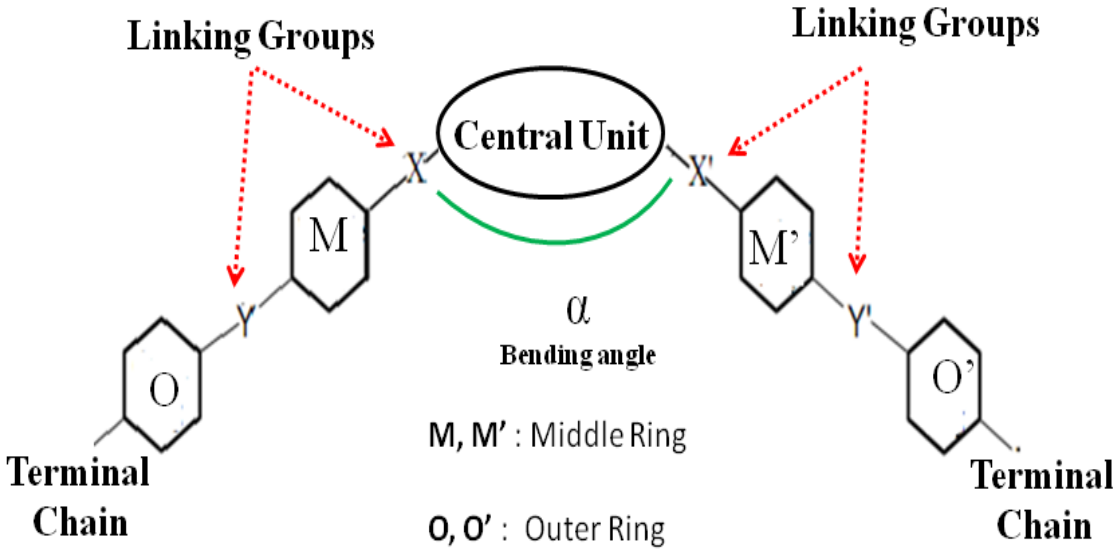

Figure 1.8: General molecular structures of bent-shaped molecules.

Meta substituted benzene rings result in bending angle α as shown in figure 1.8. Terminal chains are connected at para position of benzene rings. Terminal chains are long alkyl or alkoxy hydrocarbon chains. Length of terminal chain will decide packing structure of bent core liquid crystals in bulk. With longer alkyl chains as compared to spacer a biaxial structure is formed [39, 40], if length of alkyl chain is small molecules arrange themselves to form SmC phase.

1.6 Phases of Bent core Liquid Crystals ($B_1 - B_8$)

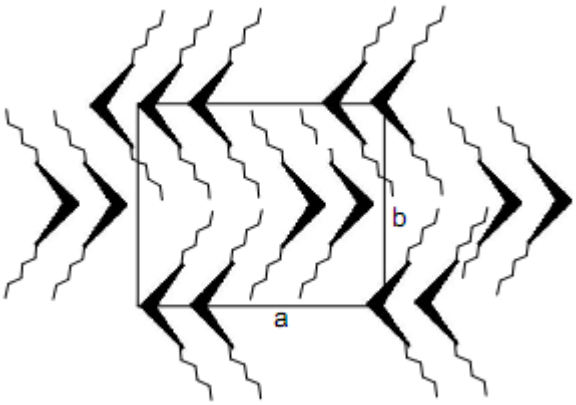

Figure 1.9: It shows molecular arrangement of $\mathbf{B_1}$ phase [28].

Bent core liquid crystals are divided into $\mathbf{B_1}$-$\mathbf{B_8}$ phases depending upon their molecular arrangement. Here **B** represents banana shape of the molecules. Most of the phases are formed by parallel alignment of molecules in bent direction.

Sekine et al (1997) discovered first compound having $\mathbf{B_1}$ phase. $\mathbf{B_1}$ have rectangular lattice structure as shown in figure 1.9. In this structure columns are formed by molecular arrangement of bent core molecules in layers. Molecules are arranged in adjacent layers having opposite polarization direction. Rectangular lattice is formed by having vertex at central unit. '**a**' represents number of molecules forming the lattice and '**b**' gives length of individual molecule. Overlapping of aromatic parts of central unit results in stabilization of network structure. If chain length is extremely large, there will be unfavourable repulsion and $\mathbf{B_6}$ phase is formed. If chain length in $\mathbf{B_1}$ phase is very small molecules move across domains resulting in formation of $\mathbf{B_2}$ phase.

In $\mathbf{B_2}$ phase long terminal alkyl chains shows variety of textures under microscope e.g.: schlieren, focal conic and fringe pattern textures. This phase is most common in observed bent shaped liquid crystal molecules. In molecular structure of bent core LC optics axis is tilted normal to layer normal. Layer polarization is also perpendicular to optic axis as shown in figure 1.10.

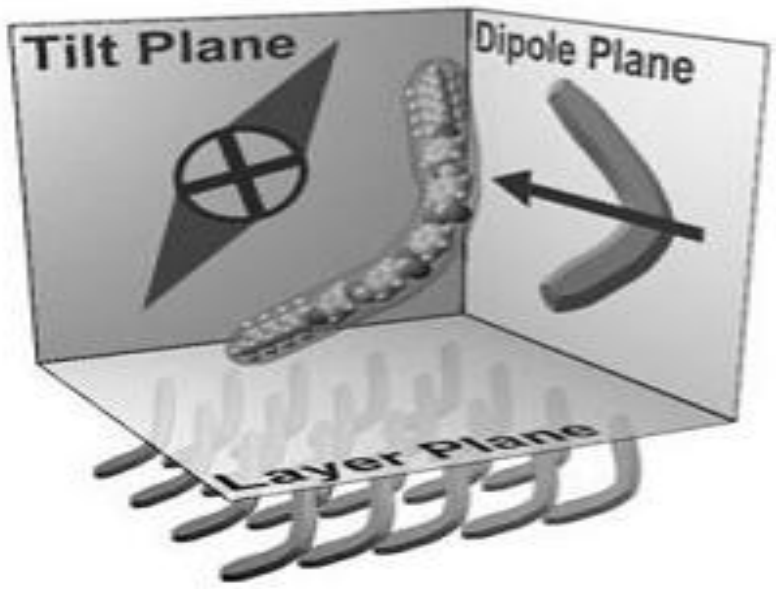

Figure 1.10: It shows molecular arrangement of $\mathbf{B_2}$ phase [28].

B_3 appears on decreasing temperature from **B_2** phase with no textural change on rapid cooling. Although breaking of domains can be observed on slow cooling. It is inferred from XRD data of these phases that they posses crystalline structure. But on the basis of dielectric spectroscopic results they show dynamic similar to **B_2** phase. Hence **B_3** phase can be termed as highly ordered smectic phase.

B_4 mesophase is observed under **B_2** phase or **B_3** phase. This phase shows coloured (blue) domains under cross polarizer. Because of blue coloured domains this phase is also named as smectic blue phase. The XRD pattern reveals small angle as well wide angle peaks indicating crystalline order.

B_5 mesophase appears below **B_2** phase. This phase is observed in molecules which are fluoro substituted at place of alkyl chains. It is proposed that **B_5** phase have rectangular lattice and in-plane molecular packing as shown in figure 1.11.This phase is reported only in a few systems.

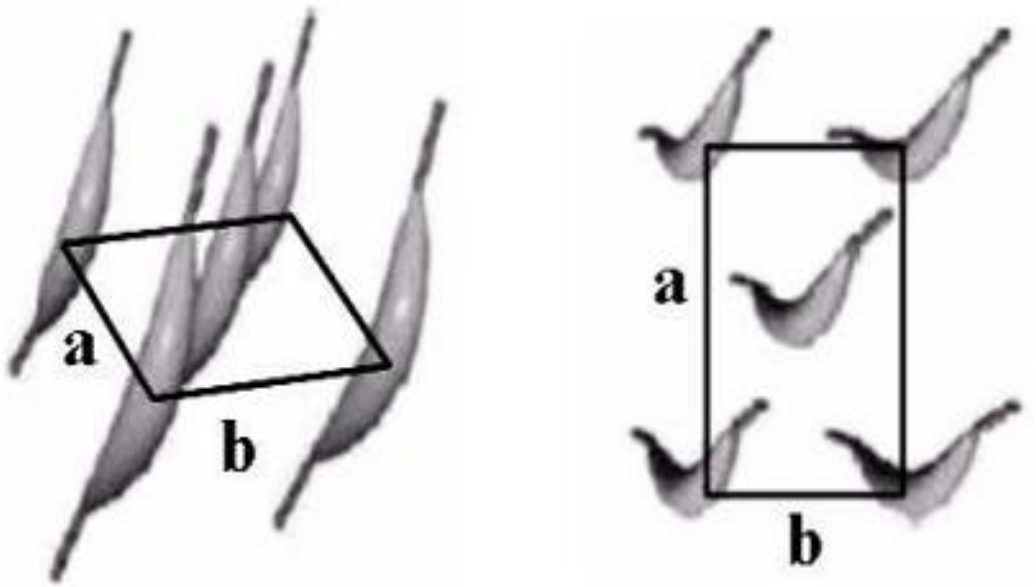

Figure 1.11: Molecular arrangement of bent core LC in **B_5** phase [41].

B_6 mesophase has intercalated structure. In molecular structure gap between the aromatic (electronegative) cores is filled by alkyl chains. Due to the pattern in packing of aromatic cores, only alkyl chain having lesser length can form **B_6** phase (figure 1.12). This phase exhibits a fan-shaped texture similar to SmA phase.

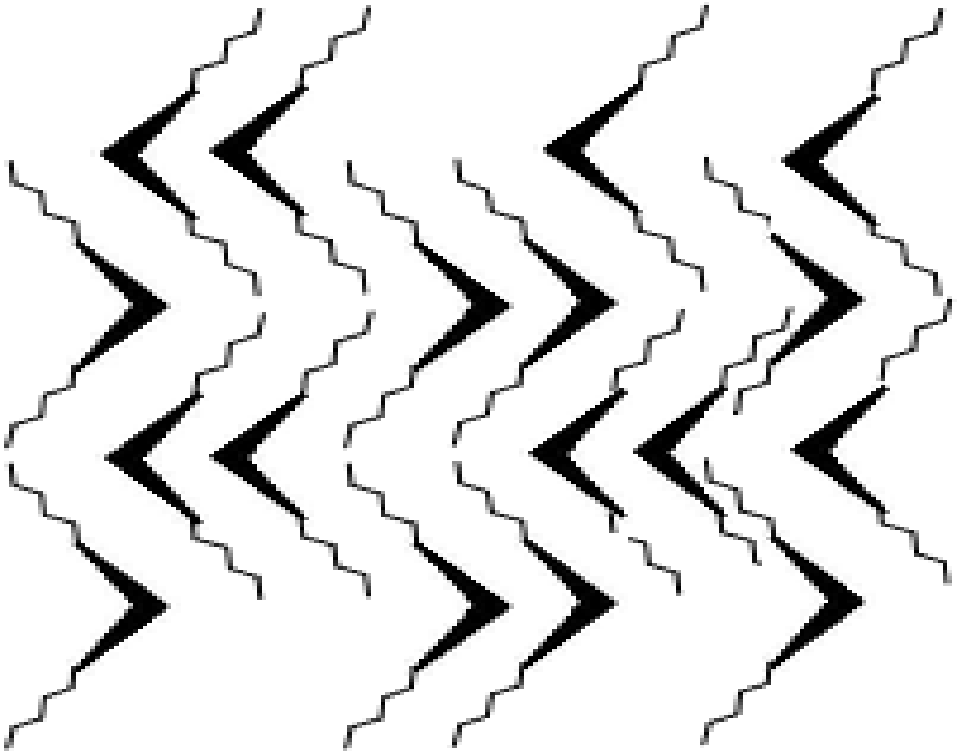

Figure 1.12: Molecular arrangement of bent core LC in $\mathbf{B_6}$ phase [11].

$\mathbf{B_7}$ phase shows helical nuclei textures. They appear when bent core molecules are slowly cooled from isotropic state. Textures usually resembles with telephone wires, textures are extremely beautiful and fascinating.

$\mathbf{B_8}$ compounds are derived from isophthalic acid, which contain carboxylic groups in terminal alkyl chains. They possess a bilayer texture. Anti-ferroelectric behaviour is observed in $\mathbf{B_8}$ phase at higher temperature

1.7 Langmuir-Blodgett Films

Benjamin Franklin studied the behaviour of thin film on air- water interface [44-43]. He observed that surface tension at interface is different from tension faced by molecules in bulk. Interface tensions helped in alignment of molecules. Later on, Agnes Pockles found that impurities of sub phase had their influence on arrangement of molecules [44-45]. Irving Langmuir, an American scientist, had performed systematic studies on monolayers floating on air-water interface. He gave understanding about the structure of monolayer and proposed that the preferred orientation of monolayer was attained due to presence of

amphiphilic character of molecule. Monolayers formed at air water interface are referred as **Langmuir** monolayers. Later his work was further preceded by Katherine Blodgett who gave detailed description of sequential monolayer transfer to solid substrate. She developed experimental set up for making monolayer and multilayers on solid substrates. Thus, monolayers transferred to substrates are named as **Langmuir-Blodgett (LB)** films [46].

1.8 Langmuir Monolayer

Amphiphilic character of molecules is the major requirement to form Langmuir monolayer. Proper balance between hydrophilic groups and hydrophobic groups of amphiphilic molecules is necessary to ensure insolubility at water surface. Solution is prepared by dissolving low concentration of amphiphilic molecules in volatile solvent such as chloroform. This dilute solution is spread drop wise on water surface. The solvent will evaporate leaving a well aligned layer on interface. Hydrophilic groups of molecules align towards water surface and hydrophobic groups are repelled away from water surface. Monolayers formed by this procedure at molecular level are named as Langmuir monolayers [47].

The schematic view of Langmuir Blodgett setup is given in figure 1.13. Monolayer formed is dependent upon nature of spread material [48, 49], pH of the sub phase, compression rate, temperature of sub phase [50], ions present in sub phase etc. Trough containing water is usually made up of teflon. The most important parameter in study of LB films is surface pressure (Π). It is defined as the difference between surface pressure of sub phase in the presence of monolayer and without monolayer [51, 52].

$$\Pi = \gamma^{\circ} - \gamma \qquad (1.1)$$

Where γ° is the surface tension of water without monolayer and γ is the surface tension with monolayer. Surface pressure is measured by immersing Wilhelmy plate in to subphase. Wilhelmy plate is attached to electro-balance by a hook. Plate can be made of platinum or paper. This plate sense surface pressure of monolayer with great accuracy during compression. Constant compression of monolayer is done by moving barriers at uniform speed.

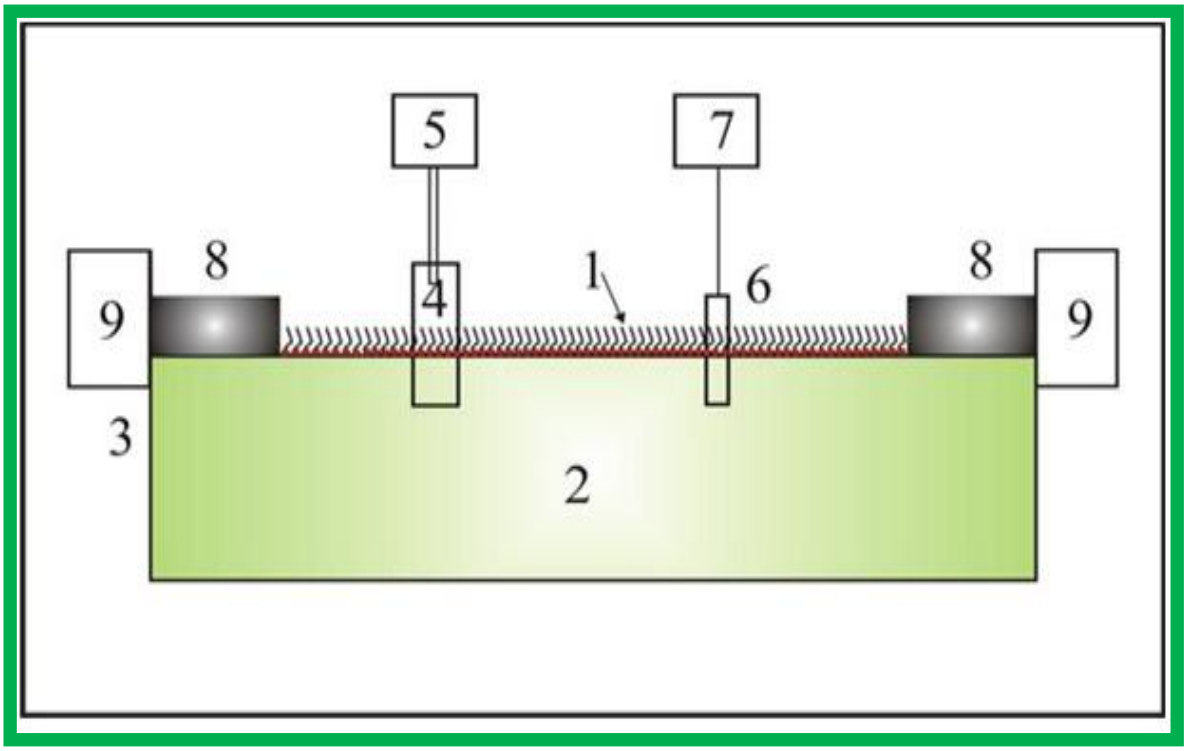

Figure 1.13: Schematic view of LB experimental set up. 1. Monolayer at interface 2. Liquid subphase (water) 3. Langmuir Blodgett Trough 4. Solid substrate 5. Dipping mechanism 6. Wilhelmy Plate 7. Electro balance (Surface Pressure) 8. Barriers 9. DC motor for driving barriers.

After required compression films are easily transferrable to substrate at constant dipping speed. Solid substrate is fixed in dipper clip. Langmuir monolayer provides very useful information about intermolecular forces and molecular sizes of materials [53, 54].

1.9 Surface pressure- Area (Π-A) Isotherm

Surface pressure-Area isotherm gives information about various phase transitions occurring during constant compression. Surface Pressure arises because molecules at interface experience unequal forces of interactions at interface as compared to molecules present in bulk.

A typical version of Surface pressure- Area isotherm is shown in figure 1.14. For simple amphiphilic materials isotherm consist of three distinct regions: **Gas** phase, **Liquid** phase and **Solid** phase [55].

Initially there is no external pressure on molecules forming monolayer. There is no interaction force among them and behave like a '**gas**' which obey ideal gas equation

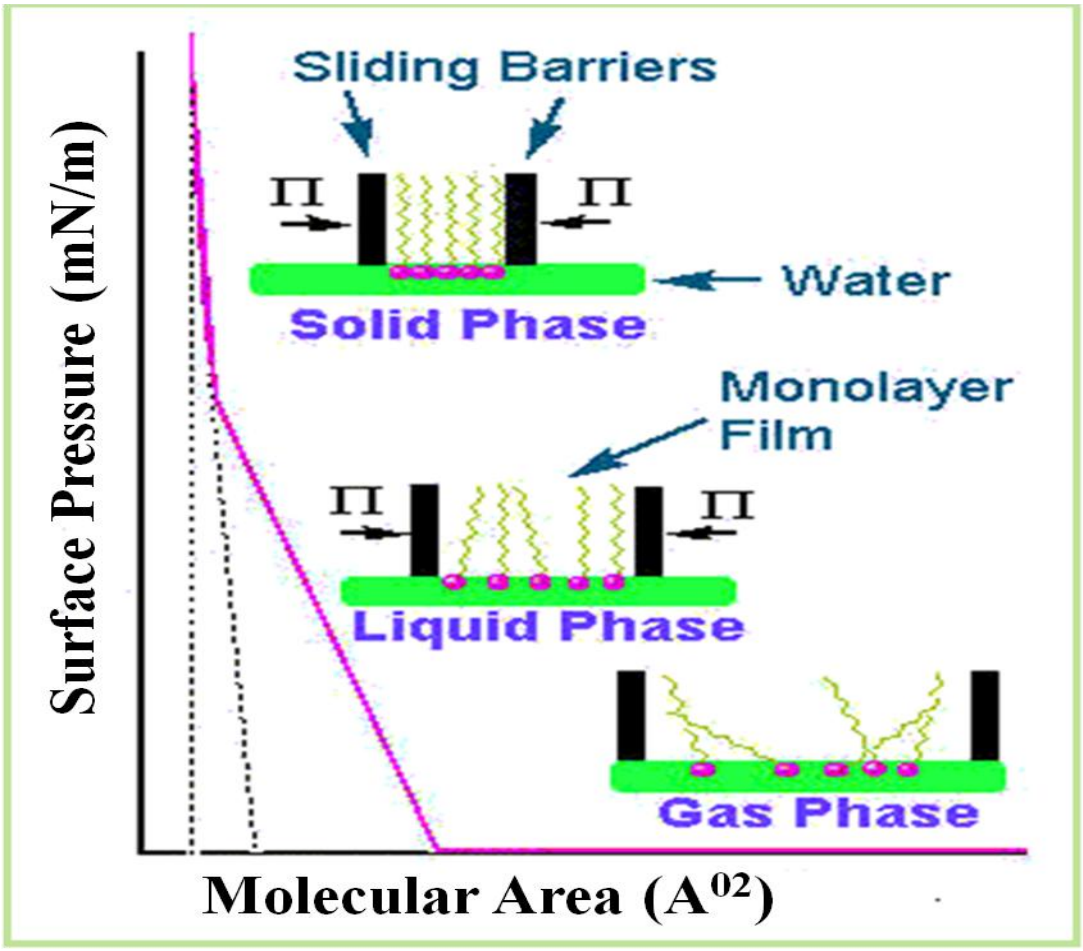

Figure 1.14: Isotherm of Langmuir monolayer on constant compression of barrier.

$$\Pi A = K T \tag{1.2}$$

Where Π is the surface pressure of molecules present at interface, A the molecular area, K denotes Boltzmann constant and T represents temperature.

Researchers have reported deviation from equation 1.2 in most of the monolayers. When compression process is initiated in gaseous phase, molecules posses weak forces of attraction. Surface pressure of monolayer will start increasing with decrease in area per unit molecule. This leads to correction in equation 1.2.

$$\left(\pi + \frac{a}{A_m^2}\right)(A_m - b) = k_b T \tag{1.3}$$

Where **a** shows surface pressure increased during compression and **b** shows reduced area.

Liquid Phase appears with compression, firstly low density phase comes with molecular ordering, it is intermediate phase between gaseous and liquid phase. In this phase molecules are randomly arranged as in liquid phase but they have slightly week

forces of attraction. When this phase is further compressed, molecules come closer to each other and they arrange themselves in such a way that hydrophobic parts of molecules are lifted upwards and hydrophilic groups are attracted towards water surface. This partial ordering of molecules leads to high density two-dimensional liquid phase [56].

With further sliding of barriers towards each other, molecules of monolayer come closer. Attraction forces among molecules are increases up to great extent which result in formation of **Solid** phase [57-60].

Further compression of monolayer form solid phase result in collapsed state. Monolayer will become 3-D in state. The pressure at which 3-D or multilayers are formed are named as collapsed surface pressure. So, the **collapse pressure** can be defined as maximum surface pressure up to which a uniform monolayer can sustain [61, 62].

As we can clearly examine from figure 1.14 each phase of monolayer has a characteristic trace on the isotherm plot with a sharp transition at the change of phase.

The monolayer phase can be easily characterized by studying compression modulus |E|.

$$|\mathbf{E}| = -A_m \frac{d\pi}{dA_m} \tag{1.4}$$

1.10 Modes of deposition

Deposition of Langmuir monolayer is dependent upon speed of transfer. At low speed of transfer, monolayer can be easily transferred to solid substrates. Packing structure and molecular orientation remain preserved during formation of Langmuir Blodgett films. If transfer speed is chosen very high, the crystalline structure is changed or lost. Chances of transfer are decreased significantly. Films are always formed at constant surface pressure [63]. There are two methods which are used to transfer Langmuir monolayer to solid substrates as shown in figure 1.15:

1. Langmuir Blodgett (Vertical deposition)
2. Langmuir-Schaefer (Horizontal Deposition)

In **Langmuir-Blodgett** deposition substrate is lowered vertically into water subphase. While lowering it becomes in contact with the monolayer present at interface. Monolayer gets attached to the substrate at constant surface pressure. Repeated immersion emersion of the substrate at interface results in formation of multilayers. Multilayers can be formed by three different types (**X**, **Y** and **Z**) of substrate movements as described below:

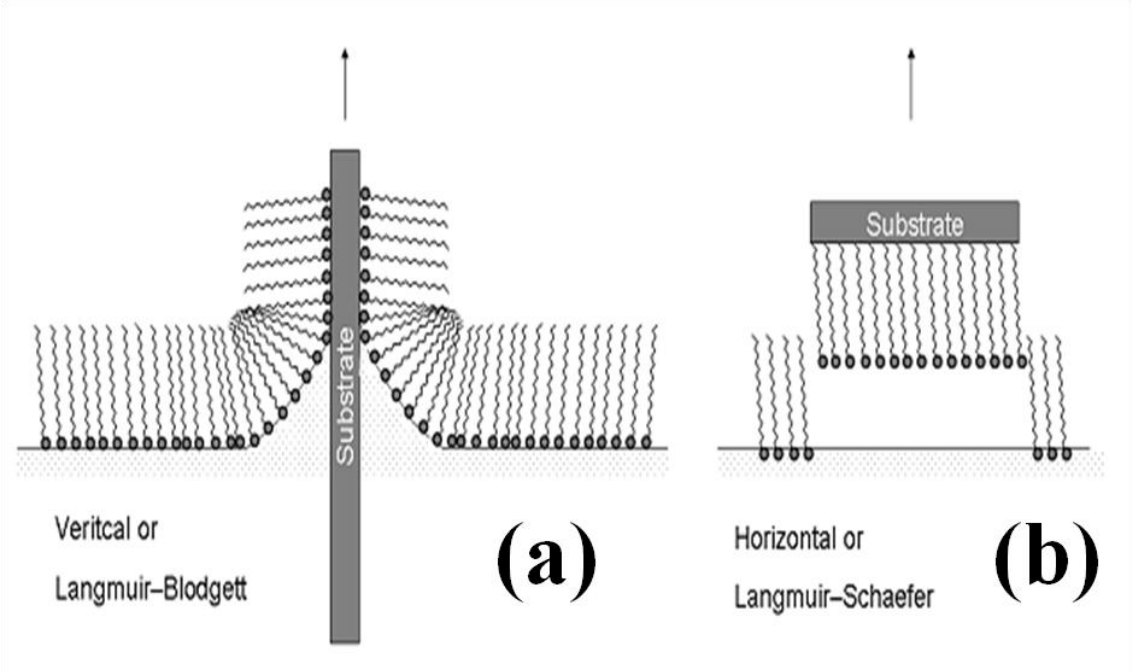

Figure1.15: Schematic representation of the vertical (Langmuir-Blodgett) and horizontal (Langmuir -Schaefer) multilayer films transfer method [64].

In **Y**-type deposition mode sequence of multilayers with alternating hydrophobic-hydrophobic and hydrophilic-hydrophilic interactions are deposited by repeating up and down stroke alternately (Figure 1.16). Multilayers can be deposited by **X** and **Z** type, when films are transferred by down stroke and upstroke movements only. Such multilayers can be formed with molecules having a weakly hydrophilic character or a slightly polar terminated alkyl chain [65-67].

In horizontal lifting method, substrate is moved up at very slow speed parallel to interface as depicted schematically in the right side of figure 1.15. Crystalline order of monolayer is preserved during transfer.

Transfer Ratio is used to calculate how efficiently LB film is transferred to solid substrate from sub phase.

$$\tau = \frac{\textbf{Decrease in Langmuir monolayer surface area}}{\textbf{Total surface area of the substrate}}$$

Where τ represents transfer ratio. For ideal deposition transfer ratio is 1. Many times this may not be the case, often during transfer, films get modified due to various reasons. Transfer ratio may deviate slightly from 1.

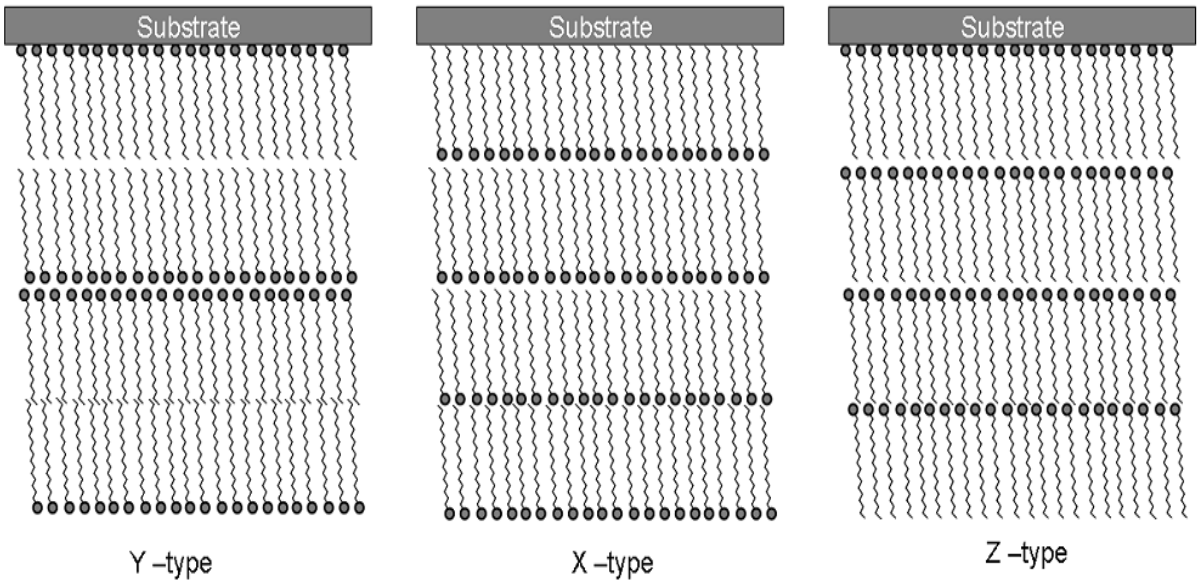

Figure 1.16: **Y**, **X** and **Z**-type of multilayer deposition (**Y**-type is centrosymmetric while the X and Z are non-centrosymmetric) [64].

1.11 Langmuir Blodgett films of Amphiphilic Liquid Crystals and Functionalized nano-particles

All thermotropic liquid crystal molecules are not amphiphiles; nevertheless many of them do posses amphiphilic properties. They create stable and compressible monolayers at air-water interface. These monolayers can be easily transferred to solid substrates [68-71].

Some liquid crystals which donot have balance between hydrophilic and hydrophobic groups, they can form LB monolayers by addition of long chain fatty acids. Nano-particles itself do not have tendency to stabilize at interface but after they are functionalized with long polar alkyl chains, they do get hydrophobic character.

In this thesis we have attempted to understand properties of stable LB films of ferroelectric liquid crystals and their composite dispersed with nano-particles [72-75].

References:

1 G L Gaines Jr. Insoluble Monolayers at Liquid Gas Interface, Interscience: NewYork, 1966.

2 K S Birdi. Lipid and Biopolymer Monolayers at Liquid Interfaces, Plenum Press: New York, 1989.

3 M L Longo, A M Bisagno, J A N Zasadzinski, R Bruni, A J Waring. A function of lung surfactant protein SP-B. Science. 1993, **261**, 453.

4 M J Rosen. Surfactants and interfacial phenomenon, Wiley Interscience Publication: New York, 1973.

5 A Singh, R Singh, Surface chemistry, Campus Books International:New Delhi India, 2005.

6 J Israelachvili. Intermolecular and surface forces, 2nd edition Academic Press: London, 1992.

7 J Seddon. Handbook of liquid crystals, Wiley: New York, 1998.

8 F Reinitzer. Beiträge zur Kenntniss des Cholesterins. Monatshefte für Chemie 1888, **9 (1)**, 421.

9 G W Gray. Molecular Structure and the Properties of Liquid Crystals, Academic Press: 1962.

10 P G Gennes, J Prost. The Physics of Liquid Crystals, Oxford University Press: UK, Second edition, 2001.

11 P J Collings, M Hird. Introduction to Liquid Crystals, Chemistry and Physics; Taylor and Francis: London, 1997.

12 S Chandrasekhar. Liquid Crystal 2nd ed, Cambridge University Press, 1992.

13 I C Khoo. Liquid Crystals: Physical Properties and Non-Linear Optical Phenomenon, John Wiley and Sons Inc.: New York, 1995.

14 S Chandrasekhar, B K Sadashiva, K A Suresh. Liquid Crystals of Disc like molecules, Pramana, 1977, **9(5)**, 471.

15 E S Blackmore, G J T Tiddy. Phase behaviour and lyotropic liquid crystal in cationic water surfactant system. J. Chem. Soc. Faraday Trans.1988, **84(2)**, 1115.

16 R G Laughlin. The Aqueous Phase Behaviour of Surfactants; London: Academic Press: 1996.

17 E D Fennell, Wennerstrom H. The Colloidal Domain; New York: Wiley VCH: 1999.

18 M Hird. Fluorinated liquid crystals – properties and applications, Chem. Soc. Rev. 2007, **36**, 2070.

19 W George, Gray, M K Stephen. Liquid crystals for twisted nematic display devices **J. Mater. Chem.** 1999, **9,** 2037.

20 I Dierking, M Mitov, A Mikhail, Osipov. Smectic layer instabilities in liquid crystals Soft Matter, 2015, **11**, 819.

21 H S Kitzerow, C Bahr. Chirality in Liquid Crystals, Springer-Verlag: New York, 2001.

22 C J Booth, In Handbook of liquid crystals, Wiley:VCH,1998.

23 N Tamaoki, M Moriyama, H Matsuda. Cholesteric Solid Films Formed by Spin-Coating Solutions of Di-cholesteryl Esters. Angew. Chem. Int. Ed. 2000,

39(3), 509.

24 N Tamaoki. Cholesteric Liquid Crystals for Color Information Technology. Adv. Mater. 2001, **13**, 1135.

25 T Niori, J Sekine, T Watanabe, H Furukawa, H Takezoe, Distinct ferroelectric smectic liquid crystals consisting of banana shaped achiral molecules. J. Mater. Chem. 1996, **6**, 1231.

26 C K Lee, A Primak, A Jakali, E J Choi, W C Zin, L C Chien. Ferroelectric smectic meso-phase formed by banana-shaped achiral liquid crystals. Liq. Cryst. 2001, **28**, 1293.

27 D R Link, G Natale, R Shao, J E Maclennan, N A Clark, E Körblova, D M Walba. Spontaneous Formation of Macroscopic Chiral Domains in a Fluid Smectic Phase of Achiral Molecules. Science. 1997, **278**, 1924.

28 T Sekine, T Niori, M Sone, J Watanabe, S W Choi, Y Takanishi , H Takezoe. Origin of Helix in Achiral Banana-Shaped Molecular Systems. Jap. J. Appl. Phys. 1997, **36**, 6455.

29 T Sekine, T Niori, J Watanabe, T Furukawa, S W Choi H Takezoe, Spontaneous helix formation in smectic liquid crystals comprising achiral molecules, J. Mater. Chem.1997, **7**, 1307.

30 Y Matsunaga, S Miyamoto, Mesomorphic Behavior of 2, 4-Bis-(4-alkoxybenzy lidene)cyclopentanones and Related Compounds. Mol. Cryst. Liq. Cryst. 1993, **237**, 311.

31 M Kr Paul, R Kumar, N Chakraborty, K K Raina, N V S Rao. Electro-optic and molecular relaxation behaviour of fluoro substituted achiral unsymmetrical four-ring bent-core mesogen. Liq Cryst. 2014, **41**, 635.

32 J Watanabe, T Niori, S W Choi, Y Takanishi, H Takezoe. Antiferroelectric Smectic Liquid Crystal Formed by Achiral Twin Dimer with Two Mesogenic Groups Linked by Alkylene Spacer. Jpn. J. appl. Phys.1998, **37**, L401.

33 R Amaranatha, B K Sadashiva. Synthesis and mesomorphic properties of banana-shaped compounds derived from 2, 7-dihydroxynaphthalene. Liq. Cryst. 2000, **27**, 1613.

34 T J Dingemans, E T Samulski. Non-linear boomerang-shaped liquid crystals derived from 2,5-bis(p-hydroxyphenyl)-1,3,4-oxadiazole. Liq. Cryst. 2000, **27**, 131.

35 J Thisayukta, Y Nakayama, J Watanabe. Effect of chemical structure on the liquid crystallinity of banana-shaped molecules. Liq. Cryst. 2000, **27**, 1129.

36 Y Matsunaga, T Hosoda. Mesomorphic Behavior of Symmetric Liquid Crystal Dimers: α,ω- Bis[4-(4-alkoxybenzoyloxy)benzylideneamino] alkanes. Mol. Cryst. Liq. Cryst. 1999, **326**, 369.

37 J Watanabe, H Komura, T Niori. Thermotropic liquid crystals of polyesters having a mesogenic 4, 4-bibenzoate unit Smectic mesophase properties and structures in dimeric model compounds. Liq. Cryst. 1993, **13**,455.

38 T Niori, S Adachi, J Watanabe, Smectic mesophase properties of dimeric compounds. 1. Dimeric compounds based on the mesogenic azobenzene unit. Liq. Cryst. 1995, **19**, 139.

39 J Watanabe, T Niori, T Sekine, H Takezoe. Frustrated structure induced on ferroelectric smectic phases in banana-shaped molecular systems. Jpn. J. Appl. Phys. 1998, **37**, L 139.

40 S W Choi, M Zennyoji, Y Takanishi, H Takezoe, T Niori, J Watanabe. Structure and Switching in Bent-Shaped Molecular Liquid Crystal Systems with Two

Mesogenic Groups Linked by Alkylene Spacer. Mol. Cryst. Liq. Cryst. A, 1999, **328**, 185.

41 G Pelzl, S Diele, W Weissflog. Banana-Shaped Compounds—A New Field of Liquid Crystals. Adv. Mater. 1999, **11(9)**, 707.

42 B Franklin, W Brownrigg, M Farish Phil. Trans.,1774, **64**, 445.

43 G Roberts. Ed. Langmuir-Blodgett Films, Plenum Press: New York 1990.

44 A Pockels. On the Relative Contamination of the Water-Surface by Equal Quantities of Different Substances Nature.1892, **46**,418.

45 A Pockels. Surface Tension. Nature. 1891, **43**,437.

46 K B Blodgett. Films Built by Depositing Successive Monomolecular Layers on a Solid Surface. J Amer. *Chem*. Soc. 1935, **57(6)**, 1007.

47 M C Petty. Possible applications for Langmuir-Blodgett films. Thin Solid Films. 1992, **210/211**,417.

48 M B Johan, L G Tomas Eriksson, P M Claesson, K G Nordli Barvet. Three-Component Langmuir-Blodgett Films with a Controllable Degree of Polarity. Langmuir. 1994, **10**, 1225.

49 J Fang, Y Wei, Fabrication of Polar films by Langmuir Blodgett technique, Chinese Phys. Lett.1991, **8(7)**, 360.

50 H M Brodowsky, U C Boehnke, F Kremer. Temperature Dependent AFM on Ferroelectric Liquid Crystalline Polymer and Elastomer Films. Langmuir.1997, **13**, 5378.

51 J H Golden, F J Di Salvo, M J Jean. Ordered Conducting Films of the Inorganic

Polymer, Cast from Solution. Chem. Mater. 1995, **7**, 232.

52 A Nayak, K A Suresh. Mechanical properties of Langmuir-Blodgett films of a discogen-DNA complex by atomic force microscopy, J. Phys. Chem. B. 2009, **113**, 3669.

53 V M Kaganer, Mohwald H, Dutta P. Rev. Mod. Phys. Structure and phase transitions in Langmuir monolayers. 1999, **71**, 779.

54 M M Lipp, K Y C Le, J A Zasadzinski, A J Waring. Phase and Morphology Changes in Lipid Monolayers Induced by SP-B Protein and Its Amino-Terminal Peptide. Science. 1996, **273**, 1196.

55 Y Tabe, T Yamamoto, I Nishiyama, K M Aoki, M Yoneya, H Yokoyama. Can hydrophobic oils spread on water as condensed Langmuir monolayers? J. Phys. Chem. B. 2002, **106**, 12089.

56 V M Kaganer. Structure and phase transitions in Langmuir monolayers. Rev. of Modern Phys. 1999, **71(3)**, 779.

57 R G Laughlin . The Aqueous Phase Behaviour of Surfactants, Academic Press Inc.: San Diego 1994.

58 D K Chattoraj, K S Birdi . Adsorption and the Gibbs Surface Excess, Plenum Press: New York, 1984.

59 A W Adamson. Physical Chemistry of Surfaces, Wiley & Sons:New York , 1976.

60 D J Shaw. Introduction to Colloid and Surface Chemistry, Butterworth & Co: London, 1980.

61 C Ybert, W Lu, G Moller, C M Knobler. Collapse of a Monolayer by Three Mechanisms. J. Phys. Chem. B 2002, **106**, 2004.

62 R D Smith, J C Berg. The collapse of surfactant monolayers at the air-water interface. J. Colloid Interface Sci. 1980, **74**, 273.

63 N G Marc de Mul, J Adin Mann, Jr. Multilayer Formation in Thin Films of Thermotropic Liquid Crystals at the Air-Water Interface. Langmuir 1994, **10**, 2311.

64 N Osvaldo, Jr. Oliveira. Langmuir-Blodgett Films - Properties and Possible Applications. Brazjljan J. of Physks. 1992, **22**, 61-69.

65 S Hénon, J Meunier. Microscope at the Brewster angle: Direct observation of first-order phase transitions in monolayers. Rev. Sci. Instrum. 1991, **62**, 936.

66 W D Harkins. The Physical Chemistry of Surface Films, Reinhold:New York 1952.

67 B P Bink. Insoluble monolayers of weakly ionising low molar mass materials and their deposition to form Langmuir-Blodgett multilayers. Adv. Coll. Int. Sci. 1991, **34**, 343.

68 X Wang, L Sun, B Zhao, W Xu, Q Xue, K Yang, Q Zhang, Y Ozaki. An infrared study of Langmuir–Blodgett films of side-chain chiral liquid crystalline polysiloxane. Thin Solid Films. 2006, **497**, 347.

69 K Inglot, T Martyński, D Bauman. Molecular organization and aggregation in Langmuir and Langmuir-Blodgett films of azo dye/liquid crystal mixtures. Opto−Electron. Rev. 2009, **17(2)**, 120.

70 J Y Fang, Z H Iu, G Ming, Z M Ai, Y Wei. Anchoring structure of liquid-crystal monolayers on polyimide Langmuir-Blodgett films observed by scanning tunneling microscopy. Phys. Rev. A, 1992, **46(8)**, 4963.

71 H K Bisoyi, S Kumar. Liquid-crystal nanoscience: an emerging avenue of soft

self-assembly. Chem. Soc. Rev., 2011, **40**, 306.

72 R K Gupta, K A Suresh, S Kumar. Monolayer of amphiphilic functionalized gold nanoparticles at an air-water interface. Phys. Rev. E. 2008, **78**, 032601 (1).

73 K Yeji, M Nobutsugu, H Weihong, K Said, A Z U M I Reiko, M Mutsuyoshi. Langmuir–Blodgett Films of Single-Wall Carbon Nanotubes: Layer-by-layer Deposition and In-plane Orientation of Tubes. Jpn. J. Appl. Phys. 2003, **42**, 7629.

74 D L Michael, L P David. Organizing Carbon Nanotubes with Liquid Crystals. Nano Lett. 2002, **2(11)**, 1197.

75 V Ramakrishnan, M D Costa, K N Ganesh, M Sastry. PNA-DNA hybridization at the air-water interface in the presence of octadecylamine Langmuir monolayers. Langmuir. 2002, **18**, 6307.

Chapter 2

Experimental techniques and Materials Used

Overview

This chapter presents the experimental techniques and materials used for preparation and characterization of LB films of liquid crystals and their composite systems. It explains various stages for preparation and deposition of LB films. Experimental techniques like FTIR used to confirm complete deposition, X-Ray Diffraction (XRD) for phase determination and Atomic Force Microscopy (AFM) for topography are discussed.

Hydrophobicity and hydrophillicity of groups present in ferroelectric liquid crystal, single wall carbon nano tube, nano-particles and bent core liquid crystal are discussed along with their molecular structure and 3-D models. A summary of methodology is also given at end of this chapter.

2.1 Langmuir-Blodgett Deposition technique

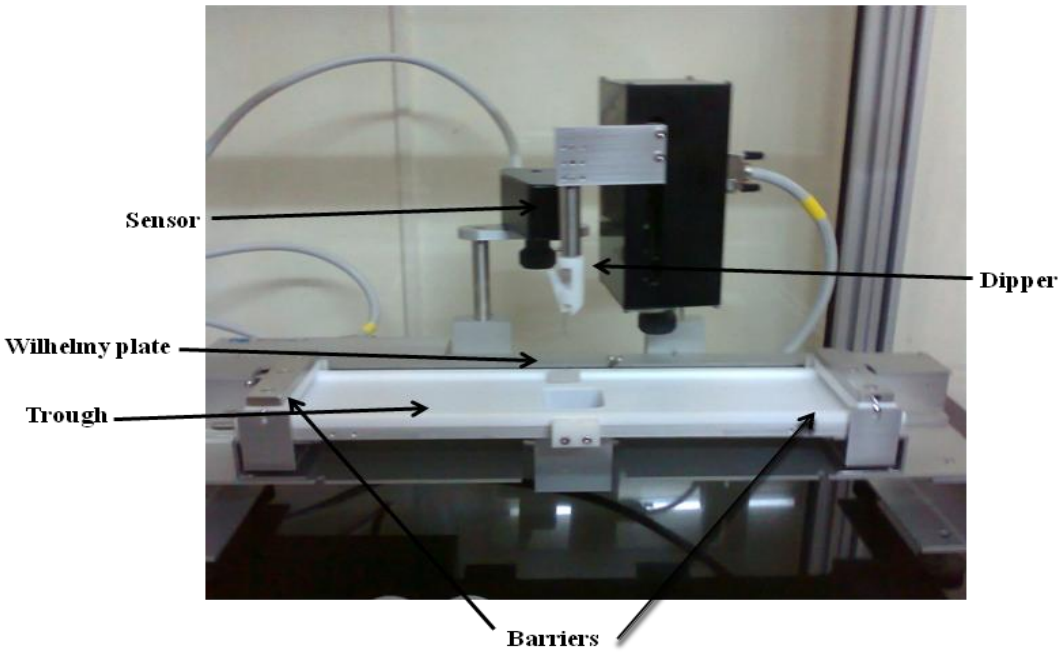

Figure 2.1: Experimental set for Langmuir-Blodgett film deposition.

We have used KSV-NIMA, Finland experimental set up. This instrument is a single minitrough (160 m*l* without dipping well) system made up of Teflon with a dipper well for dipping the substrate [figure 2.1]. The working area of the trough may be varied by moveable barriers, made up of Derlin (polyactelylene). These barriers are also used to stabilise the surface pressure of monolayer. The surface pressure was measured by Wilhelmy plate (38mm×19.62mm×10mm) with precision of 0.1mN m^{-1}[1, 2]. The deposition of films onto a solid substrate is done by holding substrate into dipper clip, then dipper is moved vertically through the floating Langmuir monolayer at the air-water interface. Movements of both the dipper and the barrier are done by computer controlled stepper motors. The speeds of the motors can be controlled precisely. The whole set-up is located in an acrylic small glass cabinet (CABI S) to avoid air streams and dust deposition and to allow temperature control at 23.0 $\pm$ 0.1°C. Temperature was measured using a probe (KN0054), which was immersed in Langmuir trough from one side and the other side being containing the temperature measuring probe having a wire connected to an interface unit of KSV NIMA. The whole LB film deposition system is computerized through interface unit having display. Display shows both barrier position (mm min^{-1}) and surface pressure (mN m^{-1}) while running experiment. pH measuring probe for KSV-NIMA System (KN 0011) was also attached through interface [3,4].

2.1.1 Trough Cleaning and Subphase:

Proper cleaning of trough is very important to study molecular interactions at interface air-water. Trough is cleaned with ethanol [Merck (AR)] and then rinsed with deionised water. The proper cleanliness of trough can be ensured when Millipore water (Direct Q_3) completely dewetted the surface after draining it. Most common sub phase used for the study of mono-molecular film is ultra pure water. Other liquids can be used if they posses high surface tension as water. We have used water from Milli-Q ultra pure water purification system. The resistivity of the water was 18.2 MΩ.cm. The pH of the water is ~6.0. Addition of ions (changing acidity or basicity) into sub phase will provide considerable amount of degree of control over monolayer behaviour and the successful deposition of the monolayer.

2.1.2 Solution Preparation and spreading on Subphase:

Solution (mg ml^{-1}) of desired amphiphilic material is prepared using highly volatile water insoluble solvent such as chloroform. Solutions are ultrasonicated for required amount of time to ensure proper dissolution. Solutions are kept in air-tight container so that their concentrations remain unaltered.

Solution is spread on the aqueous surface by Hamilton micro syringe. Small drops at distance of a few millimeters above the subphase are placed uniformly. Before starting compression process with barriers, solvent evaporation time is given in each experiment.

2.1.3 Cleaning of Substrates and Deposition:

Silicon substrates were cleaned by solvent clean method. Silicon wafers were placed in warm acetone (60˚C) in a covered petri dish for about 10 minutes, and then substrates were placed in methanol for about 3 minutes. They are rinsed with deionised water and a short dip of silicon substrate was made into 2% dilute hydrofluoric acid. This acid helps in removal native silicon dioxide from wafers so that direct covalent linkage to the Si surface via a Si-C bond made monolayer chemically and thermally stable as compared to organic layers on other substrates like glass, mica, quartz etc [5]. At end, substrates were rinsed with deionised water. Glass substrates are cleaned by using acetone to remove organic impurities from surface and rinsing is done by using deionised water.

Monolayer and multilayers formed at water surface are successfully transferred to substrate at constant surface pressure with constant dipper speed (mm min^{-1}). Transfer

ratio should be close to 1.0 for all depositions to ensure complete transform of monolayer to substrate. After detaching substrate from dipper, films are dried in vacuum desicators.

2.2 Fourier Transform Infra-red Spectroscopy:

Figure 2.2: Image of FTIR Spectrometer present at laboratory.

FTIR measurements are carried out by spectroscope (BX-II, Perkin Elmer) as shown in figure 2.2, resolution 4 cm^{-1}, scan range 400 cm^{-1} to 4000 cm^{-1} at room temperature. 16 scans are performed to ensure results for each film.

When LB film is placed on sample holding stage, IR radiation is passed through film deposited on glass substrate. Some of the infrared radiation is absorbed by the film and some of it is passed through (transmitted). The resulting spectrum represents the molecular absorption and transmission, creating a molecular finger prints of the film.

So, infrared spectroscopy can result in a positive identification (qualitative analysis) of every different kind of material present in film. In addition, the size of the peaks in the spectrum is a direct indication of the amount of material present. Intensity of peaks will change with increasing layer number of deposition. The normal instrumental layout of FTIR is shown in figure 2.3. Source emits Infrared energy which is then passed through an aperture, to get desired and controlled amount of energy.

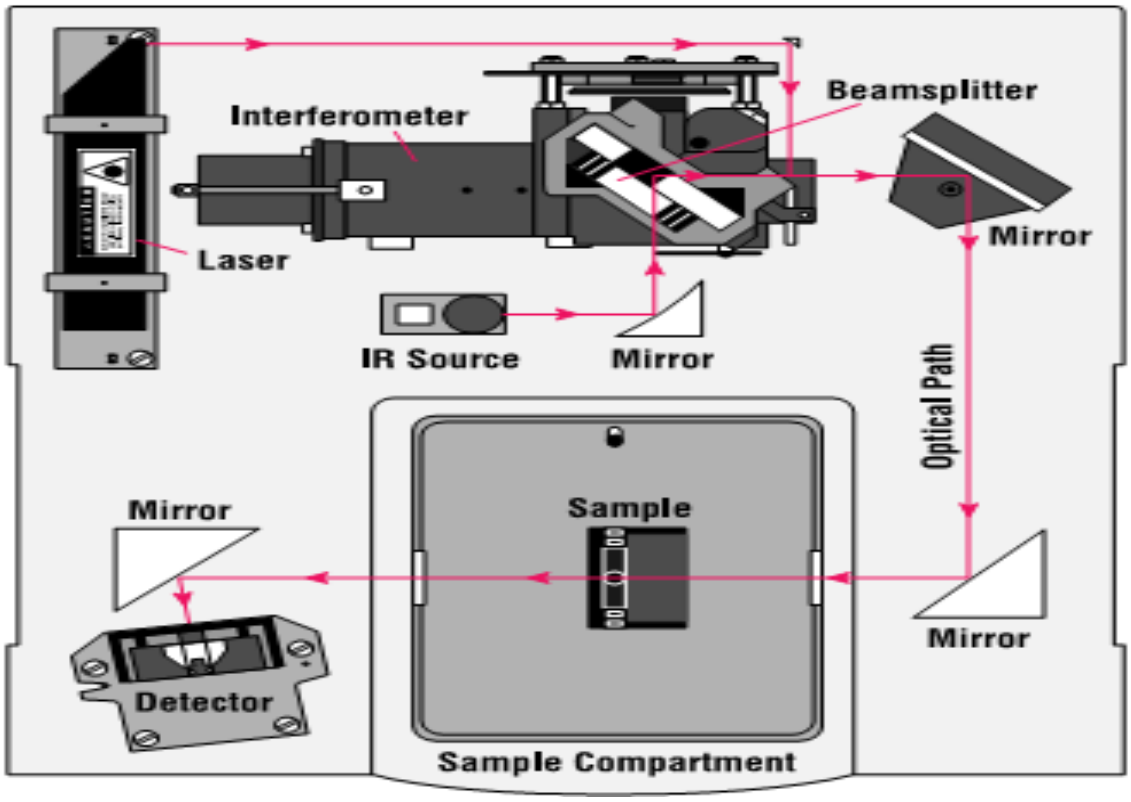

Figure 2.3: Simple layout of FTIR Spectrometer

This controlled energy beam is passed through interferometer before sending to sample compartment. Optical path of beam is controlled by its reflection from mirror. When beam falls on film mounted on sample holder, it gets transmitted from surface of sample. Specific amount of frequency is absorbed by the sample. The beam passes through detector for final measurements after getting reflection from beam. Detectors are specially designed to measure interferogram signal. This measured signal is again converted into digital signal before sending to computer. In computer Fourier transformation of signal take place. Infrared spectrum is presented to user for interpretation

2.3 X-Ray Diffraction Spectroscopy

We have used Philips XPERT–PRO MPD X-Ray Spectrometer. Laboratory view of XRD is shown in figure 2.4. For XRD analysis of LB films, films were deposited on Glass substrate, to avoid substrate peak. LB films of liquid crystal materials are detected at low angles. X-ray diffraction is the most wide spread technique for determining the phase identification, crystal structure, lattice parameter of the crystalline solids. A typical XRD consist of four main components such as X-ray source, specimen stage, receiving optics

Figure 2.4: Laboratory view of X-Ray Diffraction spectrometer.

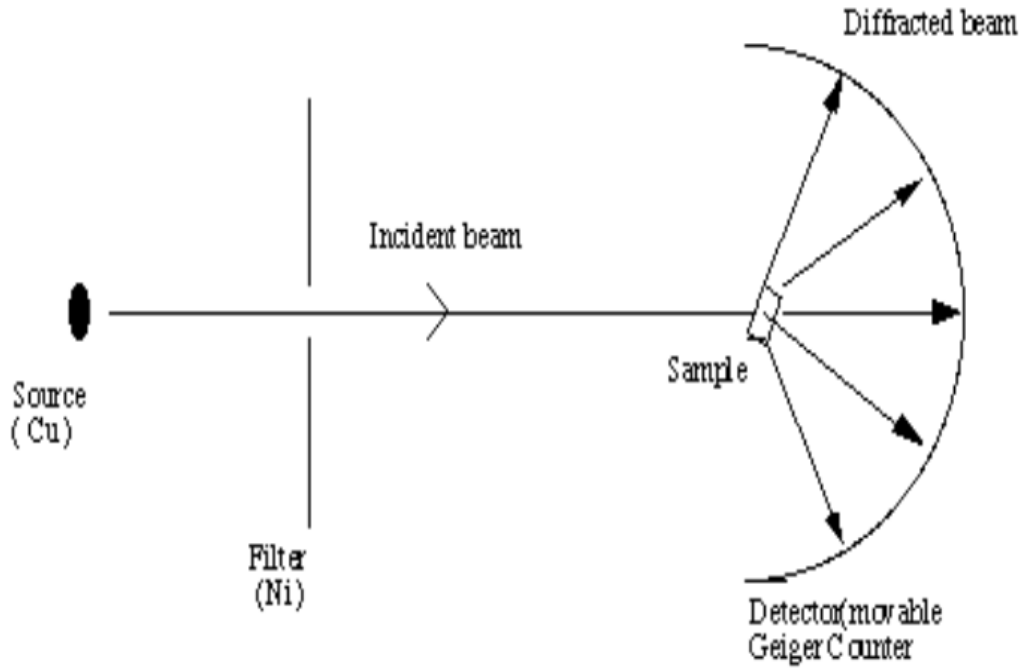

Figure 2.5: Schematic view of Optical axis of X-Ray Diffraction spectrometer

and X-ray detector as shown in figure 2.5. The source and detector with its associated optics lie on the circumference of circle focusing circle and the sample stage at the centre of circle. The angle between the plane of the specimen and the X-Ray source is θ, known as Braggs angle and the angle between the projection of X-ray and the detector is 2θ [6,7].

2.4 Atomic Force Microscopy

Atomic force microscopy (AFM) (Solver-NEXT NT-MDT; Zelenograd, Moscow, Russia) is used for topographical investigations of the thin films as shown in figure 2.6. AFM images are taken in non-contact mode (scan rate 1 Hz). Silicon nitride (SiN) probe of tip curvature radius 2 nm is attached to a cantilever (resonance frequency; 87-230 kHz, typical force constant 5.1nN m^{-1}). The topography data are sampled in a grid of 512 × 512 points. The imaging is carried out under ambient laboratory conditions. Initially properly cleaned substrate is scanned under AFM and root mean square roughness < 1nm is observed. It ensures smoothness of the silicon and its sustainability for monolayer deposition. AFM images are processed with NOVA P9 Software (Image Analysis 2.1.0.800) which is used also to determine 3-D view and height profiles.

Figure 2.6: Front view of Atomic Force Microscope.

A schematic view of an Atomic Force Microscope is shown in figure 2.7. Tip is attached at edge of cantilever. The head of the tip is usually coated with a reflecting material like SiN. When laser light falls, it gets illuminated. The reflected light from tip surface is collected on a quadrant photodiode. Sample is mounted on a piezo scanner. It can move in all X, Y and Z direction. When deflection of tip occurs due to its interaction with the sample, it is monitored by measuring change of light intensity on the photodiode. There are numerous modes of operation of AFM. Langmuir-Blodgett films are of soft organic material. They are analysed under non-contact mode of scanning.

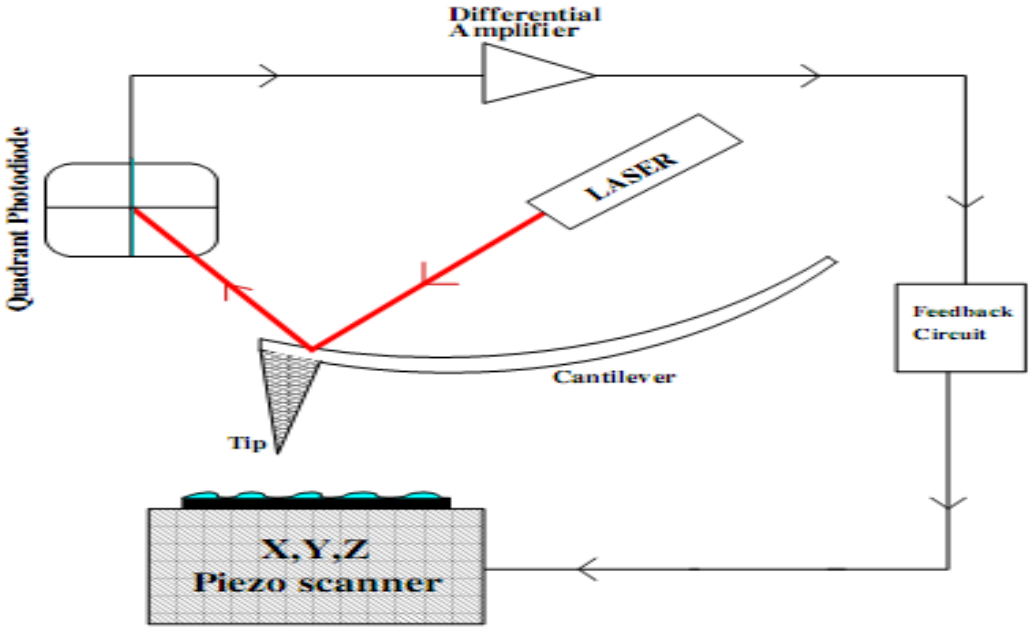

Figure 2.7: Schematic diagram of an atomic force microscope (AFM)

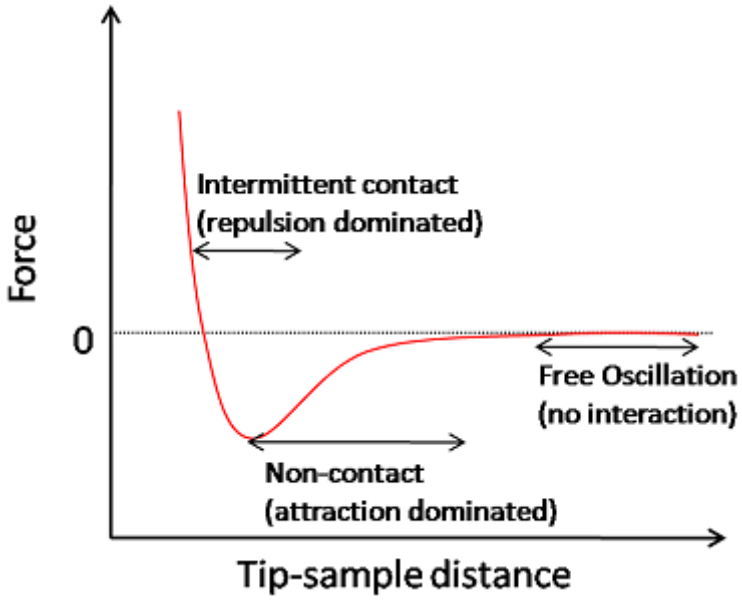

Figure 2.8: Typical force versus tip-sample distance curve in an atomic force microscopy.

In non-contact mode AFM, attractive forces which are of long range are used to monitor the tip-sample interaction as shown in force-distance curve in figure 2.9 [8,9]. In this mode oscillations are produced in cantilever by using electrical oscillator [10]. When the cantilever was away from sample free oscillations occurs due to non interaction zone.

When it approaches the sample surface, the tip is attracted toward sample material via Van der Waals interactions, hence it results in reduces amplitude of cantilever oscillation. The amplitude of the oscillations can be kept constant at a fixed cantilever-sample distance. The sample surface is scanned at constant amplitude using a feedback loop as shown in figure 2.7.

2.5 Ferroelectric liquid crystal molecules

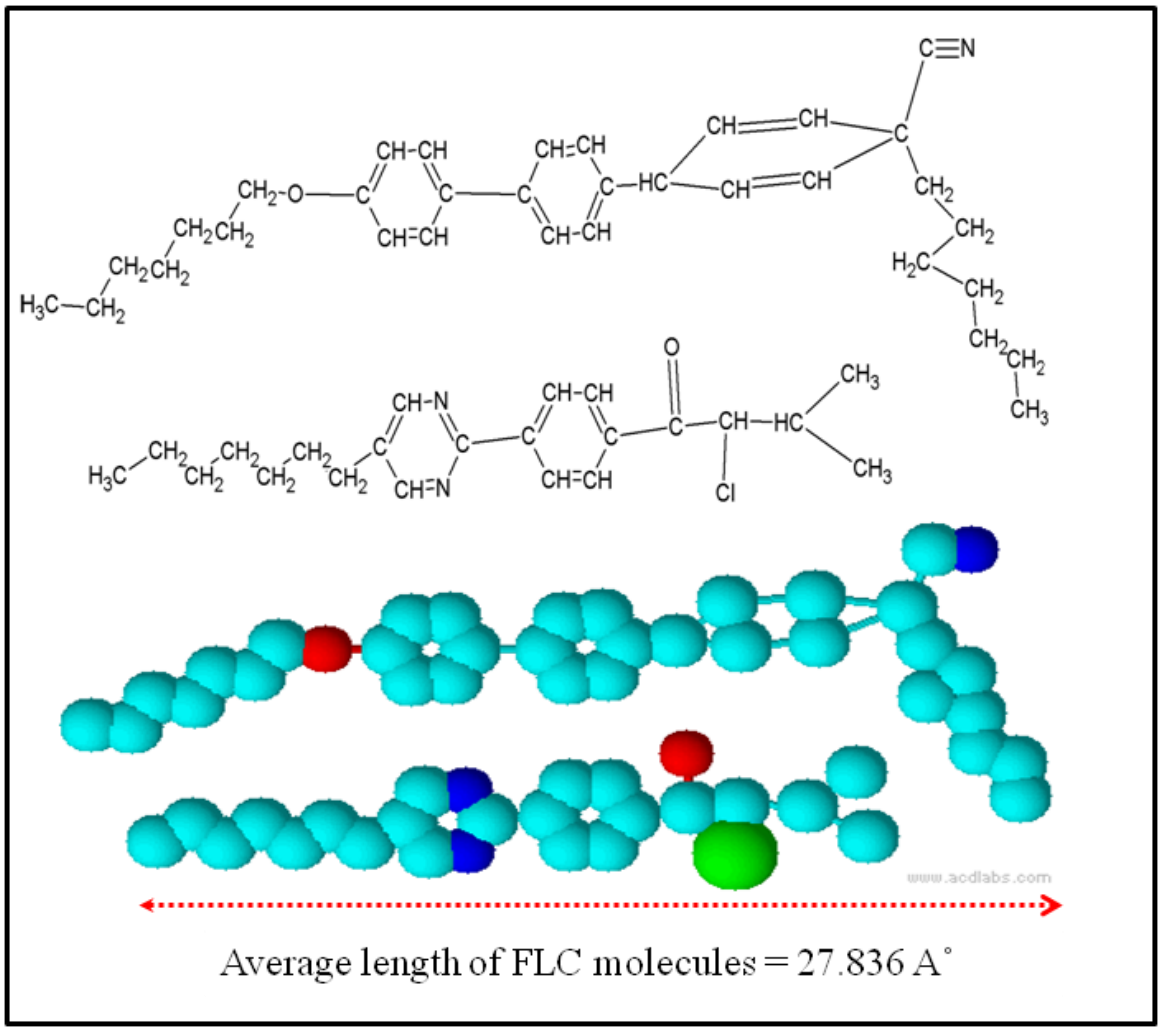

Figure 2.9: Molecular structure of the ferroelectric liquid crystal mixture showing hydrophilic and hydrophobic groups, and its 3D molecular structure [15].

A room temperature FLC [ZLI-3654 (E. Merck Darmstadt)] is taken as a basic material. Its chemical and three dimensional molecular structures are given in figure 2.9. The average molecule length ≈ 27.836 A° as determined by Chem Sketch-Advanced Chemistry Development (ACD) software. It has biphenyl rings as a back bone where as

alkyl chains at the ends are hydrophobic in nature. Hydrophillicity is provided by chiral carbon -*CH with chlorine attached to it, the carbonyl groups (- OOC), cyanide (-CN), and secondary amine's nitrogen present at meta-carbon in benzene ring [11]. The phase sequence of this compound is

$$\text{Cr} \xrightarrow{-32^{\circ}\text{C}} \text{SmC*} \xrightarrow{62^{\circ}\text{C}} \text{SmA*} \xrightarrow{76^{\circ}\text{C}} \text{N*} \xrightarrow{86^{\circ}\text{C}} \text{I.}$$

Where Cr, SmC*, SmA*, N*, I represents crystalline, Smectic C*, Smectic A*, Nematic and Isotropic phase of liquid crystals respectively [12-14]. These transition temperatures were determined by differential scanning calorimeter (DSC model LINSEIS L-63) with heating @ 5 degree minute^{-1} and verified by thermal polarzing microscopy set up (Linkam TP 94 and THMS 600) with in ±0.1°C temperature precision fitted on the polarizing microscopy (Olympus BX-51P) stage. Since the molecule exhibit chiral smectic phase at room temperature, it is a favourable condition to study and understand the mechanism of thin film deposition by Langmuir-Blodgett method [15].

2.6 Functionlaized Single Wall Carbon Nanotubes and nano-particles

We have used Octadecylamine (ODA) functionalized single-walled carbon nano tube having diameter d ≈ 2-10 nm and length L ≈ 0.5-2 μm, bundle dimensions [Sigma Aldrich] for preparing LB films. Figure 2.10 shows its molecular structure and 3D model. These pre-functionalized SWCNTs were used to prepare composites with FLC. ODA functionalized SWCNTs have amine group, which provide hydrophilic character whereas hydrophobic character is provided by long alkyl chain of ODA and walls of carbon nano tubes. Composites of FLC-SWCNTs were made by weight mixing (1, 5) wt % of single wall carbon nanotubes – FLC in chloroform solution via ultrasonication for 45 minutes [16].

We have also formed composite of FLC with AZO [AZO= ZnO + 6% Aℓ, size <50 nm (Sigma Aldrich)] nanoparticles after functionalizing them with octadecylamine (figure 2.11). 0.54 gm of octadecylamine was dissolved into 180 ml of chloroform and then 1gm of 6% Aℓ doped ZnO was also added to solution. The mixture was sonicated for at least 2 hours. The particles were precipitated from chloroform by adding 400ml anhydrous ethanol with deionised water till the clear solution is obtained. The powder was dried and AZO nano particles were doped in FLC matrix. Octadecylamine (ODA) functionalized AZO nano particles having amine group and oxygen of metal oxide, which provide

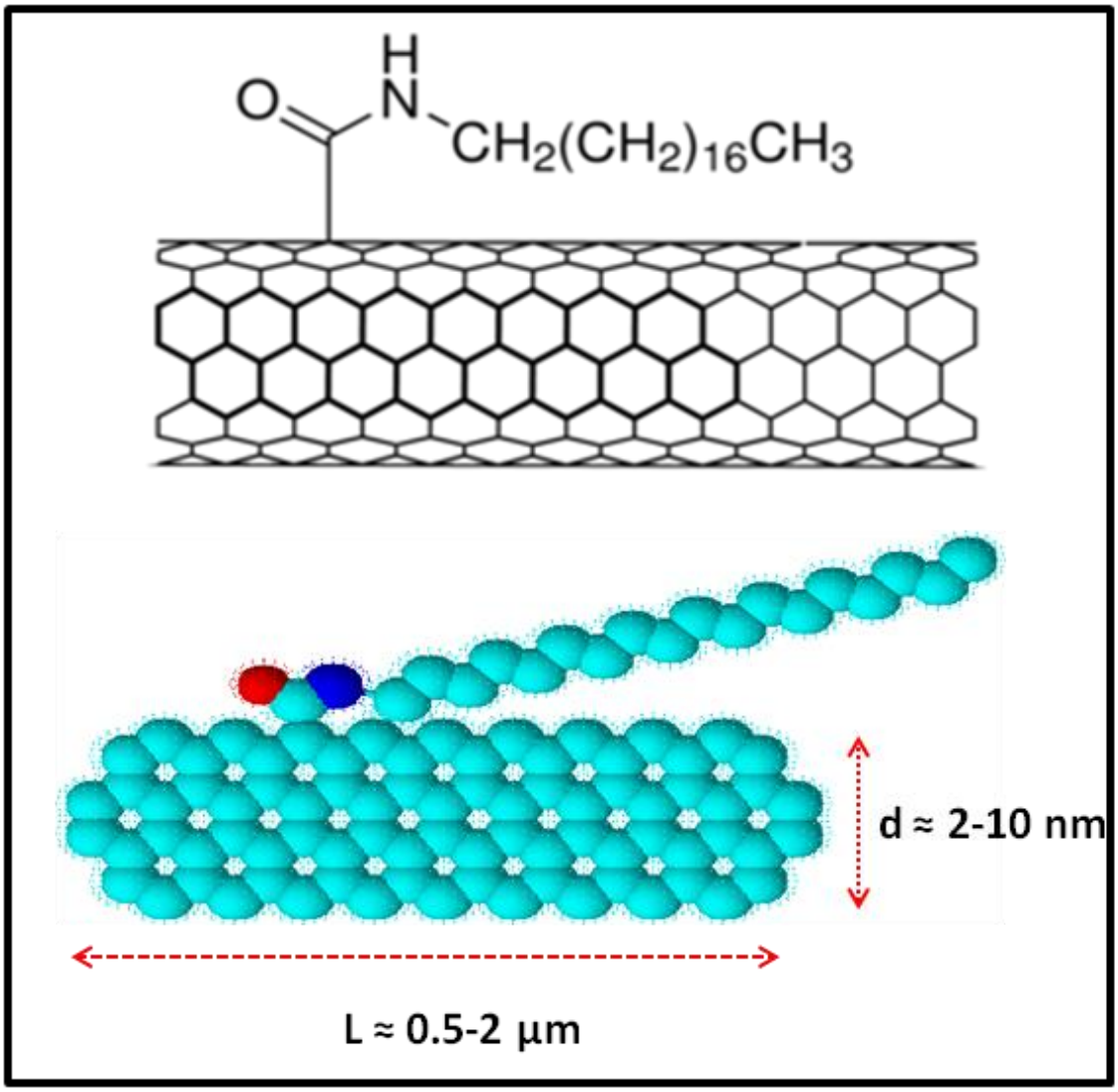

Figure 2.10: Molecular Structure and 3-D model of Octadecylamine functionalized Single Wall Carbon Nanotubes.

hydrophilic character whereas hydrophobic character is provided by long octadecyl chain.(1, 5) wt % of functionalized AZO – FLC composite material were prepared in chloroform (1 mg ml^{-1}) after 30 minutes of sonication. The proper dispersion of nano-particles in FLC matrix was ensured by uniform solution obtained after sonication [17].

Another nano-particles used are dodecanethiol functionalized silver nano-particles (5-15 nm) 0.25 % (w/v) in hexane [Sigma Aldrich]. Its molecular structure and 3D molecular model are given in figure 2.12. Dodecanethiol (DDT) functionalized Ag nano particles have thiol group which provide hydrophilic character whereas hydrophobic character is provided by long dodecyl chain.

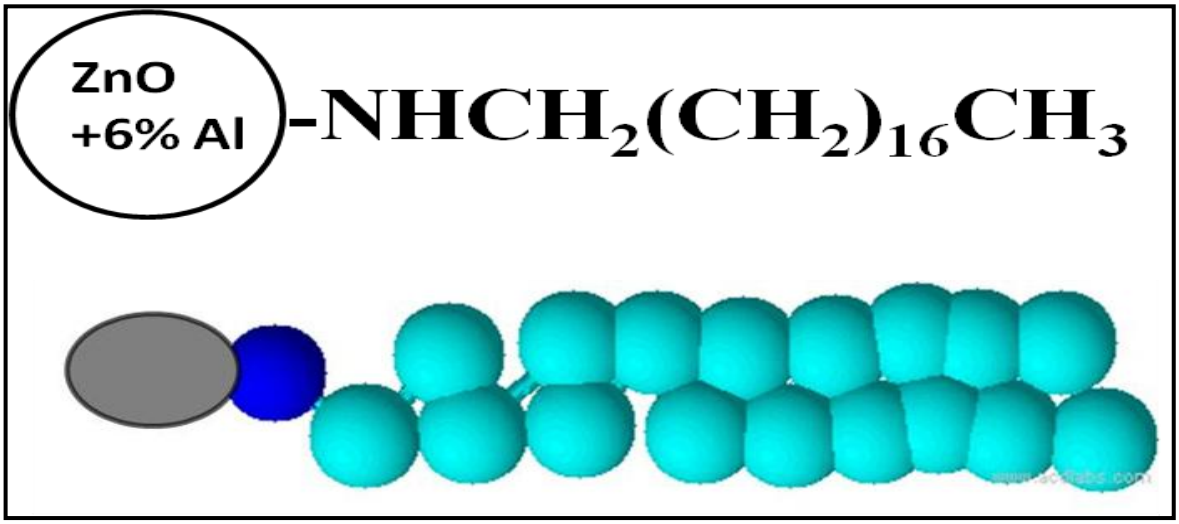

Figure 2.11: Molecular Structure and 3-D model of ODA functionalized AZO [AZO = ZnO + 6% Aℓ] nano particles [17].

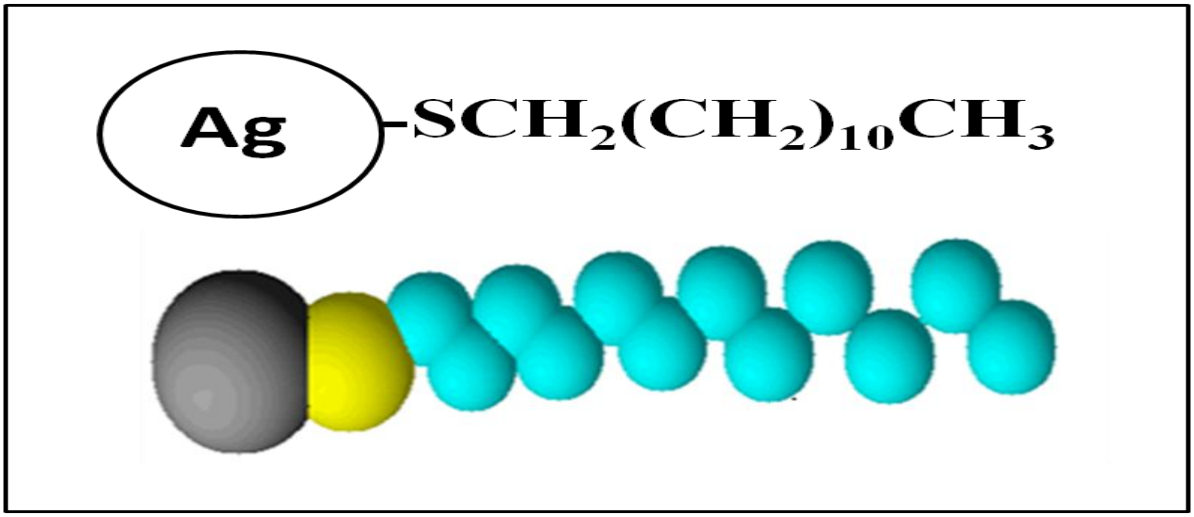

Figure 2.12: Molecular Structure and 3-D model of dodecanethiol functionalized silver nano-particles**.**

2.7 Bent core Liquid Crystalline molecules

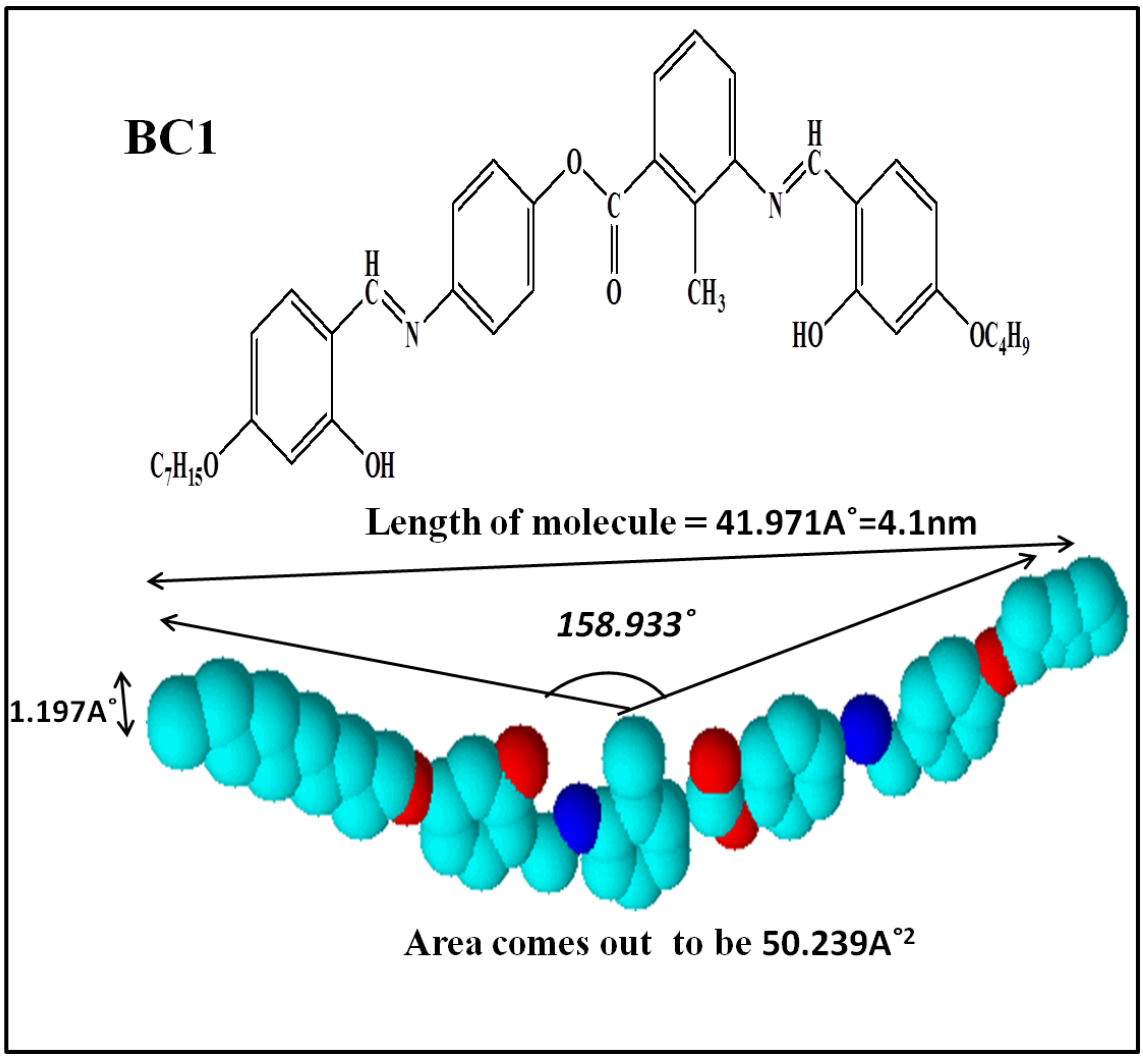

Figure 2.13: Molecular structure and 3-D view of bent-core liquid crystal molecules **BC1** [21].

Langmuir-Blodgett films were prepared of two bent core liquid crystal molecules having molecular structure {[*4-(N-4'*-n-heptyloxy-*2*-hydroxy-benzylidene)-amino)phenyl]-[*3-(N-4'-n*-butyloxy-*2*-hydroxybenzylidene)-amino) benzoate]}(**BC1**) and{[*4-(N-4'-n*-tetradecyloxy-*2-h*ydroxy-benzylidene*)*-amino)phenyl]-[*3*-(*N-4'-n*-undec-yloxy-*2-h*ydroxy benzylidene)-amino) benzoate]}(**BC2**) as shown in figure 2.13 and figure 2.14 respectively [18, 19]. The molecules have four-phenyl rings as a core where as alkyl chains at the ends are hydrophobic in nature. The hydrophillicity is provided by carbonyl

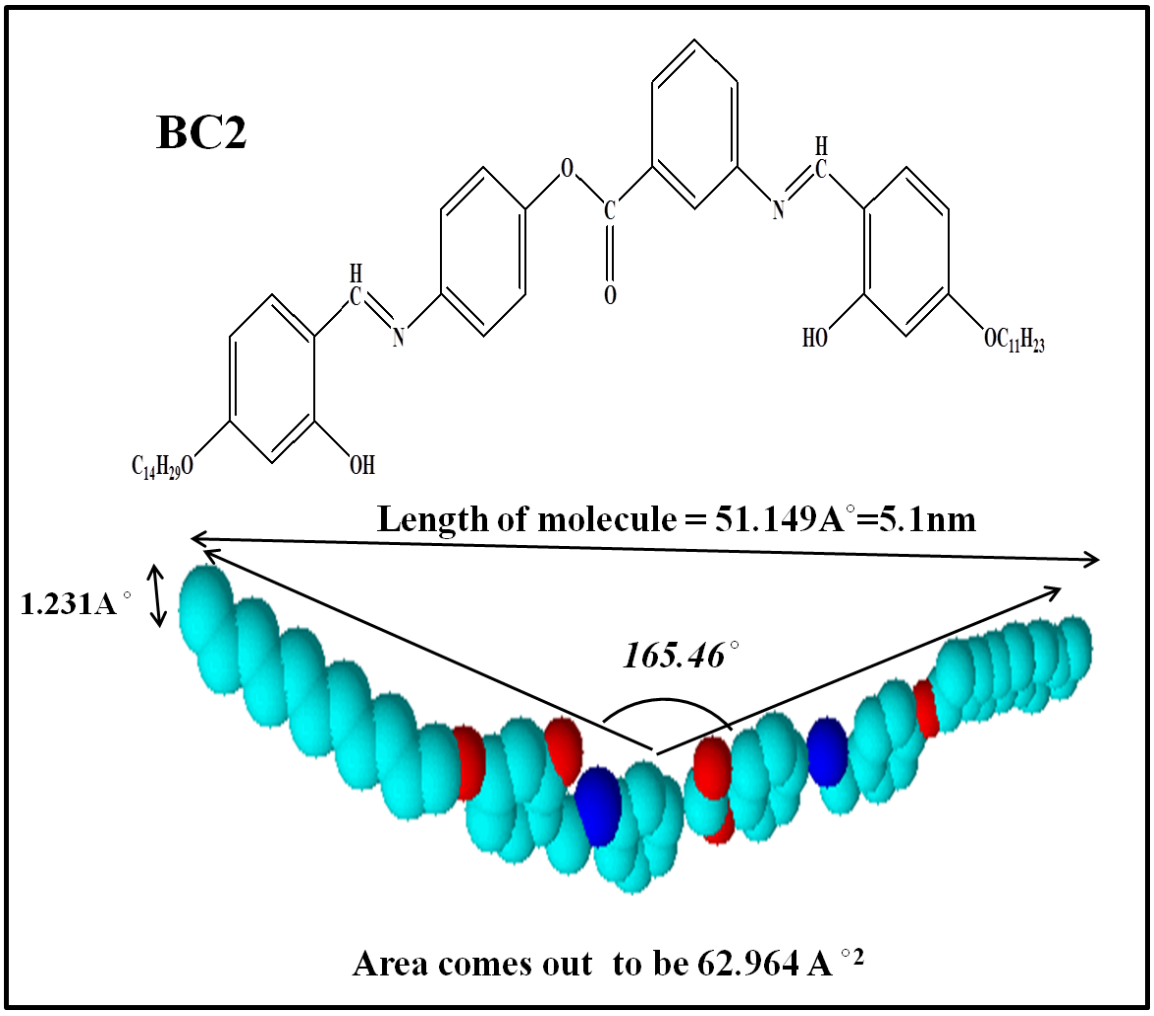

Figure 2.14: Molecular structure and 3-D view of bent-core liquid crystal molecule **BC2** [21].

groups (- OOC), alcohol (-OH), and secondary amine's nitrogen present at core of the molecule. The molecular lengths are about 4.1 nm and 5.1 nm respectively as determined by software. Different lengths of alkyl chains attached at ends result in different bent core angles, **BC1** (158.933˚) < **BC2** (165.46˚). [ACD/Chem. Sketch software (Advanced Chemistry Development, Inc, version 11.01)] was used to estimate the value of area per molecule assuming a flat film formation. **BC1** and **BC2** have molecular areas 50.239A$^{\circ 2}$ and 62.964 A$^{\circ 2}$ respectively [20].

BC1

$$K \xrightarrow{87.2^{\circ}C} M2 \rightarrow M1 \rightarrow N \xrightarrow{174.8^{\circ}C} I$$

BC2

$$Cr \xrightarrow{96.3^{\circ}C} Cr \xrightarrow{105.0^{\circ}C} B7 \xrightarrow{113.5^{\circ}C} I$$

The phase sequences as detected by POM and the transition temperatures are confirmed by differential scanning calorimetry (DSC) of the compounds are given above. **BC1** and **BC2** both show crystalline phase at room temperature. **BC1** has nematic to isotropic transition at 174.8 °C, and M2, M1 are two undefined phases. **BC2** have B7 to isotropic transition at 113.5 °C [21].

2.8 Methodology

To prepare LB films, solution of LC materials are prepared in chloroform by ultra sonicating it. Sub phase is prepared at required pH and temperature. A clear solution obtained by sonication is spread on subphase by using micro syringe. Generally quantities in microliters (µl) are drop wise placed on subphase in a uniform manner. A proper time is provided for evaporation of solvent. Dipper motor is allowed to take substrate through air-water interface. Then barriers are compressed uniformly at very slow rate. Isotherm is recorded with decrease in trough surface area.

Films are deposited on solid substrates by continuous strokes; choice of substrate is dependent upon type of characterization. For XRD amorphous glass is taken to avoid substrate peak and AFM images are taken on smooth Si substrates to avoid surface topography. A concise view of methodology is presented in form of flow chart in figure 2.15.

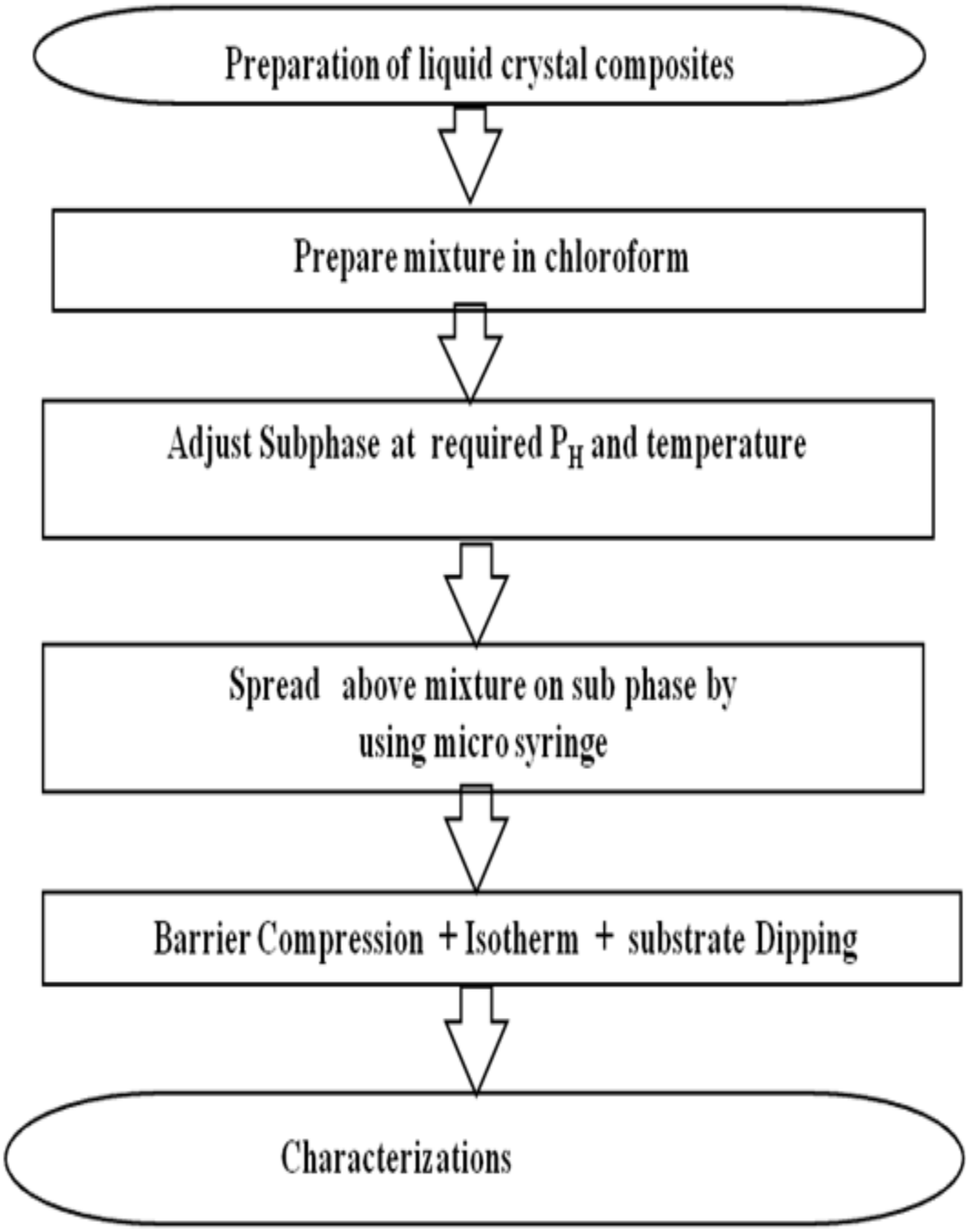

Figure 2.15: Flow Chart showing Langmuir Blodgett films preparation and characterization

References:

1 A W Adamson. Physical chemistry of surfaces. 5th ed.New York (NY): John Wiley, 1990.

2 C J L Constantino, Dhanabalan A, O N Oliveira. Experimental artifacts in the surface pressure measurement for lignin monolayers in Langmuir troughs. Review of Scientific Instruments. 1999, **70**, 3674.

3 J K Basu, M K Sanyal. Ordering and growth of Langmuir–Blodgett films: X -ray scattering studies. Phys. Rep. 2002, **363**, 1.

4 N Osvaldo, Jr Oliveira. Langmuir-Blodgett Films - Properties and Possible Applications. Brazjljan J. of Physks. 1992, **22**, 61.

5 L Scheres, A Arafat, H Zuilhof. Self-assembly of high-quality covalently bound organic monolayers onto silicon. Langmuir. 2007, **23**, 8343.

6 R Sharma, D P Bisen, U Shuklaand, B G Sharma. X-ray diffraction: a powerful method of characterizing nano-materials. Recent Res. Sci. Tech. 2012, **48(8)**, 77.

7 H F Poulsen. An introduction to three-dimensional X-ray diffraction microscopy. J. Appl. Cryst. 2012, **45**, 1084.

8 Y Martin, C C Williams, H K Wickramasinghe. Atomic force microscope–force mapping and profiling on a sub 100Å scale. J.Appl.Phys.1987, **61**, 4723.

9 G Binnig, C F Quate. Atomic Force Microscope Phy. Rev. Let. 1986, **56(9)**, 930.

10 V J Morris, A R Kirby, A P Gunning. Atomic Force Microscopy for Biologists, Imperial College Press: London, 1999.

11 A Fukuda, Y Takanishi, T Isozaki, K Ishikawa, H Takezoe. Antiferroelectric chiral smectic liquid-crystals. J. Mater. Chem. 1994, **4(7)**, 997.

12 V S Chandel, S Manohar, S P Singh, A K Singh, R Manohar. Dielectric and optical study of the ferroelectric liquid crystal mixture ZLI-3654. Akademeia. 2013, **3(1) ea0119**, 1.

13 P Malik, A Chaudhary, K K Raina. Dielectric Studies of Carbon Nanotube Doped Ferroelectric Liquid Crystal Films. Asian J.Chem. 2009, **21(10)**, S095.

14 P Malik, J K Ahuja, K K Raina. Effect of polymer viscosity on morphological and electro-optic properties of aligned polymer dispersed ferroelectric liquid crystal composite films. Curr. Appl. Phys. 2003, **3**, 325.

15 R Kaur, G K Bhullar, K K Raina. Behaviour of an ultrathin ferroelectric liquid crystal Langmuir–Blodgett film at an air–water and air–solid interface.Liq Cryst. 2012, **39**, 1375.

16 R Kaur, K K Raina. Influence of single-wall carbon nanotubes on Langmuir–Blodgett films of ferroelectric liquid crystals as studied by atomic force microscopy. Liq Cryst. 2014, **41**, 1065.

17 R Kaur, K K Raina. Effects of nano-particle doping on the Phase transitional behaviour of ferroelectric liquid crystal Langmuir -Blodgett composite films. Phase Transition. 2015, doi:10.1080/01411594.2015.1044900.

18 R Deb, R K Nath, M K Paul, N V S Rao, F Tuluri, Y Shen, R Shao, D Chen, C Zhu, I I Smalyukh, N A Clark.Four-ring achiral unsymmetrical bent core molecules forming strongly fluorescent smectic liquid crystalswith spontaneous polar and chiral ordered B7 and B1 phases. J Mater Chem. 2010, **20**, 7332.

19 M Kr Paul, R Kumar, N Chakraborty, K K Raina, N V S Rao. Electro-optic and molecular relaxation behaviour of fluoro substituted achiral unsymmetrical four-ring bent-core mesogen. Liq Cryst. 2014, **41**, 635.

20 R S Brown, U J Krull. Automation of simple instrumentation for Langmuir-Blodgett

technology. Analyst.1987, **112**, 1165.

21 R Kaur, G K Bhullar, N V S Rao, K K Raina. Effect of pH on the control of molecular orientation in monolayer of bent-core liquid crystal materials by Langmuir–Blodgett method. Liq Cryst. 2014, **42(1)**, 8.

CHAPTER 3

Langmuir-Blodgett ultrathin thin films of Ferroelectric liquid crystal and its composites with Single Wall Carbon Nanotubes

Overview

Monolayer of the ferroelectric liquid crystal formed at the air-water interface has been deposited onto solid substrates by Langmuir Blodgett technique. On compressing molecules at the sub-phase, a stable monolayer is formed at room temperature. Isotherms were recorded in constant compression mode. Monolayer and Multi-layers were successfully transferred to quartz substrate by using Y-Type deposition.

Langmuir-Blodgett films of ferroelectric liquid crystal-Single Wall Carbon Nanotubes (SWCNTs) composites have been also prepared and characterized. Pressure - area isotherms show that the films are stable and have good spreading properties. The interaction between nanotubes in the monolayer was increased during barrier compression, resulting in increased surface pressure. We observed phase change with increasing nanotubes concentration in ferroelectric liquid crystal matrix. Fourier Transform Infrared (FTIR) spectra of deposited LB films confirm complete transfer of molecules and X-Ray Diffraction (XRD) spectroscopy shows smectic layer ordering in composite films. Atomic force microscopy images indicate uniform deposition of material on single crystal silicon wafer.

3.1 Introduction

Ferroelectric Liquid crystals (FLCs) are an important class of smart electro-optic materials in soft condensed matter physics. In the last decades, significant research work has been carried out on several important FLC (having polarizing groups) materials to understand their material physics for display devices [1-4]. Typically they have anisotropy in shape and flat segments of benzene ring which form rigid backbone for long axis of the molecule. Strong dipoles and easily polarisable groups are present in structure of many liquid crystals which makes them amphiphilic in nature.

Several research groups investigated physical aspects of liquid crystal thin films deposited by Langmuir Blodgett technique [5-8], but not much effort has gone to understand the interfacial properties of ferroelectric liquid crystal. The existence of polar order in ferroelectric liquid crystals is scientifically fascinating and technologically important. Thermotropic liquid crystal molecules cannot be directly treated as amphiphilic, but many of them are able to create stable compressible monolayer at the liquid surface, which can be easily transferred to solid substrates [9-14].

Some of the recent research reports suggest novelty in carbon nano tubes CNTs–LC (carbon nano tubes - liquid crystal) combination, the LC behaviour in electro optic devices such as displays possibly being improved by the presence of small amounts of CNTs and nano material can easily modify their properties which influence their physical properties and device behaviour [15–23]. Carbon nano tubes (both Single Walled and Multi Walled) when doped in FLCs give rise to many interesting properties however, practical applications have been hindered by the poor dispersibility and solubility. Due to an organic nature of long alkyl chains functionalized nanotubes; they are dispersible in organic solvents where as covalent attachments of functional groups influences on tube-tube stacking.

The effective interactions between carbon nanotubes (CNTs) and the polar LC molecules result in the formation of soft material composites [24]. This results in the formation of permanent dipoles near the surface of functionalized SWCNTs. Several research groups have studied the role of CNT in nematics LC systems. The results reveal enhanced dielectric constant [25], fast switching time and lower switching threshold voltage [26] homogeneous dispersion [27, 29], suppressed back flow effect [21], faster electro-optic effects [15], etc. These effects are more pronounced at lower CNTs concentrations [28–31]. Some recent reports show that rotational viscosity of FLC

decreases the doping of SWCNTs while anchoring energy increases due to electron stacking between host FLC and functionalized nano tubes. Inclusion of MWCNTs in FLC significantly affects the dielectric, electrical and electro-optical properties [32- 38]. Thus, carbon nano tubes (both single walled and multi walled) when doped in FLCs give rise to many improved properties however, practical applications have been hindered by the poor dispersibility and solubility. Due to an organic nature of long alkyl chains functionalized nanotubes; they are dispersible in organic solvents where as covalent attachments of functional groups influences on tube-tube stacking.

Dispersion of SWCNTs in FLC is significant because it possess large surface area and π-π surface electron that results in the strong electrostatic interactions between SWCNTs and the surrounding host medium [39-50].

In this chapter, we have made an attempt to study the organization and orientation of FLC molecules and FLC-SWCNTs composite systems at room temperature by Langmuir Blodgett technique. Surface Pressure- Area (Π-A) isotherms, Multiple isotherms during compression and expansions cycles of barriers, Low angle X-Ray diffraction profile, Fourier Transfer Infrared spectroscopy (FTIR) and Atomic Force microscopy (AFM) image analysis have been carried out to study LB films.

3.2 FLC Monolayer at air-water interface:

3.2.1 Π-A Isotherm

1 mg ml^{-1} solution of FLC mixture (figure **2.9**) was dissolved in chloroform by sonicating the mixture for half an hour. 50µl of this solution was then taken out in Hamilton micro syringe and spread over Millipore Q filtered water (pH=6.00) contained in the LB trough. After 20 minutes of the solvent evaporation, the monolayer was compressed @ 10mm min^{-1} using derlin (polyactelylene) barriers.

Figure 3.1 shows a typical profile of surface pressure (Π) as a function of mean molecular area (Mma) of the FLC monolayer. The compression isotherm was taken by compressing barriers at constant speed (@ 5mm min^{-1}) on water sub-phase. Initially with open barriers, molecules were randomly oriented having negligible interactions between them. While closing the barriers at a constant speed, compression resulted in various molecular interactions at the air-water interface. Further compression of monolayer, results in the orientation and ordering of liquid crystal. Molecules were initially in gaseous phase at negligible surface pressure but on compression the isotherm

showed lift-off area per molecule (A_i ~13.6 $A^{\circ 2}$). We observed a gradual rise in the surface pressure up to 3mNm^{-1}. Before attaining this pressure, the monolayer was in liquid expanded phase and condensed phase was formed at A_0 ~ 7 $A^{\circ 2}$ when the FLC molecules got aligned as stable monolayer on air-water interface. A further increase in compression results in the collapse of monolayer and multilayer would be formed on the sub-phase.

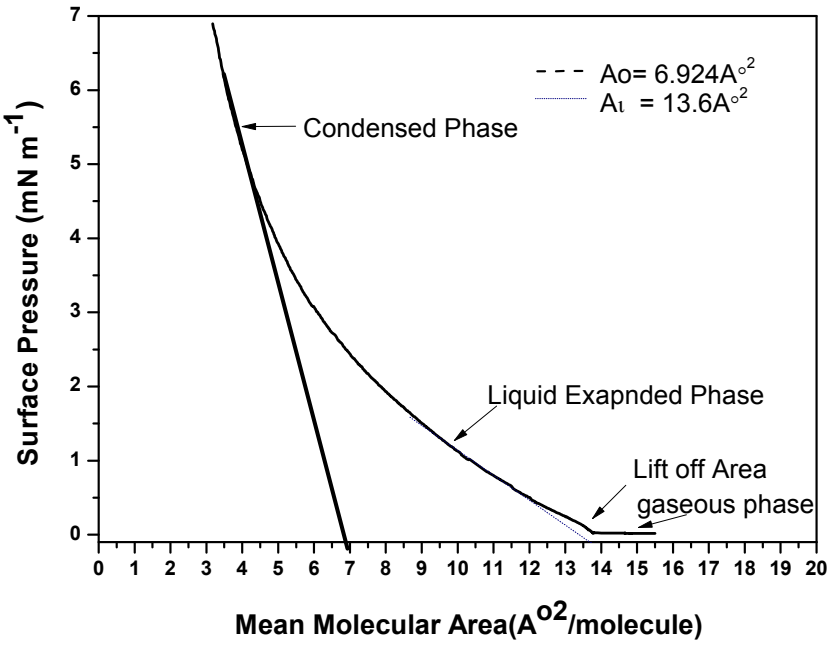

Figure 3.1: Compression isotherm of FLC shows the phase change as the mean molecular area keeps on decreasing.

3.2.2 Hysteresis in Isotherm cycles

We performed three compression-expansion cycles to stabilise the film at air-water interface as shown in figure 3.2. We noticed hysteresis behaviour during compression and expansion cycles of isotherm. This arises due to mixed amphiphilic nature of FLC molecules and can be related to the chain entanglement and molecular reorganizations [51, 52].

Figure 3.3 shows a typical profile of surface pressure as a function of time taken for cycles in the range of 0-6 mN m^{-1}. We noted three apex points at 6 mN m^{-1} which corresponds to the maximum surface pressure attained during each cycle. It shows that the monolayer at the sub phase has taken equal time for each compression and expansion

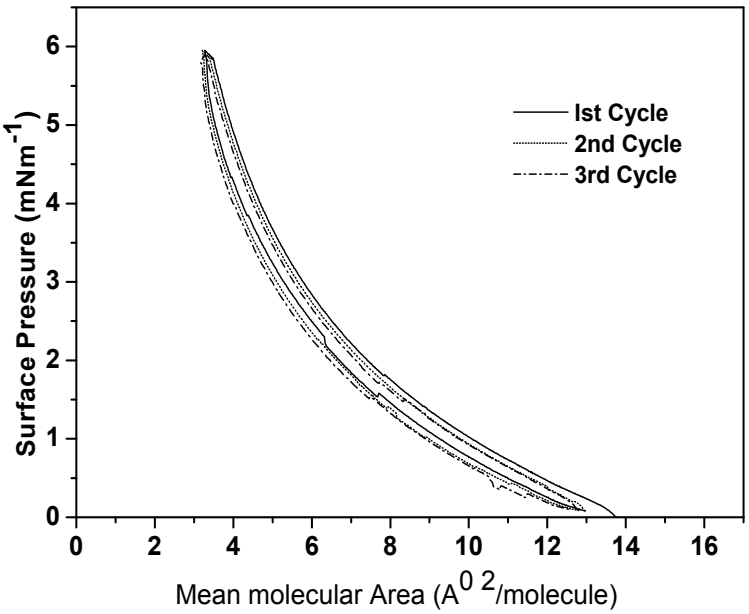

Figure 3.2: Surface pressure as a function of mean molecular area (Π –A) compression–expansion cycles showing negligible hysteresis.

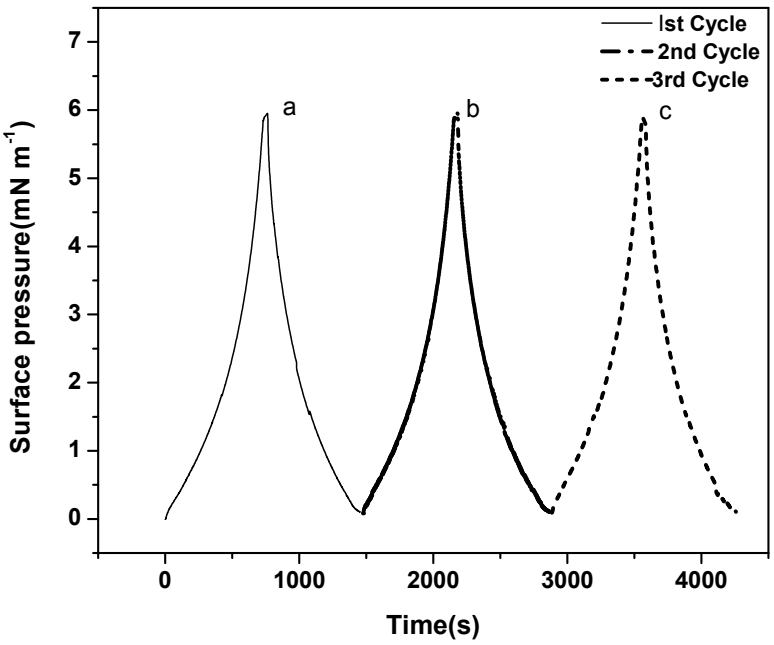

Figure 3.3: Variation in surface pressure of the FLC monolayer as a function of time during compression–expansion of barriers. Cycles have been repeated between 0–6 mN m^{-1}.

cycle and hints that monolayer was stable as molecules retain their orientation and positional order during these cycles.

The variation of surface pressure as a function of time during compression and deposition of monolayer is shown in figure 3.4. We found that the surface shows a steep increase due to the formation of monolayer initially, whereas on reaching the equilibrium position it saturates. Films were transferred to the substrate at constant surface pressure (@ 5mN m^{-1}). During the deposition process, number of molecules got decreased as they are attached to quartz substrate and barriers automatically move to adjust this surface pressure [11].

3.3 Octadecylamine functionalized SWCNTs and FLC-SWCNTs composites at air-water interface:

3.3.1 Π-A Isotherm of ODA functionalized SWCNTs

1 mg ml^{-1} solution of functionalized SWCNTs was prepared in chloroform by sonicating the mixture for half an hour. 100µl of this solution was spread on subphase. After 20 minutes of the solvent evaporation, the monolayer was compressed @ 10mm min^{-1} for recording isotherm.

Figure 3.5 shows a typical surface pressure profile of functionalized SWCNTs during first compression of barriers at air-water interface. We noticed that the surface pressure increases with increasing compression. At 240 cm^2 **(a)**, monolayer of SWCNTs is equivalent to two dimensional gas where inter tube interaction is very weak. We attained surface pressure ~ 0.96 mN m^{-1}. Further compression results in plateau region up to **(b)**, indicating liquid expanded phase of Single Wall Carbon Nanotubes. Surface pressure increases rapidly when barriers are constantly compressed at (~140 cm^2). At this stage, the nanotubes are in contact with each other and their mutual interaction in this limited area has increased the surface pressure. A condensed phase **(c)** was observed at 9 mN m^{-1} where SWCNTs might have arranged themselves to form a stable monolayer at air-water interface [53]. Figures 3.5 also shows two continuous expansion and compression cycles of barriers having SWCNTs monolayer at interface. It is clearly seen that expansion cycles do not retrace the compression cycles as it gets shifted towards lower trough areas. This hysteresis behaviour is evident and indicates that some aggregation might have occurred amongst nano tubes of monolayer which was not immediately reversed when the trough area was increased.

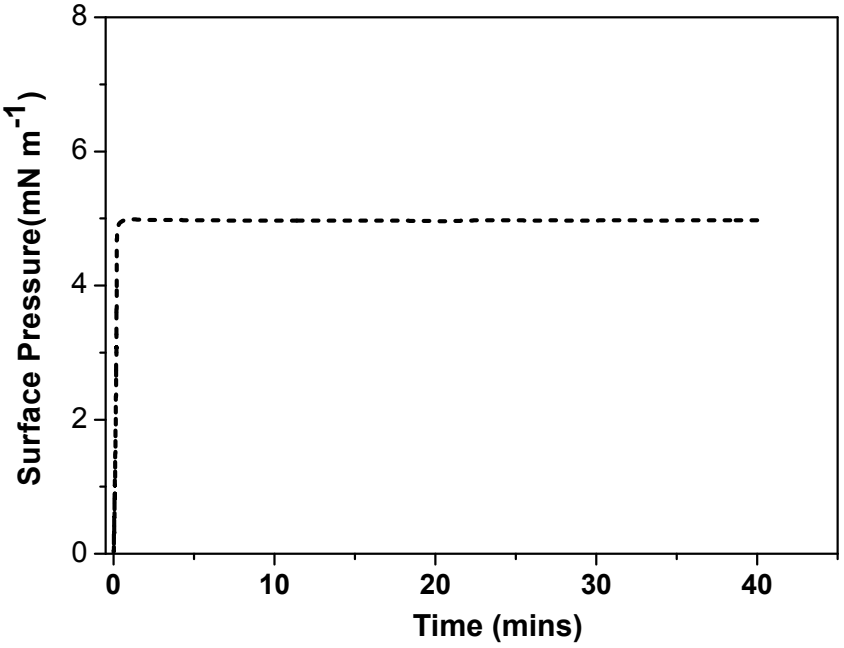

Figure 3.4: Equilibrium surface pressure (ESP) as a function of time. FLC monolayer at air–water interface stabilises at 5mNm^{-1}.

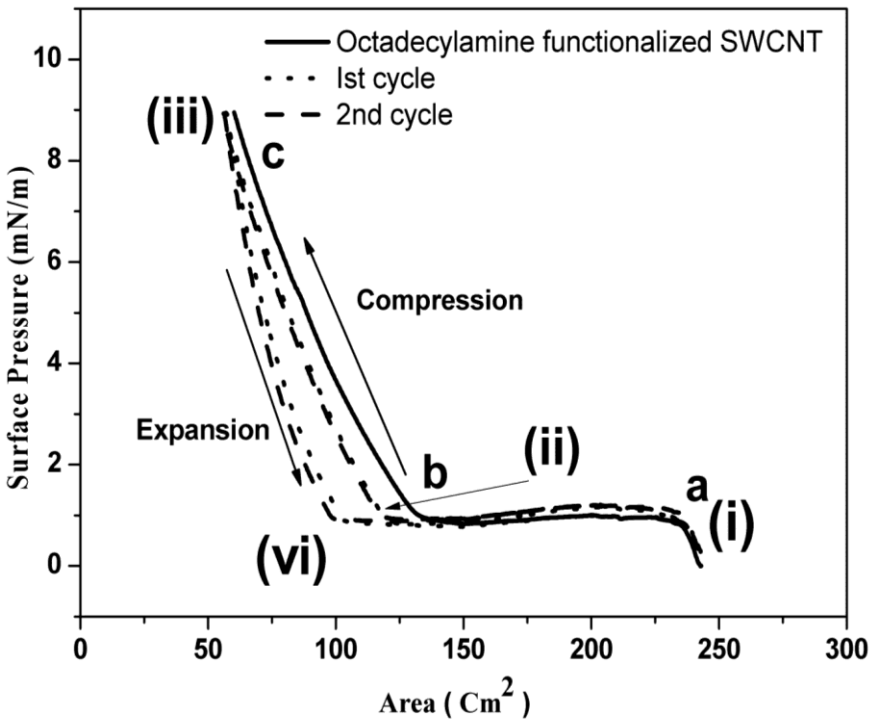

Figure 3.5: Compression isotherm of functionalized SWCNTs shows phase change, as area keeps on decreasing from 245 to 46 cm^2 and hysteresis is observed during two cycles (compression–expansion) of barriers having SWCNTs at air–water interface.

During the first down stroke, no material was transferred onto the Si substrate because it entered the sub phase, with open barriers. But after the compression process, nanotubes got transferred to the solid substrate during the upstroke, with typical transfer ratio of 1.02. 11 multilayers were deposited by Y-type method.

3.3.2 Isotherms of FLC - functionalized SWCNTs composites

(1, 5) wt % of FLC- SWCNTs composite materials were prepared in chloroform (1 mg ml^{-1}) after 30 minutes of sonication. The proper dispersion of nanotubes in FLC matrix was ensured by uniform solution obtained after sonication. 100 µl mixtures of both composites were spread on water sub phase separately. Isotherms were obtained by constant compression (@10 mm min^{-1}) of barriers and monolayers were transferred to individual Si substrates.

The surface pressure-area isotherm of undoped FLC and FLC doped with SWCNTs composite materials are shown in figure 3.6. They indicate that the monolayers have good surface spreading properties. In undoped FLC isotherm, increase in compression resulted in orientation and ordering of liquid crystal molecules at air-water interface. Initially molecules were in gaseous phase but then alignment of monolayer increased surface pressure up to 14 mN m^{-1}. Surface pressure variation of 1 wt% FLC composite

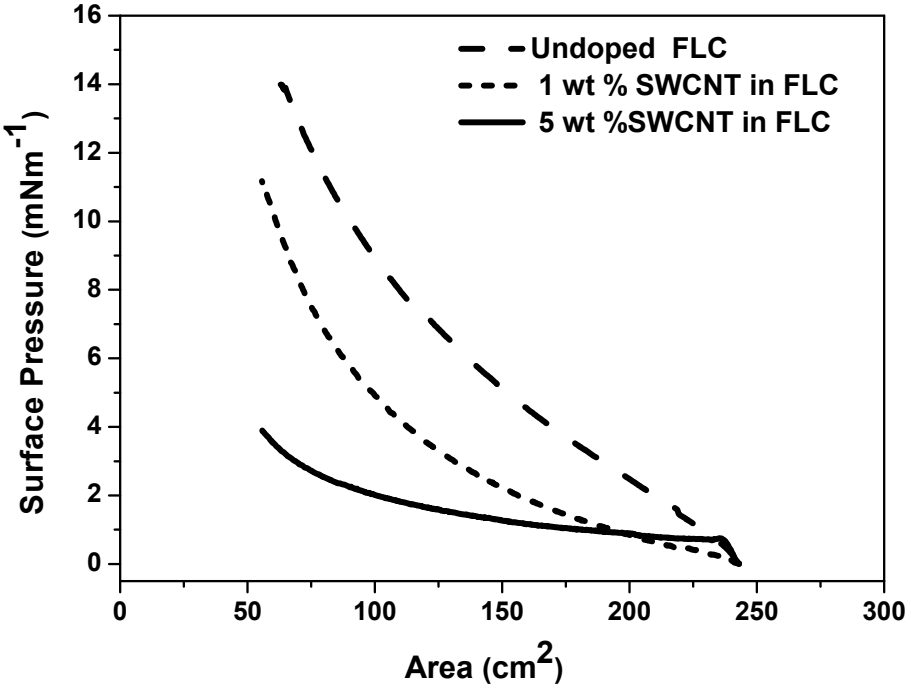

Figure 3.6: Isotherms of undoped FLC and composite systems (1, 5) wt% functionalized SWCNTs in FLC in matrix.

indicates that molecules are getting aligned with reduction in the surface area. In this case surface pressure of well aligned monolayer rise up to 9 mN m^{-1} which is lower than surface pressure attained by pure FLC, hinting at the influence of 1 wt% CNT present at the interface.

Isotherm for 5wt% functionalized SWCNTs in FLC reveals smooth transitions from the gas to the liquid phase and from the liquid phase to the condensed phase at 1mN m^{-1} and 3 mN m^{-1} respectively. This system attains maximum pressure ~ 4 mN m^{-1}, which is lower than surface pressure of 1wt % composite system.

At this composition SWCNTs and FLC are competing for better alignment as –NC═O group of functionalized nano tubes is getting affinity from –OH group of aqueous sub phase, simultaneously –F and –COO groups of FLC are aligning on surface. So a packed network is found up to a little extent. This results in lowering of surface pressure for 5wt% composite system, likely due to molecular stability with nanotubes.

Monolayers and 11 multilayers of composites were deposited on Si and glass substrates at 9 mN m^{-1} and 4 mN m^{-1} respectively. The premises about the molecular alignment of FLC-SWCNTs composite systems at air-water interface, is further confirmed by topographical investigations by using AFM on their films transferred to Si substrate.

3.4 Fourier transform infrared spectroscopy

(a) FLC films

FTIR spectras of the 11 and 22 multilayer thin films of FLC have been studied using (BX-II, Perkin Elmer) as shown in figure 3.7. Interpretations of molecules containing one halogens was straightforward, because with the polar nature of this chlorine group, we expected the spectral contribution to be distinctive (C-Cl; 800–700 cm^{-1}). Absorption at 866.4 cm^{-1} confirmed hydrocarbon chain bond with halide group CH_2-X where X= Cl. Absorption at 1175 cm^{-1} and 1169 cm^{-1} in 11 layers and 22 layers of FLC spectra respectively corresponded to C-O stretch, (C-O-C; 1200–1050 cm^{-1}) with alkyl substitution. Absorptions at 1255.88 cm^{-1} and 1264.24 cm^{-1} corresponded to Φ-O-C stretch (1270–1230 Cm^{-1}) Aromatic substitution (Φ) for 11 and 22 layers FLC respectively. Absorptions at 1316.51 cm^{-1} corresponded to aromatic secondary amine C-N stretch. Absorption at 2363.90 cm^{-1} corresponded to nitrogen compounds featuring triple or cumulated double bonds, such as cyanides (CN; 2285–1990 cm^{-1}). The band was assigned to the stretching vibration, which was the asymmetric stretch in the case of the

cumulated double-bonded compounds. All the functional groups present in FLC had been analysed in FTIR spectrum [54-56].

(b) FLC - functionalized SWCNTs composites films

Figure 3.8 shows FTIR spectra of the 11 multilayers of SWCNTs (a) and their composite systems (b). The interpretation of long chain is straight forward as we have observed a jagged absorptions at approximately 2908.74 cm^{-1} and 2842.10 cm^{-1}. These correspond to C-H stretching anti symmetric and symmetric vibrations for saturated aliphatic chain.

Another absorption is observed at 1381.76 cm^{-1}, corresponding to simple bending vibrations of C-H bonds. Presence of amide group is confirmed by absorption at 3439.96 cm^{-1}, it corresponds to N - H mode where as absorption present at 1046.49 cm^{-1} corresponds to C - N stretching.

Absorption present at 1589.99 cm^{-1} corresponds to carbonyl C = O (stretching) of amine group [54-56]. FTIR spectra confirm complete transfer of SWCNTs. Transfer of FLC multilayer has already been reported [57].

In figure 3.8 (b) the disappearances of amide group broadening (3439.96 cm^{-1}) from spectra clearly indicate that FLC and functionalized SWCNTs exhibit electrostatic interaction at the surface of nanotubes.

Absorptions at 2948.60 cm^{-1} and 2918.95 cm^{-1} are due to asymmetric and symmetric vibrations of C-H, which has remained the same as these are in FTIR spectra of functionalized SWCNTs film, just a slight shift is observed. Absorption at 1724.08 cm^{-1} confirms presence of carbonyl C=O group of FLC. Absorption at 1606.47 cm^{-1} is probably due to C=N bend of the aromatic ring.

Absorption at 1581.73 cm^{-1} confirms both aromatic C=C bonding of phenyl rings and unsaturated wall of nanotubes. Absorption at 1467.84 cm^{-1} is due to C-H bending vibrations of composites. Absorptions at 1244.87 $cm^{-1}$and 1173.47 cm^{-1} correspond to –O–C stretch (1270–1230 cm^{-1}) of aromatic substitution and C–O–C substitution (1200–1050 cm^{-1}) respectively.

The interpretation of molecules containing one halogen is straightforward, since due to the polar nature of the chlorine group its contribution to the spectrum was expected to be distinctive (C–Cl; 800–700 cm^{-1}). The absorption at 846.42 cm^{-1} confirms the presence of a hydrocarbon chain bonded with a halide group, CH2–X, where X = Cl. So, FLC-SWCNTs composite were deposited on substrates.

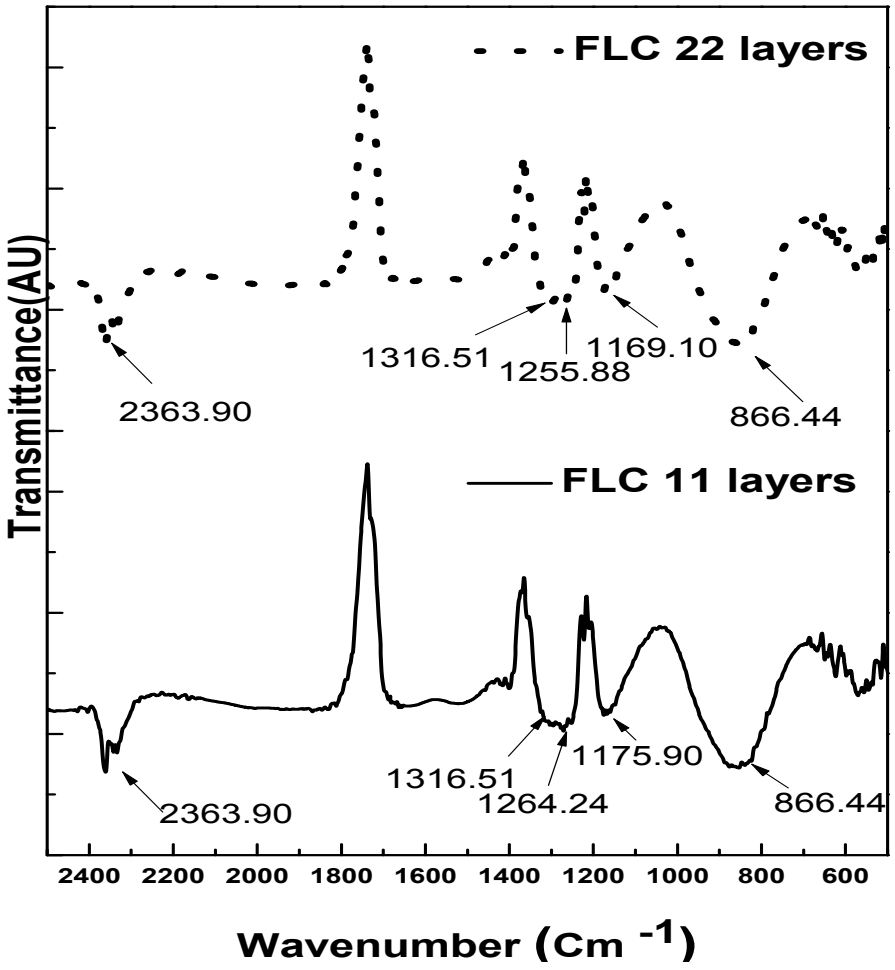

Figure 3.7: Fourier Transform Infrared spectroscopy profile of FLC multilayers.

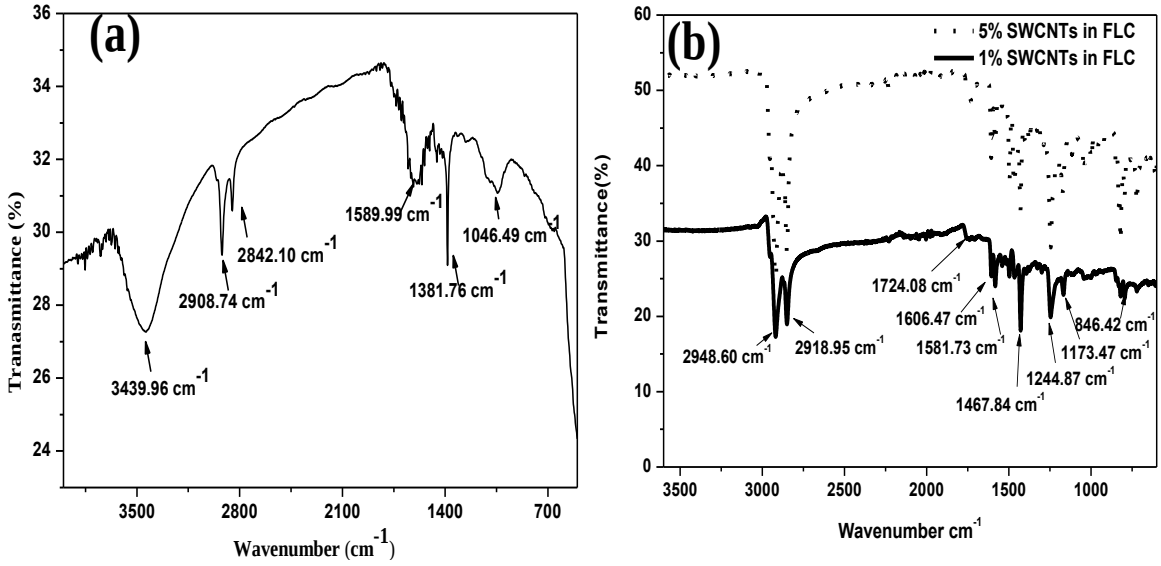

Figure 3.8 (a) FTIR spectroscopy profile of functionalized SWCNTs, (b) FTIR spectra of composite systems (1, 5) wt% functionalized SWCNTs in FLC.

3.5 X-ray diffraction spectras of FLC film and its composite with SWCNTs:

In order to ascertain the formation of smectic layer ordering in the layers to a set of 11 and 22 multilayers, LB films deposited on quartz substrate were exposed to Cu-k_α radiation source at low angle (2 θ = 1–10°) as shown in figure 3.9. The X-Ray diffraction

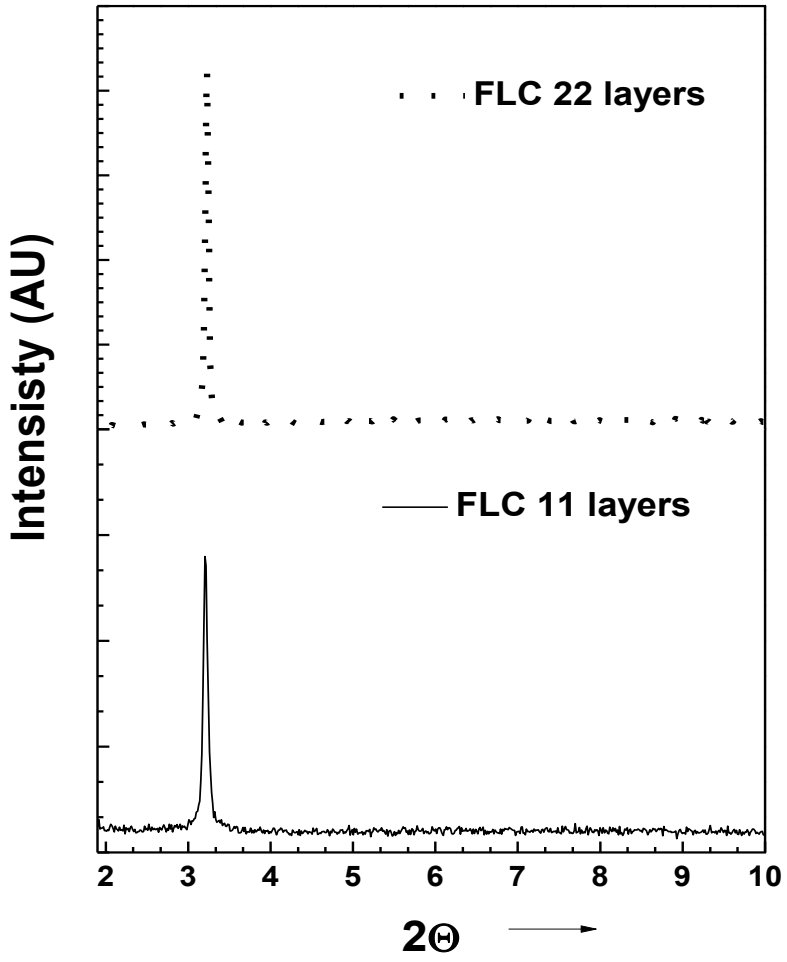

Figure 3.9: Low Angle XRD profile of FLC peaks for 11 and 22 multilayers.

profile shows an intense peak at 2Θ = 3.2° which correspond to the smectic layer ordering of liquid crystal molecules with a layer spacing of ~ 27.52 A^0 [58].

As number of layer increased from 11 to 22 layers, we noticed an increase in intensity and decrease in peak broadening at 2Θ = 3.2° [59]. Less broadened peak in XRD spectra of 22 layers indicates an increase in film thickness [60, 61]. Figure 3.10(a) and

figure 3.10(b) show low angle and wide angle X-Ray diffraction pattern of 11 multilayers of composite LB films deposited on glass substrate.

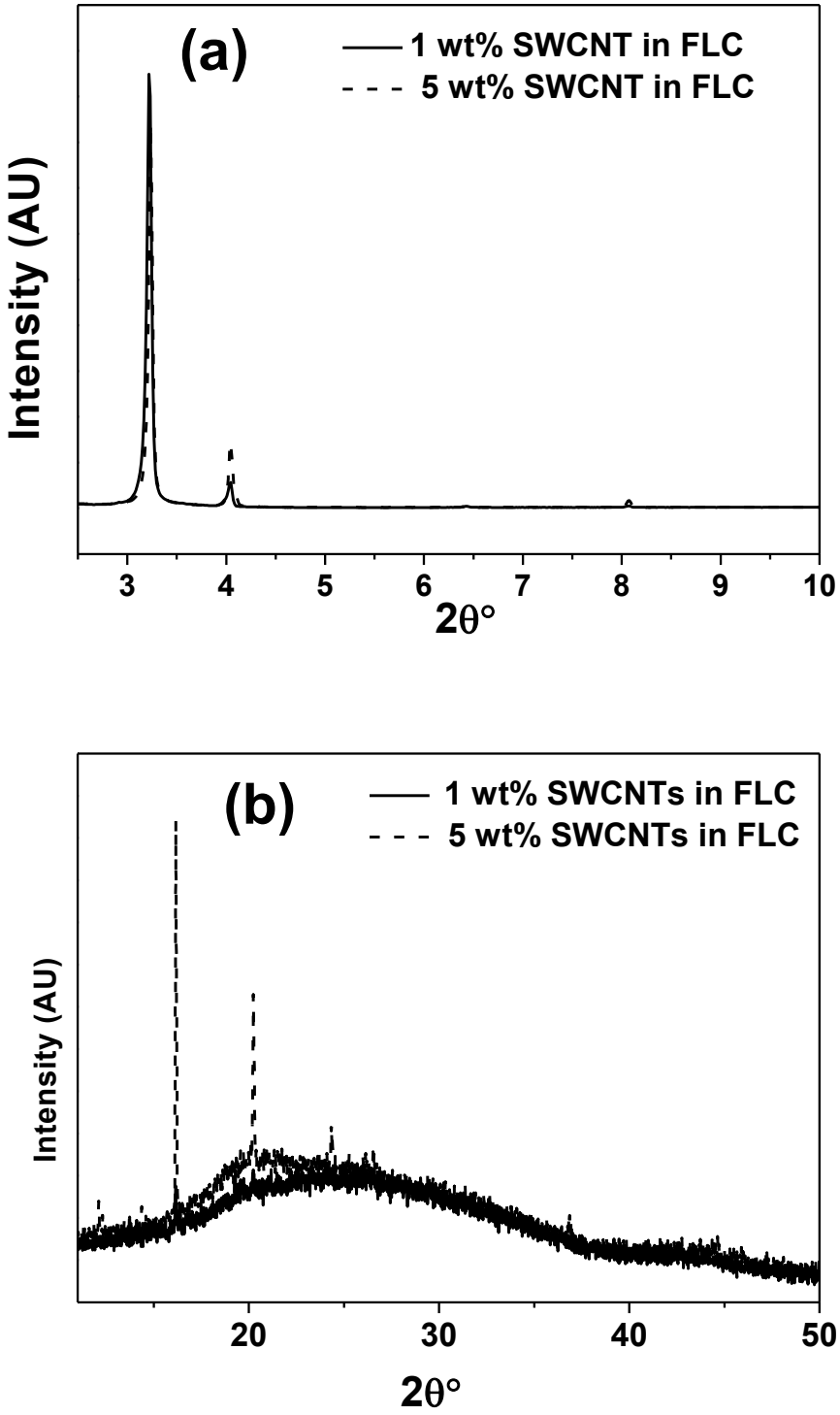

Figure 3.10: (a) Low angle X-ray diffraction profile of LB film of (1, 5) wt% functionalized SWCNTs in FLC matrix with $2\theta = (2.5^{\circ} - 10^{\circ})$ and (b) Wide angle X-ray diffraction profile of LB film of (1, 5) wt% functionalized SWCNTs in FLC matrix with $2\theta = (10^{\circ} - 50^{\circ})$.

At low angle (1, 5) wt % of SWCNTs showed an intense peaks at 2θ = 3.2°, corresponding to the smectic layer ordering of liquid crystal molecules. As the concentration of nanotubes is increased from 1 to 5 wt %, a decrease in peak intensity was noticed. From this we conclude that at low concentration doping layer structure of liquid crystal matrix is not disturbed. Peaks at 2θ = 4°, 12.0° and 14.0° are due to oriented octadecylamine chains.

Wide angle X-ray diffraction profile in range (2θ = 10 ° - 50°) shows intense peaks at 2θ = 20.06° and 24.40° are due to functionalized nanotubes doped in FLC matrix [41-1487: JCPDS]. The broader peaks are due amorphous nature of liquid crystalline host matrix.

3.6 Topography of LB film

Topography of monolayer deposited on quartz and Si substrate was investigated using atomic force microscopy (solver-next NT-MDT). Silicon nitride (SiN) probe of tip curvature radius 2nm was attached to a cantilever (resonance frequency; 87-230 kHz, typical force constant 5.1nNm^{-1}). Initially properly cleaned quartz substrate was scanned under AFM and root mean square roughness < 1nm was observed. It ensured smoothness of the quartz and its sustainability for monolayer deposition. Then, topography of the FLC monolayer deposited on quartz substrate was observed under AFM in non-contact mode.

3.6.1 Topography of FLC monolayer

The images shown in Figure 3.11 were taken at scan range 5×5 μm^2. AFM image in figure 3.11(a) showed elongated ferroelectric liquid crystal domains where as figure 3.11(b) represents three dimensional (3D) view with roughness parameter along z-axis. The black line on the figure 3.11(a) was drawn to measure the roughness variation along it; corresponding height profile is shown in figure 3.11(c). Average height profile indicated roughness about of 2.5 nm. Narrower peaks in height profile indicate the monodispersity whereas Figure 3.11(d) represents magnitude profile image.

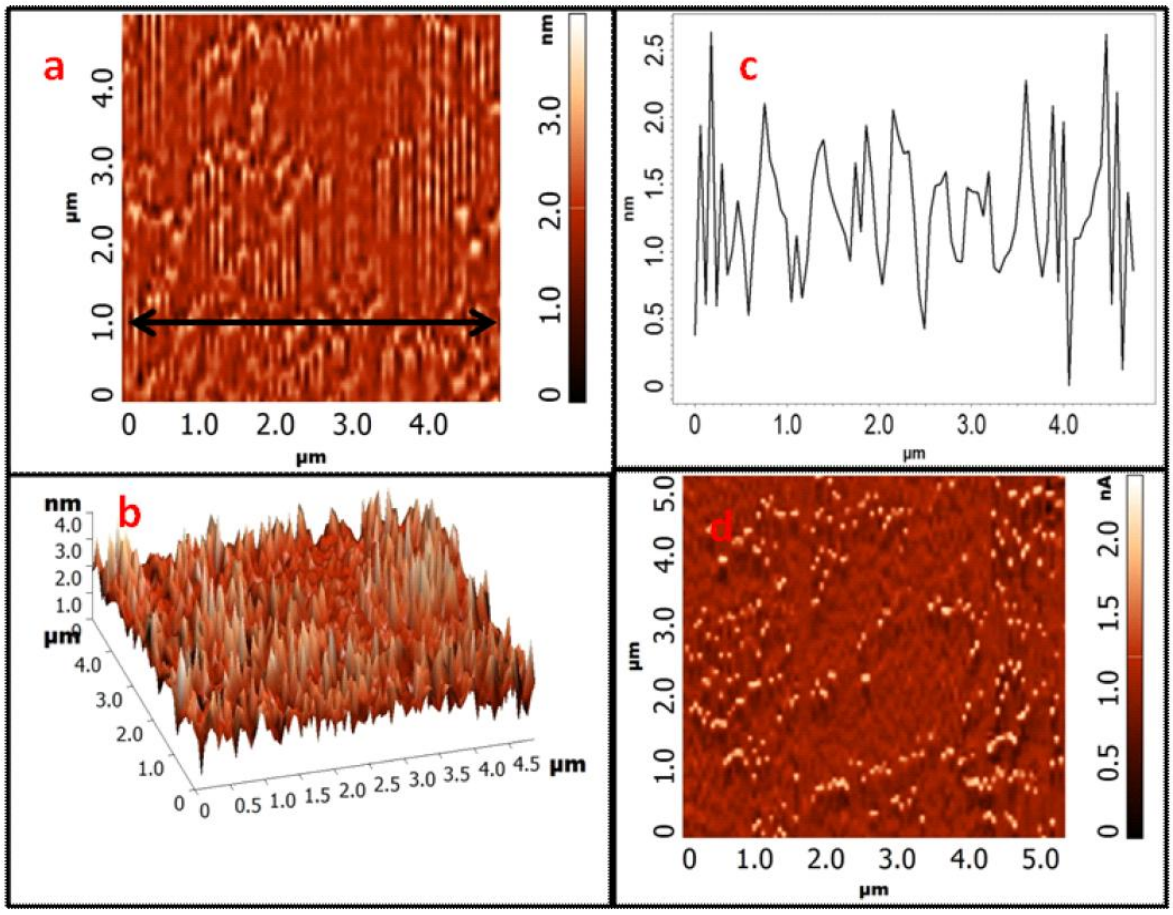

Figure 3.11: Atomic force microscopic (AFM) image of FLC deposited on a smooth quartz substrate at 5 mN m^{-1}:(a)images of FLC monolayer at a scan range 5 × 5 μm^2 , (b) 3D view of FLC monolayer, (c) height profile along black line of image (a),(d) magnitude profile of monolayer.

3.6.2 Topography of LB Films of functionalized SWCNTs and FLC-SWCNTs composites

AFM image of a LB monolayer of ODA functionalized SWCNTs on a single crystal silicon wafer substrate in a scan range 5×5 μm^2 is shown in figure 3.12. The deposition was done at constant surface pressure 8 mN m^{-1}. In image 3.12(a) film of nanotubes appears to be consisting of a network having interconnected bundles of nanotubes. 3-D topography of the deposited film is shown in scan image 3.12(b), which indicates its uniform deposition. The bundle diameters for the octadecylamine functionalized SWCNTs is lying in range 2-10 nm as inferred from figure 3.12(c) showing average height profile of deposited film [62].

During two continuous compression and expansion cycles, some SWCNTs get attached with others which resulted in hysteresis behaviour. When we deposit monolayer

after completion of two cycles, a topographical pattern obeying isotherm data was observed. In figure 3.13(a) nanotubes having tubular topography are attached with each other are shown in scan range 500 ×500 nm^2. Image 3.13(b) gives 3D view of attached nano tubes which hints at some aggregation occurring amongst Single Wall Carbon Nanotubes in the monolayer, which was not immediately reversed on expansion. Height profile in figure 3.13(c) shows average diameter of tubes ~ 8nm. High coverage of nano tubes on the surface enables us to see the result by statistical analysis.

Thus we find maximum number of counts of particles having size in range of 2-10 nm as shown in figure 3.13(d).Figure 3.14 shows AFM image of 1 % functionalized SWCNTs in FLC deposited at 9 mN m^{-1}. The AFM image having scan range 1×1 μm^2 shown in image 3.14(a) have elongated ferroelectric liquid crystal domains, tubular topography is not observed because of very less weight percent of SWCNTs in it and image 3.14(b) gives a three-dimensional (3D) view, with the roughness parameter along the z-axis. The corresponding average height profile is shown in figure 3.14(c), the average height profile indicating a roughness ~ 2.5 nm, which is near to average length of FLC molecules. Narrower peaks in the height profile indicate mono dispersity

Figure 3.15 shows image in scan range 5×5 μm^2 for 5 % mixture, where as topography of aligned SWCNTs along with ferroelectric liquid crystal domains is shown in figure 3.15(a). 3-D view as shown in image 3.15(b) infer about complex pattern of both globular as well as tubular topography and 3.15(c) shows average height profile having average tube diameter ~ 6nm, this is because of strong (π-π) electrostatic interaction between SWCNTs wall and FLC's biphenyl rings.

This suggest the possibility of aligning carbon nano tube using FLC as enabling material, it has many important applications in nano tube based electronics [63], where large scale alignment is required to avoid short circuit and undisturbed tube interaction.

3.7 Conclusions

It is concluded that the amphiphilic nature of the FLC and functionalized nanotubes played a vital role in the orientation and ordering of films at interface. Reproducibility of the Π–A isotherm confirmed the stability of the mono-layer. The XRD profile indicated smectic layering of the FLC molecules and FTIR spectra confirmed complete deposition

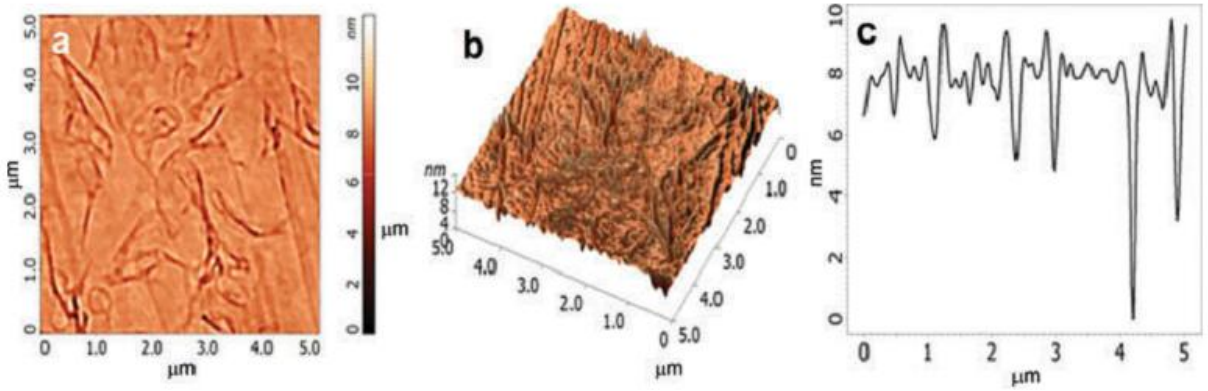

Figure 3.12: AFM image of functionalized SWCNTs deposited at 8 mN m^{-1} on single crystal silicon wafer. (a) 5 × 5 μm^2 2-D image (b) 3-D view and (c) shows average height profile.

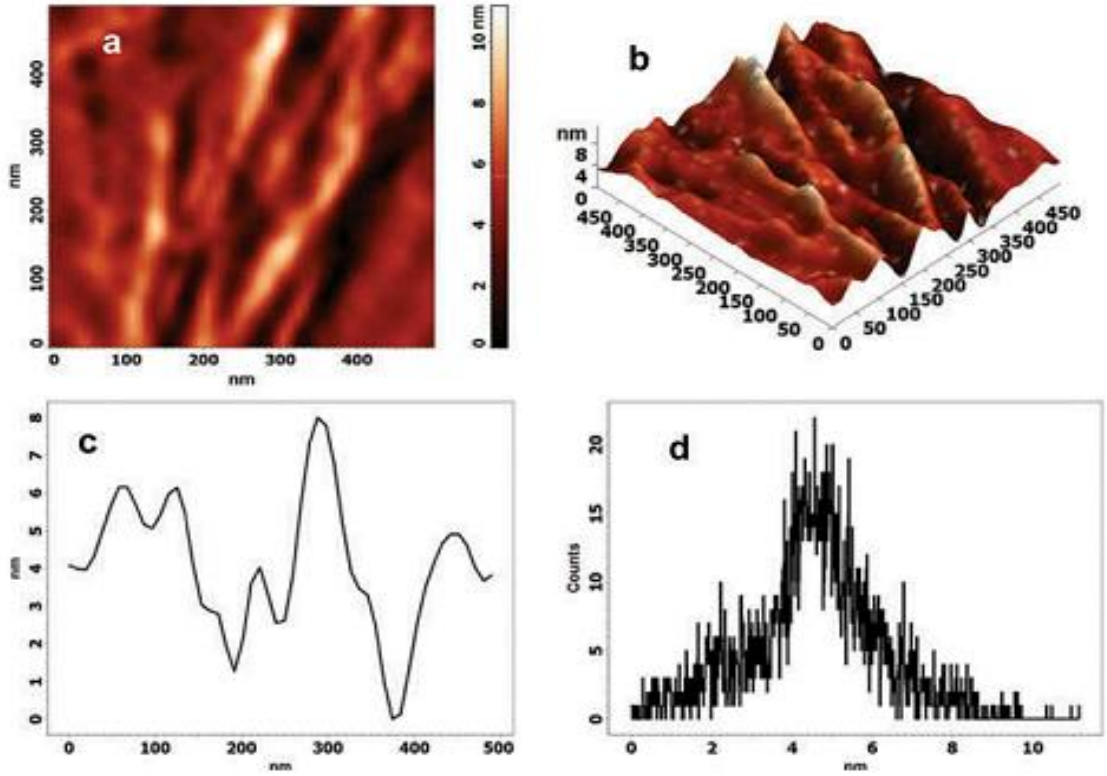

Figure 3.13: Image of 500 × 500 nm^2, interconnected SWCNTs are observed. (a, b) shows 2-D and 3-D image, while (c) shows average height profile and (d) provides count of size distribution.

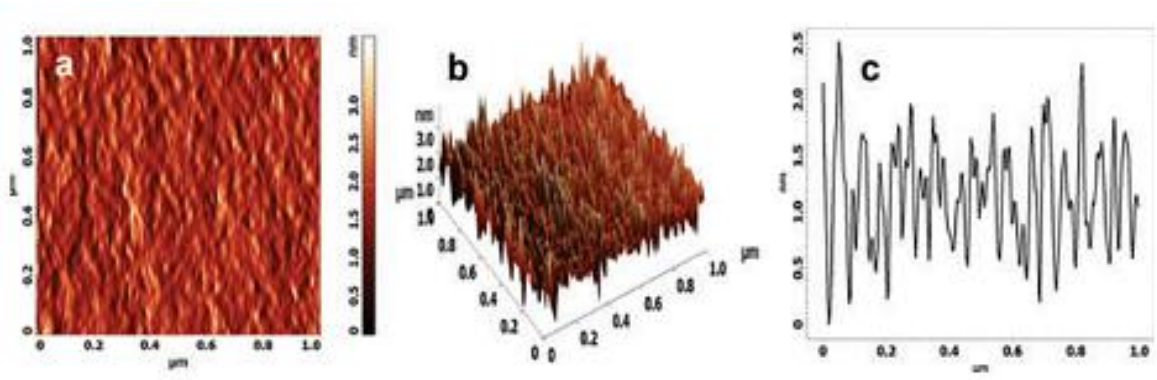

Figure 3.14: Images of 1 wt% ODA-functionalized SWCNTs in FLC deposited at 9 mN m^{-1} on single crystal silicon wafer. (a) It shows 1 × 1 μm^2 2D image, (b) shows 3-D view and (c) shows average height profile.

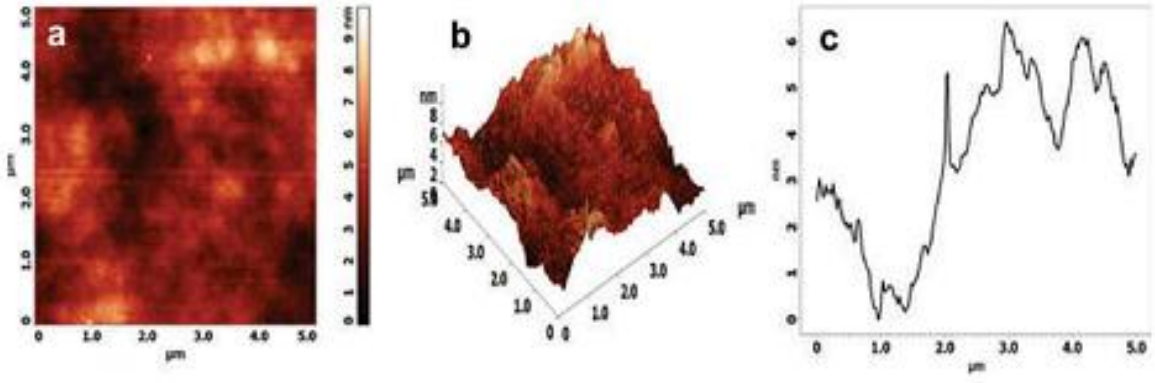

Figure 3.15: Images of 5 wt% functionalized SWCNTs in FLC deposited at 4 mN m^{-1} on single crystal silicon wafer. (a), (b) and (c) show 5 × 5 μm^2 2-D image, 3-D view of deposited LB film and average height profile, respectively.

of the FLC and composite films. SWCNTs in FLC matrix enhances stability due to π–π stacking of SWCNTs with the FLC molecules. Thus LB technique provides new insight into ultrathin films of LCs, which will find a variety of applications in sensor devices. These investigations have opened up vistas for understanding the switching and other electrical properties of FLC–SWCNTs thin films by providing molecular level ordering of nanotubes in FLC matrix.

References

1 R B Meyer. Ferroelectric liquid crystals, A Review. Mol. Cryst. Liq. Cryst. 1977, **40**, 33.

2 N A Clark, S T Lagerwall. Submicrosecond bistable electrooptic switching in liquid crystals. Appl. Phys. Lett. 1980, **36**,899.

3 A Fukuda, Y Takanishi, T Isozaki, K Ishikawa, H Takezoe. Antiferroelectric chiral smectic liquid-crystals. J. Mater. Chem. 1994, **4(7)**, 997.

4 M Hird. Ferroelectricity in liquid crystals-materials, properties and applications. Liq. Cryst. 2011, **38**, 1467.

5 A Ulman. An Introduction to Ultrathin Organic Films: From Langmuir-Blodgett to Self Assembly, Academic Press: Boston, 1991.

6 G G Roberts. Langmuir-Blodgett Films; Plenum Press: New York, 1990.

7 R H Tredgold. Order in Thin Organic Films; Cambridge University Press, Cambridge, 1994.

8 M F Daniel, O C Lettington, S M Small. Investigations into the Langmuir-Blodgett film formation ability of amphiphiles with cyano head groups. Thin Solid Films**.** 1983, **99**, 61-69.

9 T Sakuhara, H Nakahara, K Fukuda. Control of structure in Langmuir-Blodgett films of terphenyl liquid crystal compound. Thin Solid Films. 1988, **159**, 345.

10 Xue J, C S Jung, M W Kim. Phase transitions of liquid-crystal films on an air-water interface. Phys. Rev. Lett. 1992, **69**, 474.

11 M C Friedenberg, G G Fuller, C Frank, C R Robertson. Formation of Bilayer Disks and Two-Dimensional Foams on a Collapsing/Expanding Liquid-Crystal

Monolayer. Langmuir. 1994, **10**, 1251.

12 T Martynski, R Hertmanowski, D Bauman. Molecular organization in two-dimensional films of liquid I. Langmuir films of binary mixtures of liquid crystals with a crystalline mixtures terminal cyano group. Liq. Cryst. 2001, **28**, 437.

13 T Martynski, R Hertmanowski, D Bauman. Molecular organization in two-dimensional films of liquid crystalline mixtures III. Langmuir films of binary mixtures of liquid crystal materials with terminal CN or NCS group. Liq. Cryst. 2002, **29**, 99.

14 K Inglot, T Martynski, D Bauman. Influence of the alkyl chain length of some mesogenic molecules on their Langmuir film formation ability. Liq. Cryst. 2006, **33**, 855.

15 H Y Chen, W Lee, N A Clark. Faster electro-optical response characteristics of a carbon-nanotube-nematic Suspension. Appl. Phys. Lett. 2007, **90**, 033510.

16 S Y Jeon, S H Shin, S J Jeong, S H Lee, S H Jeong, Y H Lee, H C Choi, K J Kim. Effects of carbon nanotubes on electro-optical characteristics of liquid crystal cell driven by in-plane field. Appl. Phys. Lett. 2007, **90**,121901.

17 W Lee, C Wang, Y Shih. Effects of carbon nanosolids on the electro-optical properties of a twisted nematic liquid-crystal host. Appl. Phys. Lett. 2004, **85**, 513.

18 C Huang, C Hu, H Pan, K Lo. Electrooptical responses of carbon nanotube-doped liquid crystal devices. Jpn. J. Appl. Phys. 2005, **44**, 8077.

19 I S Baik, S Y Jeon, S H Lee, K A Park, S H Jeong, K H Anand, Y H Lee. Electrical-field effect on carbon nanotubes in a twisted nematic liquid crystal cell. Appl. Phys. Lett., 2005, **87**, 263110.

20 C Huang, H Pan, C Hsieh. Electrooptical Properties of Carbon-Nanotube-Doped Twisted Nematic Liquid Crystal Cell. Jpn. J. Appl. Phys. 2006, **45**, 6392.

21 H Chen, W Lee. Suppression of field screening in nematic liquid crystals by carbon nanotubes Appl. Phys. Lett. 2006, **88**, 222105.

22 G Scalia, J P F Lagerwall, S Schymura, M Haluska, F Giesselman, S Roth. Carbon nanotubes in liquid crystals as versatile functional materials. Phys. Status Solidi B 2007, **244**, 4212.

23 N Ould-Moussa, C Blanc, C Zamora-Ledezma, O D Lavrentovich, I I Smalyukh, M F Islam, A G Yodh, M Maugey, P Poulin, E Anglaret, M Nobili. Dispersion and orientation of single-walled carbon nanotubes in a chromonic liquid crystal. Liq. Cryst. 2013, **40(12)**, 1628-1635.

24 L D Sio , V C C Paolo, Umeton. Using soft composite materials for a tuneable broadband optical filter. J. Opt., 2014, **16**, 065703.

25 R Basu, G S Iannacchione, Orientational coupling enhancement in a carbon nanotube dispersed liquid crystal. Phys Rev E. 2010, **81**, 051705.

26 H Wang, P Weib, Y Lic, J Hanb, H R Leec, B D Naabd, N Liub, C Wange, E Adijantob, B C K. Teec, S Morishitab, Q Lib, Y Gaoe, Y Cuia, Z Bao. Tuning the threshold voltage of carbon nanotubes transistors by n-type molecular doping for robust and flexible complementary circuits. PNAS, 2014, 111(13), 4776.

27 G Scalia. Alignment of carbon nanotubes in thermotropic and lyotropic liquid crystals. Chem. Phys. Chem, 2010 **11**, 333.

28 I Dierking, G Scalia, P Morales. Liquid crystal–carbon nanotube dispersions J. Appl. Phys. 2005, **97**,044309.

29 Z K Husain, M Husain. Carbon nanotubes and its possible applications. Indian J. Eng. Mater. Sci. 2005, **12**, 529.

30 J P F Lagerwall, G Scalia. Carbon nanotubes in liquid crystals. J. Mater. Chem. 2008, **18**, 2890.

31 G De Filpo, S Siprova, G Chidichimo, A I Mashin, F P Nicoletta, D Cupelli. Alignment of single-walled carbon nanotubes in polymer dispersed liquid crystals. Liquid Crystals. 2012, **39(3)**, 359.

32 J Prakash, A Choudhary, D S Mehta, A M Biradar. Effect of carbon nanotubes on response time of ferroelectric liquid crystals. Phys. Rev. E. 2009, **80**, 012701.

33 F V Podgornov, A M Suvorova, A V Lapanik, W Haase. Electrooptic and dielectric properties of ferroelectric liquid crystal/single walled carbon nanotubes dispersions confined in thin cells. Chem. Phys. Lett. 2009, **479**, 206.

34 Neeraj, K K Raina. Dynamic Responses of Dispersed Ferroelectric Liquid Crystal Composite Materials. Integr Ferroelectr. 2011, **125**, 104.

35 Neeraj, K K Raina. Multiwall carbon nanotubes doped ferroelectric liquid crystal composites: Astudy of modified electrical behavior. Physica B. 2014, **434**, 1.

36 P Ganguly, A Kumar, S Tripathi, D Haranath, A M Biradar, Effect of functionalisation of carbon nanotubes on the dielectric and electro-optical properties of ferroelectric liquid crystal. Liq. Cryst. 2014, **41(6)**, 793.

37 R K Shukla, K K Raina, V Hamplova, M Kaspar, A Bubnov. Dielectric behaviour of the composite system: multiwall carbon nanotubes dispersed in ferroelectric liquid crystal. Phase Transit. 2011, **84**, 850.

38 N Sood, S Khosla, D Singh, S S Bawa. Dielectric investigations of pure and carbon nanotube-doped deformed helix ferroelectric liquid crystals. Liq. Cryst. 2012; **39(10)**, 1169.

39 V Krstic, J Munster, G S Duesberg, G Philipp, M Burghard, S Roth. Electrical

transport in single-walled carbon nanotube bundles embedded in Langmuir–Blodgett monolayers. Synth. Met. 2000, **110**, 245.

40 R B Prabhakar. Electrical Properties and Applications of Carbon Nanotube Structures J. Nanosci. Nanotechnol. 2007, **7**, 1.

41 M Sano, A Kamino, J Okamura, S Shinkai. Self-Organization of PEO-graft-Single-Walled Carbon Nanotubes in Solutions and Langmuir-Blodgett Films. Langmuir. 2001, **17**, 5125.

42 J Cui, C P Daghlian, U J Gibson. Gold Nanoparticle Mediated Formation of Aligned Nanotube Composite Films. J. Phys. Chem. B. 2005, **109**, 11456.

43 J B Cui, C P Daghlian, U J Gibson. Solubility and electrical transport properties of thiolated single-walled carbon nanotubes. J. Appl. Phys. 2005, **98**, 044320.

44 J L Hernandez-Lopez, E R Alvizo-Paez, S E Moya, J Ruiz-Garcia. Trapping, Pattern Formation, and Ordering of Polyelectrolyte/Single-Wall Carbon Nanotube Complexes at the Air/Water and Air/Solid Interfaces. J. Phys. Chem. B 2006, **110**, 23179.

45 L Jia, Y F Zhang, Y J Li, C You, E Q Xie. Highly ordered in-plane orientation of single-walled carbon nanotubes. J Optoelectron Adv M. 2008, **10**, 2743.

46 Y Guo, N Minami, S Kazaoui, J Peng, M Yoshida, T Miyashita. Multi-layer LB films of single-wall carbon nanotubes. Physica B. 2002, **323**, 235.

47 Y Kim, N Minami, W Zhu, S Kazaoui, R Azumi, M Matsumoto. Langmuir–Blodgett Films of Single-Wall Carbon Nanotubes: Layer-by-layer Deposition and In-plane Orientation of Tubes Jpn. J. Appl. Phys. 2003, **42**, 7629.

48 D S Hecht, L Hu, G Gruner. Electronic properties of carbon nanotube/fabric composites Curr. Appl. Phys. 2007, **7**, 60.

49 L Feng, H Li, F Li, Z Shi, Z Gu. Functionalization of carbon nanotubes with amphiphilic molecules and their Langmuir–Blodgett films. Carbon. 2003, **41**, 2385.

50 C L Honeybourne**,** K J Barrell**.** Langmuir–Blodgett multilayers of six compact porphyrin amphiphiles. J. Mater. Chem.1996, 6, 323.

51 C J L Constantino, A Dhanabalan, O N Oliveira. Experimental artifacts in the surface pressure measurement for lignin monolayers in Langmuir troughs. Rev. of Sci. Inst., 1999, **70**, 3674.

52 Z Gang, F Kun, S Xia, He Pingsheng. Elasticity of 10, 12-Pentacosadiynoic Acid Monolayer and the Polymerized Monolayer at Varying pH and Temperatures. Langmuir. 2002, **18**, 6602.

53 A W Adamson. Physical Chemistry of Surfaces. 5th edition. New York USA: John Wiley, 1990.

54 N B Colthup, L H Daly, S E Wiberley. Introduction to Infrared and Raman Spectroscopy. 3rd edition. San Diego CA USA: Academic Press, 1990.

55 L J Bellamy. Infrared Spectra of Complex Molecules. New York USA: Chapman and Hall, 1975.

56 G Socrates. Infrared Characteristic Group Frequencies. New York USA: Wiley, 1994.

57 R Kaur, G K Bhullar, K K Raina. Behaviour of an ultrathin ferroelectric liquid crystal Langmuir–Blodgett film at an air–water and air–solid interface. Liq. Cryst. 2012, **39(11)**, 1375.

58 E Olbrich, O Marinov, D Davidov. Ordering effects in thin smectic-**C*** films: An x-ray-reflectivity study. Pys. Rev. E. 1993, **48**, 2317.

59 S Okada, H Matsuda, H Nakanishi, M Kato, Inventors; Agency of Industrial Science & Technology, Ministry of International Trade and Industry, assignee. Method using X-Ray to determine thickness of organic films. United States patent **US 5003569**, 1991 March 26.

60 M Ibn-Elhaj, M Z Cherkaoui, R Zniber, H Mohwald. Effect of a Siloxane Moiety on the Anchoring of Ferroelectric Liquid Crystals at the Air−Water Interface. J. Phys. Chem. B. 1998, **102**, 5274.

61 Zi Wen, Q Jiang, K Tatani, Y Ozaki. Characterization of Langmuir −Blodgett Films of a Ferroelectric Liquid Crystal. J. Phys. Chem. B, 2006,**110**, 1722.

62 C Venet, C Pearson, A S Jombert, M F Mabrook, DA Zeze, M C Petty. The morphology and electrical conductivity of single-wall carbon nanotube thin films prepared by the Langmuir–Blodgett technique. Colloid Surf. A. 2010, **354**, 113.

63 J J Lee, A Yamaguchi, Md A Alam, Y Yamamoto, T Fukushima, K Kato, M Takata, N Fujita, T Aida, Back Cover: Discotic Ionic Liquid Crystals of Triphenylene as Dispersants for Orienting Single-Walled Carbon Nanotubes. Angew. Chem. Int. Ed., 2012, **51**, 8666.

CHAPTER - 4

Effects of nano-particle doping on the Phase transitional behaviour of ferroelectric liquid crystal Langmuir -Blodgett composite films

Overview

Langmuir–Blodgett films of ferroelectric liquid crystal doped with low concentration of functionalized {ZnO: Aℓ (AZO) and Ag} nano-particles were prepared and characterised. Pressure–area isotherms show that the nano-particles as well as FLC composite systems have capability to form stable monolayer at air-water interface. The molecular interaction between nano-particles and ferroelectric liquid crystal molecules increases during barrier compression, which resulted in increased surface pressure. We observed various phases in isotherms with increasing concentration of nano-particles in the ferroelectric liquid crystal matrix. X-Ray diffraction profile at low angle confirmed that ferroelectric liquid crystal retains its layer structure at low concentration doping of nano particles in FLC matrix. Atomic force microscopy images indicate that low wt% composites are uniformly deposited without disturbing translation behaviour of Sm C* liquid crystal.

4.1 Introduction

We know that nano-particles have their effect on the electro-optic performance of ferroelectric liquid crystals [1-6], but effect is dependent on the size, intrinsic characteristics and doping concentration of nanoparticles [7-10]. Low doping concentrations usually lead to even distribution in liquid crystal matrix. We have prepared LB films of AZO nanoparticles because AZO nanoparticles posses several favourable semiconducting properties, good transparency, high electron mobility, wide band gap and Ag nano-particles have unique electro-optical response [11-14].

Liquid crystal (LC) alignment plays important role in fabricating liquid crystal displays. There are several ways to align LC materials, some conventional techniques are like photo alignment, and polymer stabilized alignment by using polyimide (PI) films [15-18] and the nano-particle induced alignment for developing thin films at room temperature [19-23].

Research groups have prepared thin films of these doped composite systems by all these methods at micro scale. But in many applications molecular level ordering is required; this ordering can be attained by Langmuir-Blodgett (LB) technique at nanometer scale [24-28].

Amphiphilic LC creates stable compressible monolayers at the air–water interface which are easily transferrable onto solid substrates [29-31]. Functionalized nano-particles also have tendency to align themselves on air-water interface. They have proper balance in hydrophilic and hydrophobic groups as shown in figures 2.11 and 2.12. The films formed by addition of nano-particles in FLC matrix forms a new class of composite materials for variety of applications [32-35].

We made an attempt to understand the effects of nano-particle doping on properties of FLC thin films. We doped ZnO:Aℓ (AZO) and Silver (Ag) nano-particles in FLC matrix.

Monolayers at air–water interface were characterised by surface pressure–area (Π–A) isotherms. Low Angle and Wide Angle X-Ray diffraction are used to study phase transition of LB films deposited on glass substrates, Fourier Transform Infrared Spectroscopy to study interaction between nano-particles and FLC matrix and atomic force microscopy (AFM) were used to investigate topography of LB films deposited on Si wafer.

4.2 Fourier Transform Infrared (FTIR) Spectroscopy of functionalized AZO and Ag nano-particles

Figure 4.1 shows FTIR spectras of Octadecylamine (ODA), ZnO: Aℓ (AZO) and ODA functionalized AZO nano-particles. In AZO, two major absorptions are present. One at 3469 cm^{-1} and other near to 503 cm^{-1}; first one is due to Zn-O bond and other is from 6% Aℓ doping in ZnO.

In ODA major absorptions corresponds to presence of amine and carbon atoms of octadecyl chain. Presence of amide group is confirmed by absorption at 3331.96 cm^{-1}. The interpretation of long chain is straight forward as we have observed jagged absorptions at approximately 2912.13 cm^{-1} and 2896.10 cm^{-1}. These correspond to C-H stretching asymmetric and symmetric vibrations for saturated aliphatic chain. Absorption present at 1583.00 cm^{-1} corresponds to carbonyl C = O (stretching) of amine group. Absorption is observed at 1360.00 cm^{-1}, corresponding to simple bending vibrations of C-H bonds.

In ODA –AZO a broad absorption is missing at 3469 cm^{-1}, which was present in FTIR of AZO nano-particles, it confirms the chemical functionalization through oxygen. The absorptions seen at 2851.00 cm^{-1} and 2903.00 cm^{-1} to saturated octadecyl chain Absorption at 3331 cm^{-1} in FTIR spectra of ODA was due to presence of free NH_2 group. This absorption peak has shifted to 3229 cm^{-1} in spectra of ODA functionalized AZO nano-particles. It is due to chemical functionalization of AZO nano-particles [36, 37].

We have purchased pre-functionalized Ag nano-particles. FTIR spectra of DDT functionalized Ag nano-particles is given in figure 4.2. In the spectrum of DDT functionalized Ag nano-particles, the CH_2 symmetrical and asymmetrical stretching bands appear at 2959.25 cm^{-1}& 2924.66 cm^{-1} and 2872.90 cm^{-1}& 2854.40 cm^{-1} respectively [38, 39] which are due to long dodecanethiol chain attached to Ag atom.

The absence of S–H stretching band at 2700–2550 cm^{-1} in spectrum is clearly observed which is resulted from the coordination –SH to the surface of the nano-Ag particles. Wagging (Wx) progression bands of dodecyl chains appear at 1459.55 cm^{-1}, 1378.50 cm^{-1} and 1117.47 cm^{-1} (1400–1150 cm^{-1}). Absorption at 724 cm^{-1} is due to Ag nano-particles. Hence long alkyl chains are attached to nano-particles provide balance between hydrophillicity and hydrophobicity to make stable monolayers at water surface.

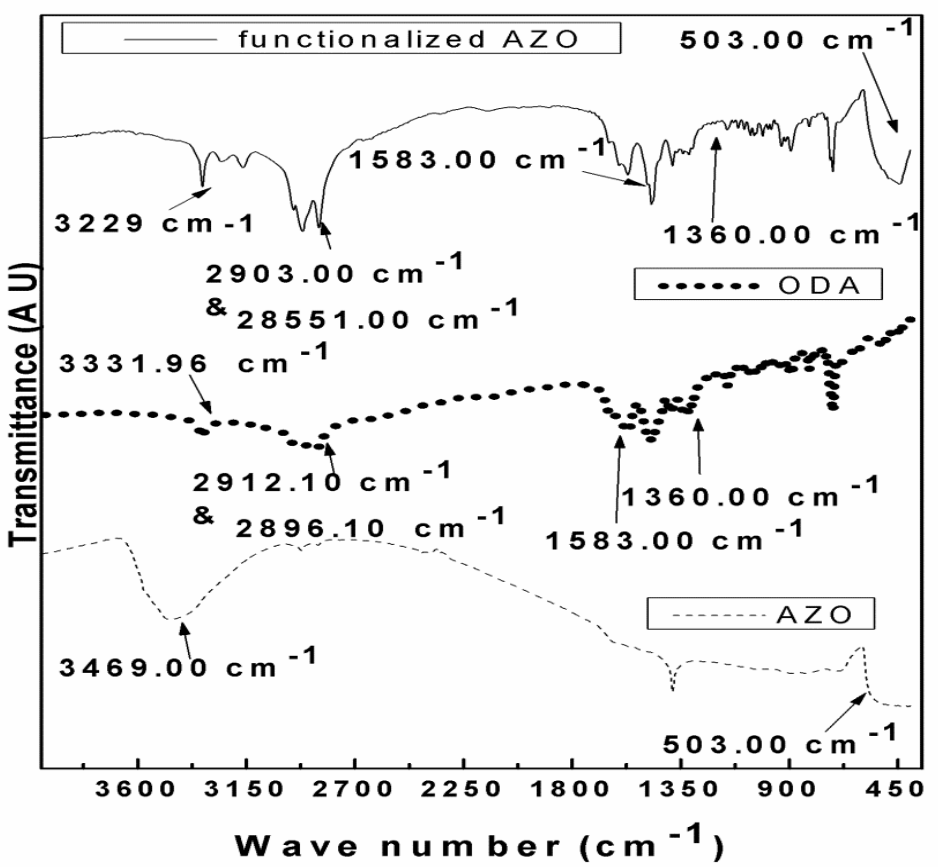

Figure 4.1: FTIR spectra of AZO nano-particles, Octadecylamine (ODA) and ODA functionalized AZO nano-particles.

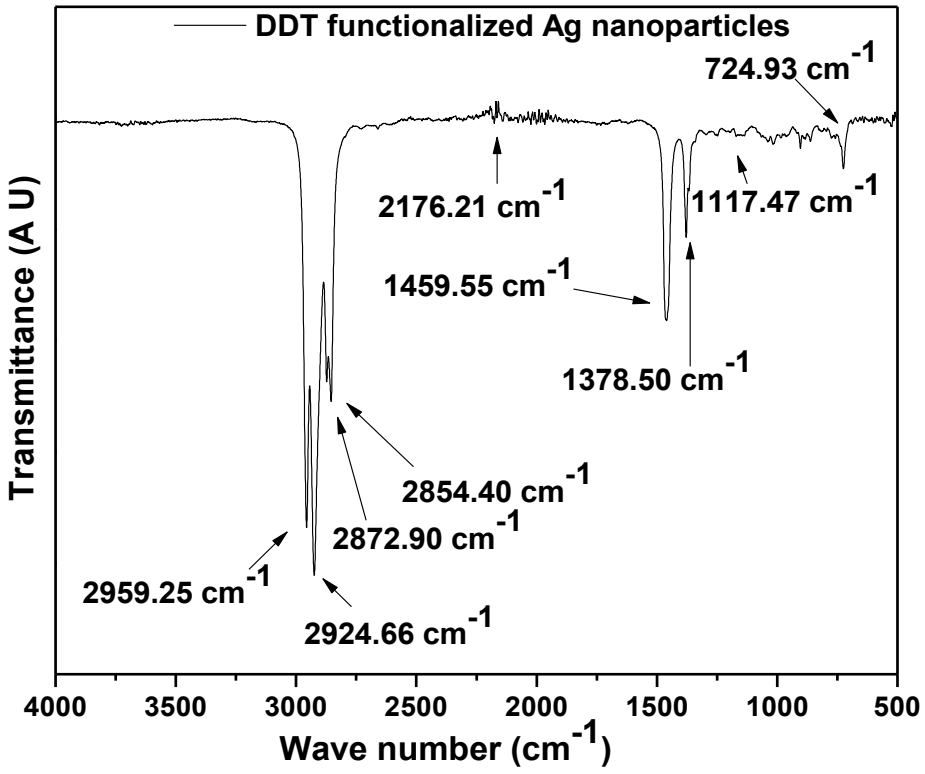

Figure 4.2: FTIR spectra of DDT functionalized Ag nano-particles.

4.3 Surface Pressure- Area (Π-A) Isotherms of nano-particles – FLC films

100 µl of solution prepared by dissolving 1.0 mg ml^{-1} of Octadecylamine functionalized AZO nano-particles in chloroform was spread on the aqueous surface by Hamilton micro syringe. After providing evaporation time of about 15 minutes, barriers were swept closer @ 10mm min^{-1}. Before starting next experiment, trough was thoroughly cleaned by using ethanol and deionised water. 50 µl of solution (1mg ml^{-1} FLC in $CHC\ell_3$) was spread on trough water and isotherm was recorded at constant barrier speed (10 mm min^{-1}) to prepare monolayer of FLC material. (1, 5) wt % of AZO – FLC composite material were prepared in chloroform (1 mg ml^{-1}) after 30 minutes of sonication. The proper dispersion of nano-particles in FLC matrix was ensured by uniform solution obtained after sonication. 50 µl mixtures of both composites were spread on water sub phase separately.

The surface-pressure isotherms of undoped FLC and AZO nano-particles doped FLC composite materials are shown in Figure 4.3. The isotherms indicate the formation of stable monolayers at constant compression speed. As in undoped FLC isotherm, increase in compression resulted in orientation and ordering of LC molecules at air–water interface. Initially molecules were in the gaseous phase but then alignment of monolayer had increased surface pressure up to 7 mNm^{-1}, at this pressure a condensed phase was formed. Surface-pressure variation of 1 wt% FLC composite at constant barriers compression 10 mm min^{-1} indicates that the molecular alignment as a function of reduced surface area. In this case, surface pressure of well-aligned monolayer raises up to 14.76 mN m^{-1}, which is greater than surface pressure attained by undoped FLC hinting at the presence of nano-particles doped system at the interface. Where as isotherm for 5 wt% functionalized AZO nano-particles in FLC reveals smooth transitions from the gas to the liquid phase and from the liquid phase to the condensed phase at 2.66 mN m^{-1} and 4.45 mN m^{-1} respectively.

This system attains maximum pressure ~30 mNm^{-1}, which is higher than surface pressure of 1 wt% composite system. At this composition, AZO nano-particles and FLC molecules are competing for better alignment. We believe that the –NC═O group of nano-particles is getting affinity with –OH group of aqueous sub phase, simultaneously –Cl and – CO groups of FLC are aligning on surface. So a packed network might get formed. This results in an increase of surface pressure for 5 wt% system, likely due to molecular stability with nano-particles. Figure 4.3 inset shows typical LB surface pressure-Area (Π-

A) isotherm of functionalized AZO nano-particles Three distinct regions are observed in this profile. Region I represents rise in the surface pressure (up to 11 mNm^{-1}) which occur due to molecular ordering in the gaseous state resulting in the formation of expanded liquid phase. On further compression of barriers, surface pressure increases up to 21.18 mNm^{-1} [Region II], representing the liquid condensed phase. Region III represents solid condensed phase, formed with a sharp rise in the surface pressure up to 43.39 mNm^{-1}. The functionalized AZO nano-particles thus have a stable monolayer at air-water interface, which was easily transferred to Si substrate at 42.0 mNm^{-1}.Monolayers and 11 multilayers of (1, 5) wt% composites were transferred to glass and Si wafer substrate at 14 and 30 mNm^{-1} respectively.

1mg ml^{-1} solution of FLC material was prepared in chloroform by sonicating the mixture for about 30 minutes. 50 µl of this solution was spread on trough water and isotherm was recorded at a constant compression (10 mm min^{-1}). (1, 5) wt % of Ag – FLC composites material were prepared in chloroform (1 mg ml^{-1}) after 30 minutes of sonication. The proper dispersion of nano-particles in FLC matrix was ensured by uniform solution obtained after sonication. 50 µl mixtures of both composites were spread on water sub phase separately.

Surface pressure–area (Π-A) isotherms profiles of undoped FLC and (1, 5) wt% of DDT functionalized Ag nano-particles in FLC matrix are given in figure 4.4. Inset (figure 4.4) shows Π-A behaviour of DDT functionalized Ag nano-particles at air-water interface. In undoped FLC isotherm condensed phase surface pressure reaches up to 7 mN $m^{-1.}$ At these stage molecular interactions among FLC molecules has resulted in formation of well orientated monolayer at air-water interface after passing through gaseous and liquid expanded phase.

In 1 wt% FLC composite isotherm molecules were in gaseous phase up to 175 cm^2. With constant compression, interaction between nano-particles and FLC resulted in increased surface pressure ~ 12.46 mNm^{-1}; whereas further rise in surface pressure up to 24.5 mN m^{-1} is observed in case of 5 wt% functionalized Ag nano-particles in FLC matrix. Thus with increasing concentration of nano-particles, increased interaction among them resulted in increased value of surface pressure. Monolayer and 11 multilayers of both composites were successfully deposited at constant surface pressure (12 mN m^{-1}, 24 mN m^{-1}) on Si wafer and glass substrate respectively.

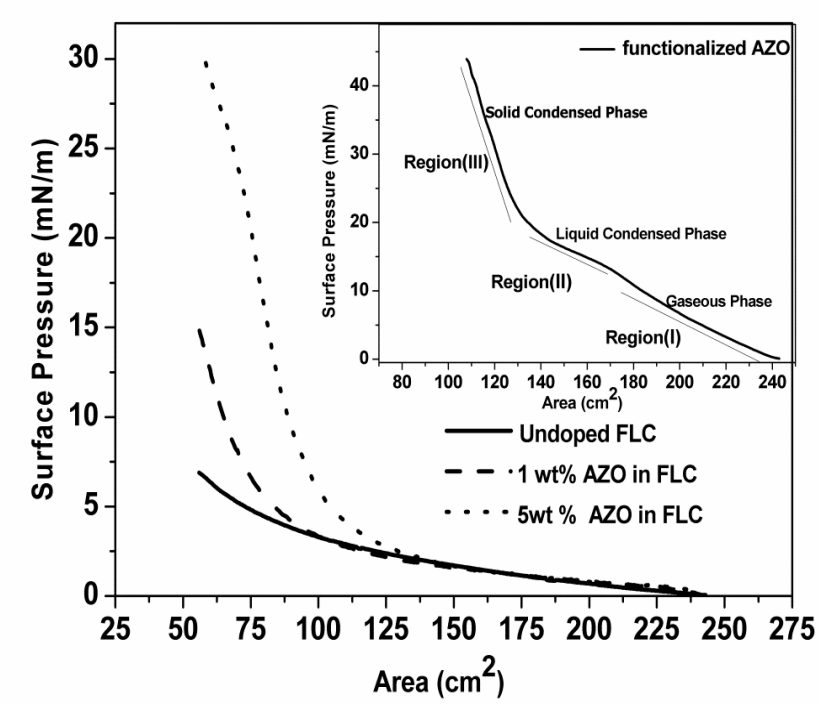

Figure 4.3 Surface pressure–area isotherm profile of undoped FLC and (1, 5) wt% functionalized AZOs in FLC matrix. [Inset] Π-A isotherm profile of functionalized AZO having three distinct phase regions (I, II and III).

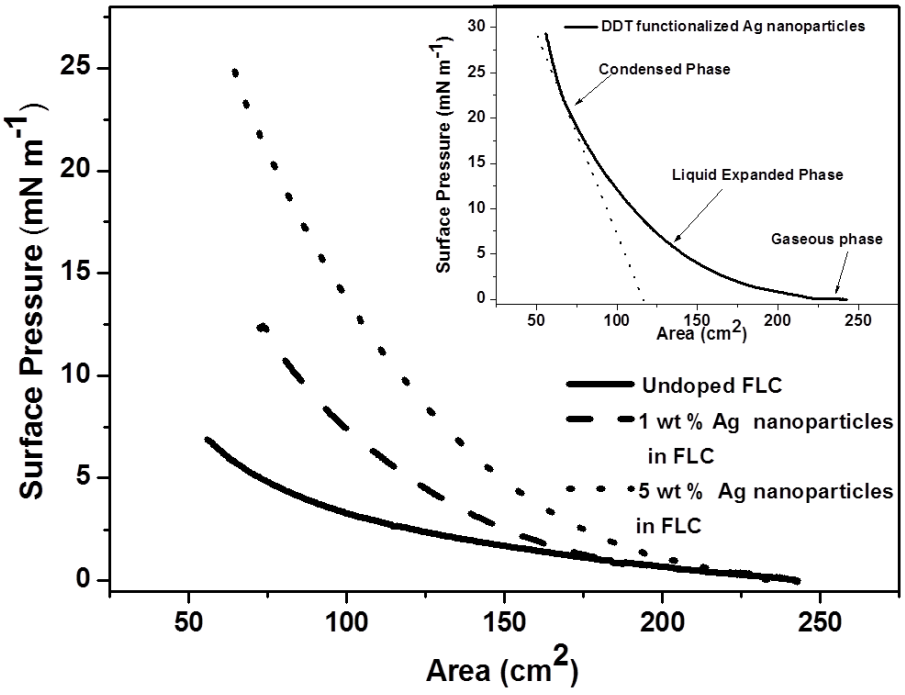

Figure 4.4 Surface pressure–area isotherms profile of undoped FLC and (1, 5) wt% of functionalized Ag nano-particles in FLC matrix. Inset figure shows Π-A isotherm profile of functionalized Ag nano-particles having three distinct phase.

In surface pressure-Area (Π-A) isotherm of dodecanethiol functionalized Ag nano-particles, various phase changes were observed with constant compression of barriers. The molecules were initially in the gaseous phase at negligible surface pressure, but on compression the isotherm move to liquid expanded phase.

A gradual rise was observed in the surface pressure up to 25 mN m^{-1}. Before attaining this pressure the monolayer was in the liquid expanded phase, and the condensed phase was formed at A ~ 116 cm^2, when the functionalized Ag nano-particles molecules had become aligned as a stable monolayer at the air–water interface. Monolayer and 11 multilayers were successfully deposited (at surface pressure 29 mN m^{-1}) on Si wafer and glass substrate respectively.

4.4 Fourier Transform Infrared (FTIR) Spectroscopy of LB films

Figure 4.5 shows FTIR spectra of composite systems (1, 5) wt% of ODA functionalized AZO nano-particles in FLC. Absorption at 845.21 cm^{-1} confirmed the presence of a hydrocarbon chain bonded with a halide group, CH2–X, where X = Cl. Absorption at 1016 cm^{-1} corresponded to C–O stretching (C–O–C; 1200–1050 cm^{-1}), with alkyl substitution of FLC. Absorption at 1166.81 cm^{-1}, 1428.36 cm^{-1} and 1466.21 cm^{-1} corresponded to C-C stretch of aromatic rings of FLC; it is due to interaction occurring between FLC and long alkyl chain of functionalized AZO nano-particles. Absorption at 1538.51 cm^{-1} corresponded to N-H bend of functionalized nano-particles. Absorption at 1758.97 cm^{-1} corresponded to C=O stretching of ODA. Absorptions at 2921.96 cm^{-1} and 2852.38cm^{-1} are cm^{-} corresponded to C-N stretch of octadecyl amine. Absorption at 1246 cm^{-1} corresponded to 1606.71 cm^{-1}, due to octadecylamine chain. Presence of absorption at 3485.80 cm^{-1} confirms presence of N-H group .Absorptionat 663.22 cm^{-1} confirms presence of 6% aluminum doping in ZnO. So FTIR spectra confirm complete transfer of molecules from air-water interface and hints at interaction occurring between them.

Figure 4.6 shows FTIR spectra of LB film of composite systems (1, 5) wt% of DDT functionalized Ag nano-particles in FLC matrix. Again absence of S–H stretching band at 2700–2550 cm^{-1} in composite spectrum confirm coordination –SH to the surface of the nano-Ag particles. The CH_2 symmetrical and asymmetrical stretching bands of dodecyl chain appear at 2956.35 cm^{-1}& 2924.78 cm^{-1} and 2872.78 cm^{-1}& 2855.11 cm^{-1}

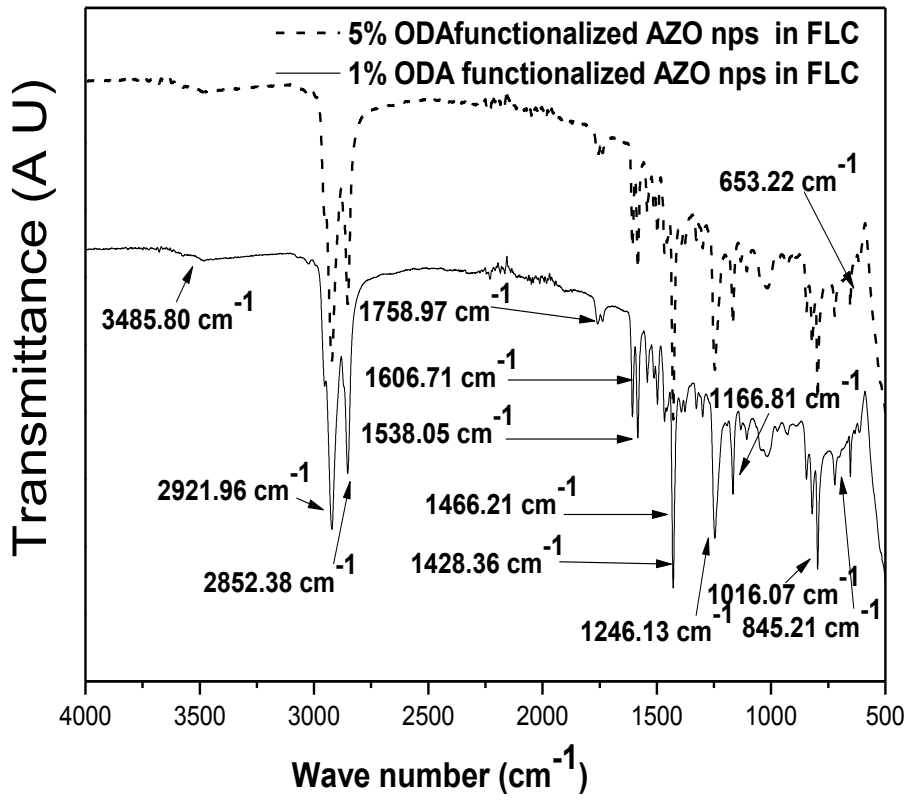

Figure 4.5 FTIR spectras of LB films of (1, 5) wt% of ODA functionalized AZO nano-particles in FLC matrix.

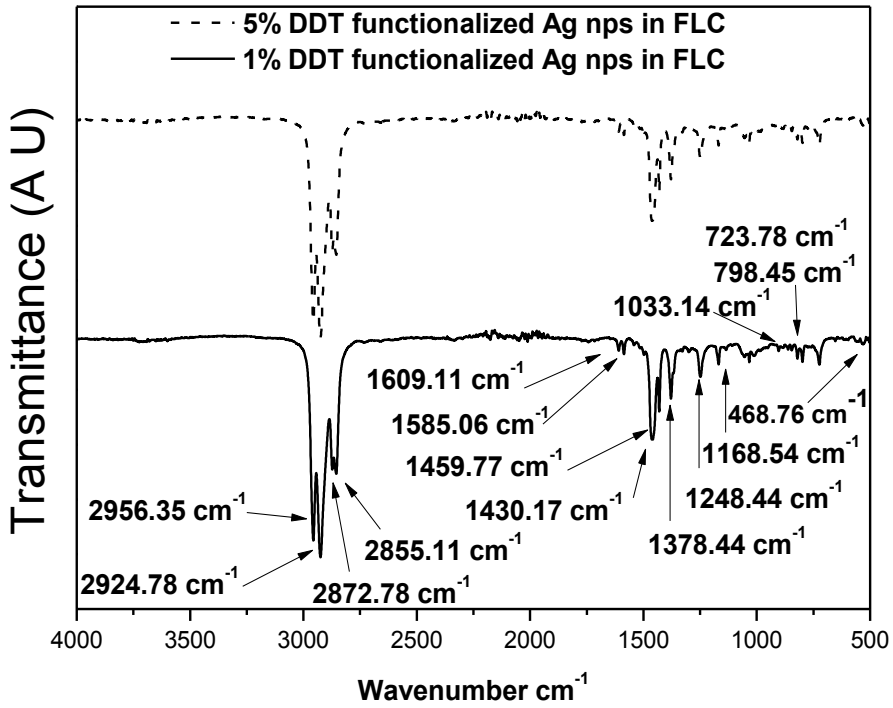

Figure 4.6 FTIR spectras of LB films of (1, 5) wt% of DDT functionalized Ag nano-particles in FLC matrix.

respectively, which are almost similar to LB film of functionalized Ag nano-particles. Absorption at 1585.06 cm^{-1} corresponds to N-H band of FLC. Absorption at 1609.11 cm^{-1} corresponded to C-C aromatic structure of FLC.

Absorptions at 1168.54 cm^{-1} and 1248.44 cm^{-1} corresponded to C–O stretching (C–O–C; 1200–1050 cm^{-1}). Absorption at 798.45 cm^{-1} confirms the presence distinctive (C–Cl; 800–700 cm^{-1}) of FLC molecule. Absorptions at 1459 cm^{-1}, 1430.17 cm^{-1} and 1378 cm^{-1} are due to CH_2 symmetrical and asymmetrical stretching bands of DDT molecule. Absorptions at 1609.11 cm^{-1} and 1585 cm^{-1} and absorption at 1248.44 cm−1 corresponded to Φ–O–C stretch (1270–1230 cm−1), aromatic substitution (Φ) for FLC. Absorptions at 1378.44 cm−1corresponded to aromatic secondary amine C–N stretch. Absorption at 724 cm^{-1} is due to Ag nano particles. All groups present in the FLC and functionalized Ag nano-particles were analyzed by FTIR spectrum [40].

4.5 X-Ray Diffraction Spectroscopy of LB films

Figure 4.7 and figure 4.8 show low angle and wide angle X- Ray diffraction pattern of 11 multilayers of (1,5) wt % composites LB films deposited on glass substrate. In figure 4.7 low angle ($2\theta = 2.5^{o} – 10^{o}$) XRD for (1, 5) wt % of AZO functionalized nano-particles in FLC matrix showed an intense peak at $2\theta = 3.2^{\circ}$, corresponding to the smectic layer ordering of liquid crystal molecules with a layer spacing of ~27.52 Å **[**41]. As the concentration of AZO nano-particles is increased from 1 to 5 wt %, a decrease in intensity was noticed.

In figure 4.8 wide angle range ($2\theta = 10^{o} – 80^{o}$) shows intense peaks at (100), (002), (101), (102), (103), (110), (112) corresponding to ZnO (36-1451 JCPDS) [42, 43]. Broader diffraction peaks observed in range ($2\theta = 20^{o}$- 24^{o}) are from long alkyl chain of octadecylamine, such a lattice can only result from the periodic arrangement of ODA-AZO nano-particles in FLC matrix. From this we conclude that with doping of nano particles, layer structure of liquid crystal matrix is not disturbed.

Figure 4.9 shows low angle X-ray diffraction profile of LB film of (1, 5) wt% functionalized Ag nano-particles in FLC matrix with $2\theta = (2.5^{\circ}$- $5^{o})$ and 4.10 shows wide angle X-ray diffraction profile of LB film of (1, 5) wt% DDT functionalized Ag nano-particles in FLC matrix with $2\theta = (5^{\circ}$- $50^{o})$.

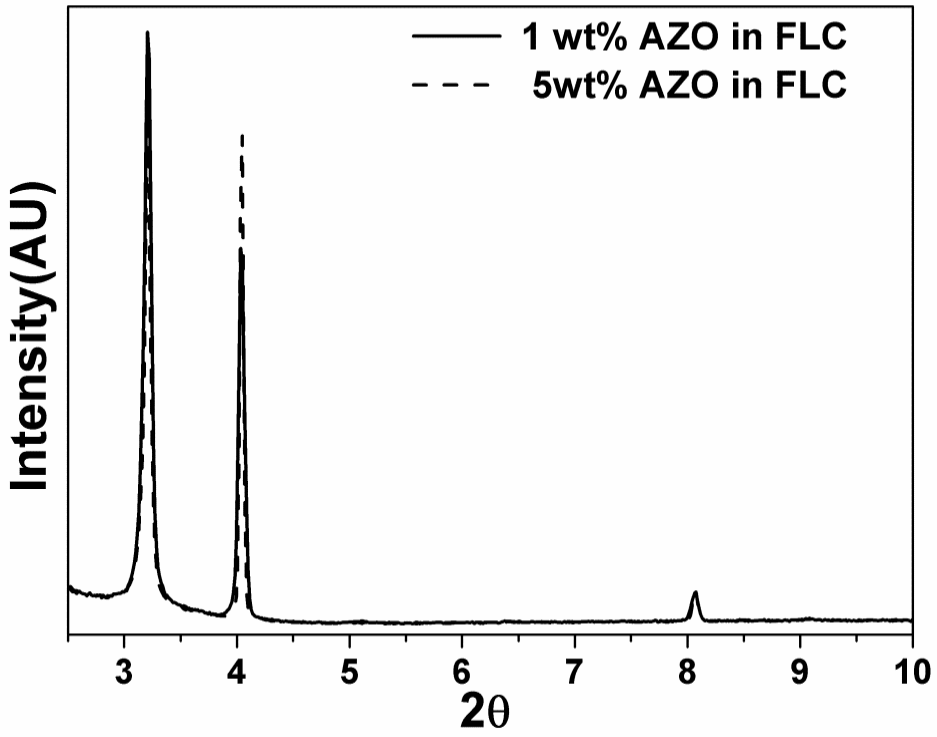

Figure 4.7: Low angle X-ray diffraction profile of (1, 5) wt% functionalized AZO nano-particles in FLC matrix with 2θ = (2.5°-10°).

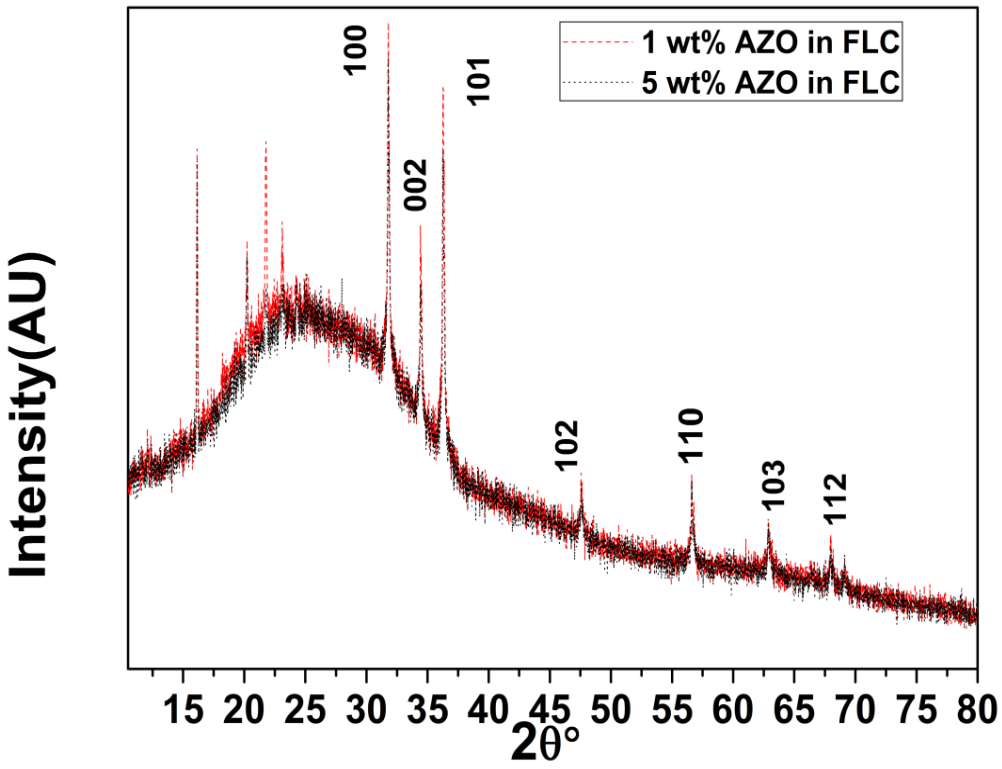

Figure 4.8: Wide angle X-ray diffraction profile of (1, 5) wt% functionalized AZO nano-particles in FLC matrix with 2θ = (10°-80°).

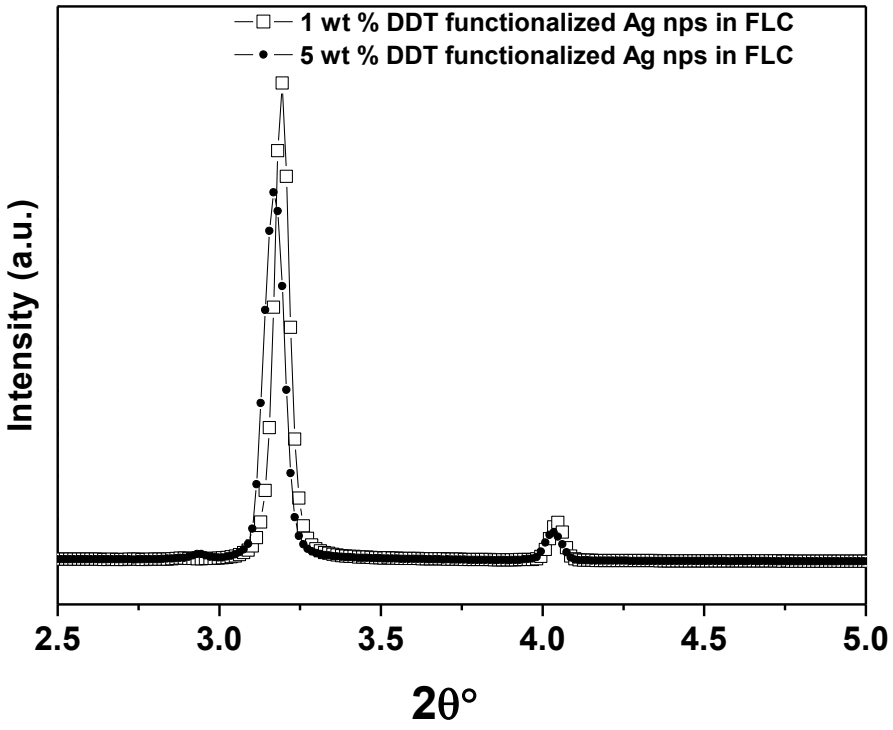

Figure 4.9 Low angle X-ray diffraction profile of LB film of (1, 5) wt% functionalized Ag nano-particles in FLC matrix with 2θ = (2.5°- 5°).

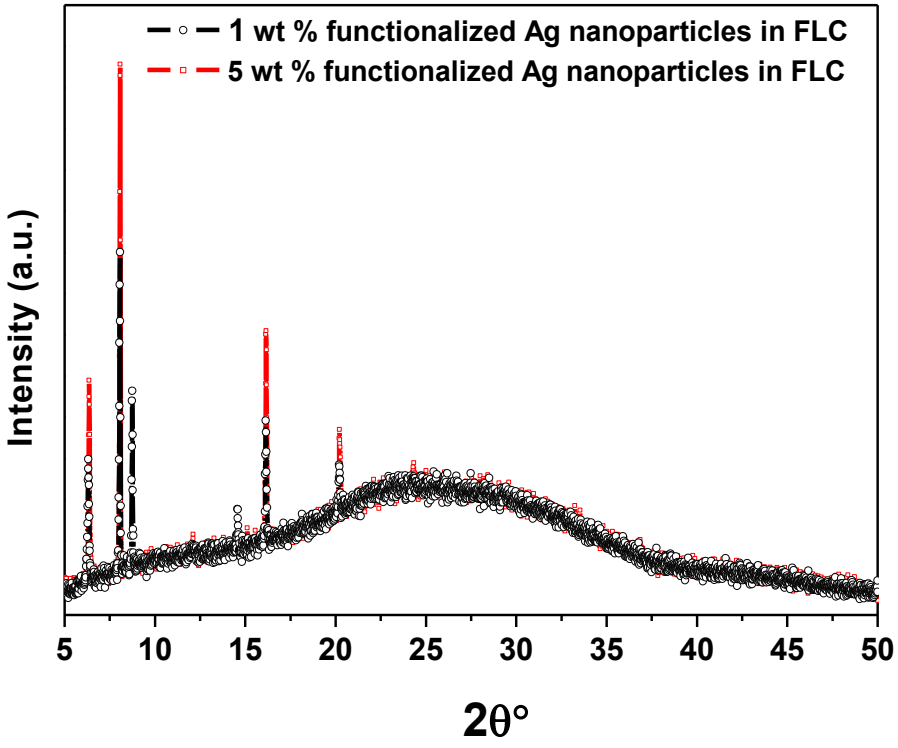

Figure 4.10 Wide angle X-ray diffraction profile of LB film of (1, 5) wt% functionalized Ag nano-particles in FLC matrix with 2θ = (5°- 50°).

In Low angle spectra an intense peak at 2θ = 3.2° and 4° are due to smectic layer ordering of FLC molecules and long dodecyl chain respectively [44]. Peaks at 2θ = 16.15 ° and 20.23° are due to Ag nano-particles (87-0598: JCPDS). Other intense peaks at 6.36°, 7.99°, 8.69° and 14.63° are due to alignment of DDT chains in LB films of composite systems.

4.6 Topographical images of LB films

Atomic force microscopy (AFM) (Solver-NEXT NT-MDT; Zelenograd, Moscow, Russia) was used for topographical investigations of thin films. AFM images were taken in non-contact mode (scan rate 1 Hz) by using Silicon nitride (SiN) probe of tip curvature radius 2 nm was attached to a cantilever (resonance frequency; 87-230 kHz, typical force constant 5.1nN m^{-1}) [45]. The topography data were sampled in a grid of 512 × 512. The imaging was carried out under ambient laboratory conditions. Initially properly cleaned silicon substrate was scanned under AFM and root mean square roughness < 1nm was observed. It ensured smoothness of the silicon and its sustainability for monolayer deposition [46, 47]. AFM images were processed with NOVA P9 Software (Image Analysis 2.1.0.800) which was also used to determine 3-D view and height profiles.

AFM image of LB monolayer of functionalized AZO nano-particles deposited on a single crystal silicon wafer substrate in a scan range 1×1 μm^2 is shown in figure 4.11. The deposition was done at constant surface pressure 42 mN m^{-1}. In image 4.11(i), film of nano-particles appears to be consisting of many grains, having mountain-valley-like morphology. 3-D view of the deposited film is shown in image 4.11(ii), which indicates its uniform deposition. The average size of octadecylamine functionalized AZO nano-particles is lying in 10-35 nm as inferred from figure 4.11(iii).

Figure 4.12 shows AFM image of 1 wt% functionalized AZO nano-particles in FLC deposited at 14 mN m^{-1}. The AFM image of scan range 2×2 μm^2, shown in image 4.12 (i) have elongated ferroelectric liquid crystal domains as well as mountain-valley-like topographical coverage in limited area because of very less weight percent of AZO nano-particles in it and image 4.12(ii) gives a three-dimensional (3D) view, with the roughness parameter along the z-axis. The corresponding average height profile is shown in figure 4.12 (iii), the height profile indicating a roughness ~ 20 nm, which refer to presence of AZO nano-particles and height peaks in the range of 2-3 nm indicate FLC host matrix, which is same as size of FLC molecules [figure 2.9]. Narrower peaks in the height profile are indicative of mono dispersity of AZO nano-particles in FLC matrix.

Figure 4.13 shows image in scan range 5×5 μm^2 for 5wt% mixture, topography of aligned AZO nano-particles along with ferroelectric liquid crystal domains is shown in figure 4.13(i). 3-D view as shown in image 4.13(ii) infer about complex pattern of FLC domains and valley like topography of nano-particles and 4.13(iii) shows average height profile having height ~ 2-20 nm having distinct peaks corresponding , so there is no severe agglomeration of the particles and they remain stabilized and well dispersed in the smectic C phase. The nano-particles appear to be stabilized by repulsive interactions between functionalized nano-particles forming stable dispersions in the SmC* phase [48].

Figure 4.14 shows atomic force microscopic images of functionalized Ag nano-particles deposited at 29 mN m^{-1} on single crystal silicon wafer. 4.14 (a) shows 5 × 5 μm^2 2-D image, 4.14 (b) shows 3-D view and 4.14 (c) shows height profile. Topography of film reveals that nano particles are well separated from its neighbouring nano-particles, indicating that Ag nano-particles are well functionalized by dodecanethiol molecules. 3D view shows that height of nano-particles monolayer lies between 6-10 nm, similar profile is shown by height image.

Figure 4.15 shows AFM images of 1 wt% DDT-functionalized Ag nano-particles in FLC matrix deposited at 12 mN m^{-1} on single crystal silicon wafer. 4.15(a) shows 5 × 5 μm^2 2D image which shows average contrast of deposition up to 8nm, 4.15 (b) shows 3-D view and 4.15(c) shows average height profile, red lines in height profile indicate peaks at 2.3nm are due to FLC and peaks up to 6-7 nm are due to functionalized Ag nano-particles. The AFM images show that there is no severe agglomeration of the particles and they remain stabilized and well dispersed in the smectic C phase.Raised humps region in figure 4.15(b) are due to individual nano-particles. The nano-particles in FLC matrix are stabilized due to repulsive interactions among them.

Figure 4.16 shows images of 5 wt% functionalized Ag nano-particles in FLC deposited at 24 mN m^{-1} on single crystal silicon wafer. 4.16(a), 4.16(b) and 4.16(c) show 5 × 5 μm^2 2-D image, 3-D view of deposited LB film and average height profile respectively. It is similar to 1 wt% nano-particles in FLC matrix, with increase in concentration density of nano-particles is increased in imaging area. As FLC domains are clearly observed in images of composite systems, it indicate translation behaviour of FLC remain unaltered with low concentration doping.

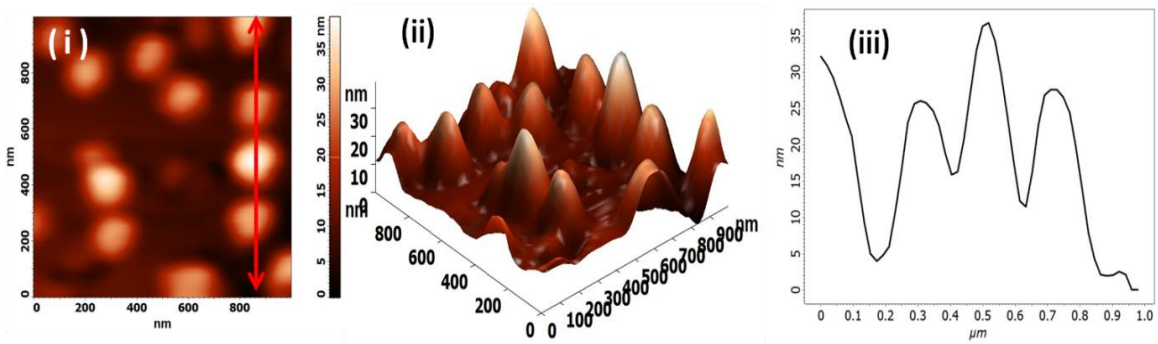

Figure 4.11: Atomic force microscopic images of functionalized AZO nano-particles deposited at 42.0 mNm^{-1} on single crystal silicon wafer. (i) 1 ×1 μm^2 2-D image (ii) 3-D view and (iii) shows average height profile.

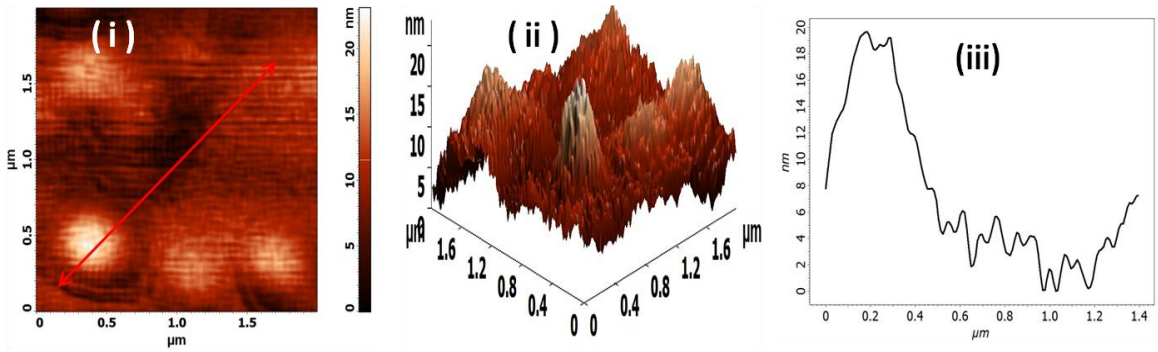

Figure 4.12: Images of 1 wt% ODA-functionalized SWCNTs in FLC deposited at 14 mN m^{-1}on single crystal silicon wafer. (i) It shows 2 × 2 μm^2 2D image, (ii) shows 3-D view and (iii) shows average height profile.

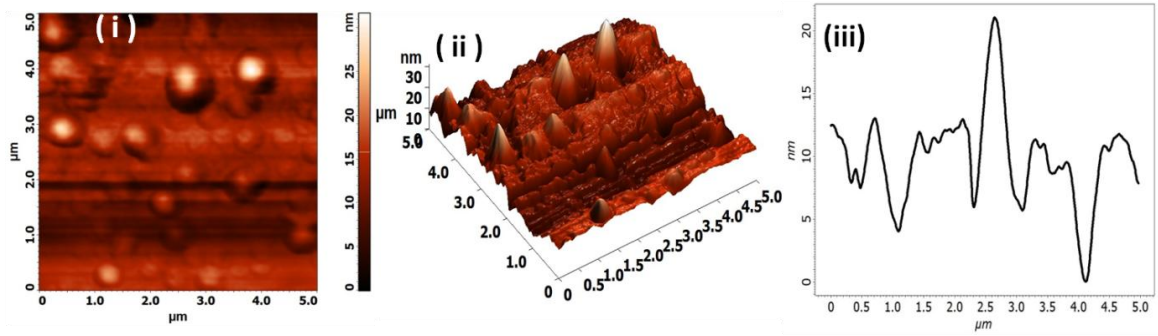

Figure 4.13: Images of 5 wt% functionalized AZO nano-particles in FLC deposited at 30 mN m^{-1} on single crystal silicon wafer. (i), (ii) and (iii) show 5 × 5 μm^2 2-D image, 3-D view of deposited LB film and average height profile, respectively.

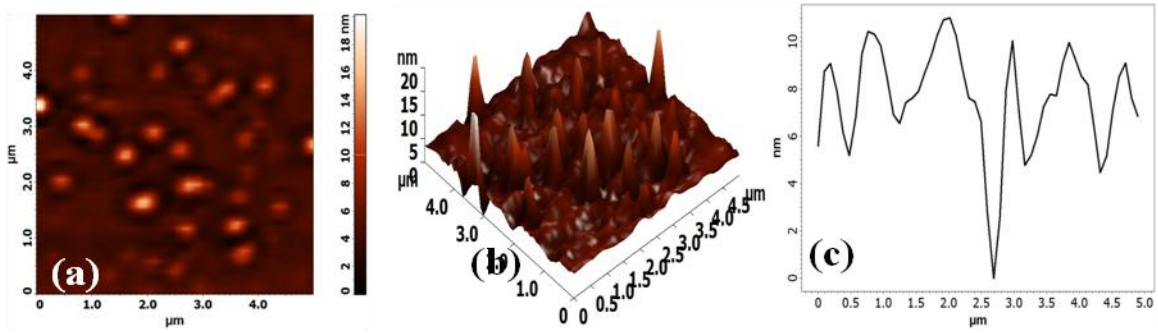

Figure 4.14 Atomic force microscopic images of functionalized Ag nano-particles deposited at 29 mN m^{-1} on single crystal silicon wafer. (a) 5 × 5 μm^2 2-D image (b) 3-D view and (c) shows height profile.

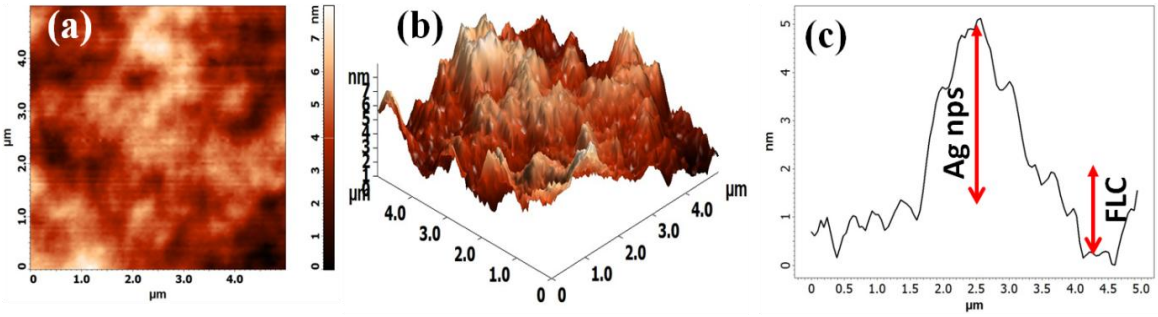

Figure 4.15: Images of 1 wt% DDT-functionalized Ag nano-particles in FLC deposited at 12 mN m^{-1} on single crystal silicon wafer. (a) It shows 5 × 5 μm^2 2D image, (b) shows 3-D view and (c) shows height profile.

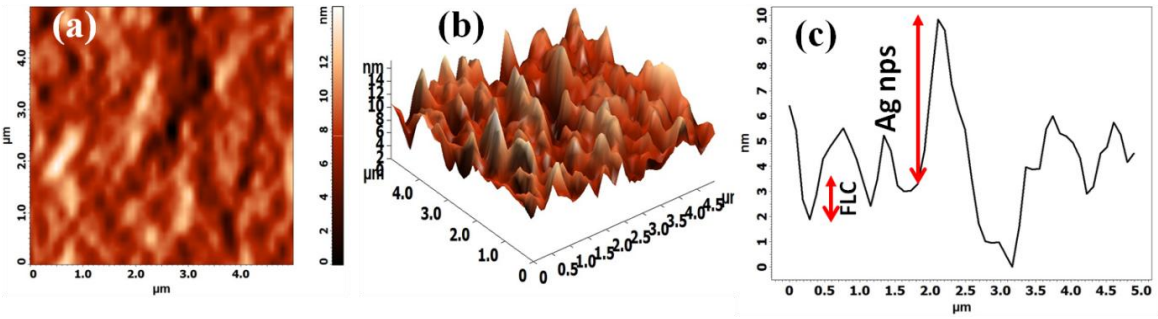

Figure 4.16: Images of 5 wt% DDT-functionalized Ag nano-particles in FLC deposited at 24 mN m^{-1} on single crystal silicon wafer. (a) It shows 5 × 5 μm^2 2D image, (b) shows 3-D view and (c) shows height profile.

Doping of nano-particles in liquid crystal matrix also help in alignment of host molecules at substrate. This aspect of composites systems is expected to have their applications in optical devices.

4.7 Conclusions

We have successfully prepared uniform Langmuir Blodgett films of functionalized AZO and functionalized Ag nano-particles. They form stable monolayers at air–water interface and stability is enhanced due to strong interaction between alkyl chains of functionalized nano-particles with the FLC molecules. LB films of nano-particles-FLC composite system have been transferred to substrates. X-Ray diffraction profile confirms dispersion of nano-particles in FLC matrix, without disturbing the SmC^* layer structure (translation behaviour) of FLC. Similar results are interpreted from AFM images of LB films. These well organized composite films can have variety of applications in sensors and optical devices.

References

1 D P Singh, S K Gupta, K K Pandey, S P Yadav, M C Varia, R Manohar. Ferroelectric liquid crystal matrix dispersed with Cu doped ZnO nanoparticles.J. Non-Cryst. Solids. 2013, **363**.178.

2 S K Gupta, D P Singh, R Manohar. Electrical and polarization behaviour of titania nanoparticles doped ferroelectric liquid crystal. Adv. Mater. Lett. 2015, **6(1)**, 68.

3 A Chandran, J Prakash, P Ganguly, Biradar. A M Zirconia nanoparticles/ ferroelectric liquid crystal composites for ionic impurity-free memory applications. **RSC Adv.** 2013, **3**, 17166.

4 A Chaudhary , P Malik, R Mehra, K K Raina. Electro-optic and dielectric studies of silica 88anoparticles doped ferroelectric liquid crystal in SmC* phase. Phase Transit Multinat J. 2012, **85(3)**, 244.

5 A Chaudhary , P Malik, R Mehra, K K Raina. Observation of memory behaviour in cadmium sulphide nanorods doped ferroelectric liquid crystal mixture. Phase Transit Multinat J. 2013, **86(12)**, 1256.

6 Neeraj , K K Raina. Influence of silica nanoparticles on dielectric spectroscopy and polarization switching responses of novel ferroelectric liquid crystals. Phase Transitions: A Multinational Journal.2010, **83(8)**, 615.

7 H H Liang, Y Z Xiao, F J Hsh, C C Wu, J Y Lee. Enhancing the electro-optical properties of ferroelectric liquid crystals by doping ferroelectric nanoparticles. Liq Cryst. 2010, **37(3)**, 255.

8 J L West, F Li, K Zhang, H Matkuri, A V Glushchenko. Electro-Optic properties of Ferroelectric Nanoparticle / Liquid Crystal Dispersions. Sid. Int. Symp. Dig. Tec. 2012, **38(1)**, 1090.

9 P Kr Tripathi, A Kr Misra, K Kr Pandey, R Manohar. Study on Dielectric and Optical Properties of ZnO Doped Nematic Liquid Crystal in Low Frequency Region. Chem. Rapid Commun. 2013, **1(1)**, 20.

10 Y S Ha, H J Kim, H GPark, D S Seo. Enhancement of electro-optic properties in liquid crystal devices via titanium nanoparticle doping. Optics Exp. 2012, **20(6)**, 6448.

11 J Hu, R G Gordon. Textured aluminum-doped zinc oxide thin films from atmospheric pressure chemical-vapor deposition. J. Appl. Phys. 1992, **71 (2)**, 880.

12 C S Hsi, B Houng, B Y Hou, G J Chen, S L Fu. Effect of Ru addition on the properties of Al-doped ZnO thin films prepared by radio frequency magnetron sputtering on polyethylene terephthalate substrate. J. Alloys Compd. 2008, **464 (1-2)**, 89.

13 M M Suzana, T Alexandra, A Mihai, G Mihai, P. Jr Traian, S Mihai, M Zaharescu . Al-doped and undoped zinc oxide films obtained by soft chemistry. Processing and Application of Ceramics.2009, **3(1-2)**, 79.

14 B Y Oh, M C Jeong, W Lee, Myoung JM. Properties of transparent conductive ZnO:Al films prepared by co-sputtering. J. Crys. Growth. 2005, **274**, 453.

15 O Yaroshchuk, A Kadashchuk. Liquid crystal photoalignment properties of polymethylphen- ylsilane. Appl. Surf. Sci. 2000, **158 (3-4)**, 357.

16 V G Chigrinov, V M Kozenkov, H S Kwok. Photoalignment of Liquid Crystalline Materials: Physics and Applications. Wiley, New York, USA 2008.

17 I Stoica, A I Barzic, C Hulubei. The impact of rubbing fabric type on surface roughness and tribological properties of some semi-alicyclic polyimides evaluated from atomic force measurements. Appl. Surf. Sci. 2013, **268**, 442.

18 S H Kim, L C Chien. Electro-Optical Characteristics and Morphology of a Bend

Nematic Liquid Crystal Device Having Templated Polymer Fibrils. Jpn. J. Appl. Phys. 2004, **43(11A)**, 7643.

19 Z Wu, P E Powers, A M Sarangan, Q Zhan. Optical characterization of wire grid micropolarizers designed for infrared imaging polarimetry. Opt. Lett. 2008, **33(15)**, 1653.

20 W Y Teng, S C Jeng, J M Ding, C W Kuo, W K Chin. Flexible Homeotropic Liquid Crystal Displays Using Low-Glass-Transition-Temperature Poly(ethylene terephthalate) Substrates. Jpn. J. Appl. Phys. 2010, **49(1)**, 010205.

21 T Maeda, K Hiroshima. Vertically Aligned Nematic Liquid Crystal on Anodic Porous Alumina. Jpn. J. Appl. Phys. 2004, **43(8A)**, L1004.

22 T Maeda, K Hiroshima. Tilted Liquid Crystal Alignment on Asymmetrically Grooved Porous Alumina Film, Jpn. J. Appl. Phys.2005, **44(26)**, L845.

23 C Hong, T T Tang, C Y Hung, R P Pan, W Fang. Liquid crystal alignment in nanoporous anodic aluminum oxide layer for LCD panel applications. Nanotechnology. 2010, **21(28)**, 285201.

24 R Kaur, G K Bhullar, K K Raina. Behaviour of an ultrathin ferroelectric liquid crystal Langmuir–Blodgett film at an air–water and air–solid interface. Liq Cryst. 2012, **39**, 1375.

25 J E Wong, B Donnio, D W Brucec, T H Richardson. Optical and structural studies of Langmuir–Blodgett films of polyalkoxystilbazole complexes of iridium(I). Appl. Surf. Sci. 2005, **246**, 451.

26 F J Pavinatto, A F Jr. Gameiro, A A Hidalgo, L R Dinelli, L L Romualdo, A A Batista, Barbosa Neto N M, Ferreira M, O N Oliveira, Jr. Langmuir and Langmuir–Blodgett (LB) films of tetrapyridyl metalloporphyrins. Appl. Surf. Sci. 2008, **254**, 5946.

27 K Meral, H Y Erbil, Y Onganer. A spectroscopic study of water-soluble pyronin B and pyronin Y in Langmuir–Blodgett films mixed with stearic acid. Appl. Surf. Sci. 2011, **258,** 1605.

28 K Sankaranarayanan, B U Nair, A Dhathathreyan. Anomalous conformational transitions in cytochrome C adsorbing to Langmuir–Blodgett films. Appl. Surf. Sci. 2013, **273**, 75.

29 K Inglot, T Martyński , D Bauman. Influence of the alkyl chain length of some mesogenic molecules on their Langmuir film formation ability. Liq Cryst.2006, **33(7)**, 855.

30 T Martynski, R Hertmanowski, D Bauman. Molecular organization in two-dimensional films of liquid crystalline mixtures III. Langmuir films of binary mixtures of liquid crystal materials with terminal CN or NCS group. Liq Cryst. 2002, **29 (1)**, 99.

31 T Martynski, R Hertmanowski, D Bauman. Molecular organization in two-dimensional films of liquid I. Langmuir films of binary mixtures of liquid crystals with a crystalline mixtures terminal cyano group, Liq Cryst.2001, **28(3)**, 437.

32 U B Singh, R Dhar, R Dabrowski, M B Pandey. Influence of low concentration silver nanoparticles on the electrical and electro-optical parameters of nematic liquid crystals. Liq Cryst. 2013, **6(13)**, 774.

33 S K Gupta, D P Singh, P K Tripathi, R Manohar, M Varia, L K Sagar, S Kumar. CdSe quantum dot-dispersed DOBAMBC: an electro-optical study.Liq Cryst. 2013, **40 (4)**, 528.

34 R K Shukla, K K Raina, W Haase. Fast switching response and dielectric behaviour of fullerene ferroelectric liquid crystal nano colloids. Liq Cryst. 2014, **41(12)**, 1726.

35 R Kaur, K K Raina. Influence of single-wall carbon nanotubes on Langmuir–

Blodgett films of ferroelectric liquid crystals as studied by atomic force microscopy. Liq Cryst. 2014, **41**, 1065.

36 L J Bellamy. Infrared Spectra of Complex Molecules, Chapman and Hall, New York, USA, 1975.

37 G Socrates. Infrared Characteristic Group Frequencies, Wiley, New York, USA, 1980.

38 L Moa, D Liua, W Li, L Li, L Wang, X Zhoua. Effects of dodecylamine and dodecanethiol on the conductive properties of nano-Ag films. App. Surface Sci. 2011, **257**, 5746.

39 I Zalakain, N Politakos, J A Ramos, R Fernandez, H Etxeberria, I Mondragon, M A Corcuera, A Eceiza. Synthesis and incorporation of dodecanethiol capped silver nanoparticles into poly(styrene-b-isoprene-b-styrene) block copolymer and their influence in the morphology. Coll. and Surf. A: Physicochem. Eng. Aspects 2013,**436**,170.

40 N B Colthup, L H Daly, S E Wiberley. Introduction to Infrared and Raman Spectroscopy, Academic Press: San Diego, CA, USA, 1990.

41 E Olbrich, O Marinov, D Davidov . Phys. Rev.E: Stat.. Nonlinear, Soft Matter Phys. 1993, **48**, 2317.

42 S Okada, H Matsuda, H Nakanishi, M Kato, Inventors; Agency of Industrial Science & Technology, Ministry of International Trade and Industry, assignee. Method using X-Ray to determine thickness of organic films. United States patent **US 5003569**, 1991.

43 M Suchea, S Christoulakis, N Katsarakis, T Kitsopoulos, G Kiriakidis. Comparative study of zinc oxide and aluminum doped zinc oxide transparent thin films grown by direct current magnetron sputtering. Thin Solid Films. 2007, **515 (16)**, 6562.

44 C J L Constantino, A Dhanabalan, O N Oliveira. Experimental artifacts in the surface pressure measurement for lignin monolayers in Langmuir troughs. Review of Scientific Instruments. 1999, **70**, 3674.

45 G K Bhullar, R Kaur, K K Raina, Hybrid Polyaniline–TiO2 Nanocomposite Langmuir–Blodgett Thin Films: Self-Assembly and Their Characterization. J Appl Polym Sci. 2015, **135(5),1**.

46 B W Lee, D R Link, N A Clark. Atomic Force Microscopy of freely suspended liquid crystal films transferred to octadecyltriethoxysilane self-assembled monolayers. Liq. Cryst. 2000, **27(4)**, 501.

47 R Kaur, G K Bhullar, N V S Rao, K K Raina. Effect of pH on the control of molecular orientation in monolayer of bent-core liquid crystal materials by Langmuir–Blodgett method. Liq Cryst. 2014, **42(1)**, 8.

48 R Pratibha, K Park, I I Smalyukh, W Park. Tunable optical metamaterial based on liquid crystal-gold nanosphere composite. Optics Express. 2009, **17(22)**, 19459.

Chapter 5

Effect of pH on the control of molecular orientation in monolayer of bent-core liquid crystal materials by Langmuir–Blodgett method

Overview

Control of molecular orientation at the substrate surface is significant to understand the surface science. Langmuir-Blodgett films of bent-core liquid crystals having alkyl chains at both ends were deposited on silicon substrate. Studies were carried out on air–water interface by changing pH of the subphase. On compression, molecules were arranged in stacks at high pH where as uniform monolayer was formed at lower pH. Limiting area gets increased at low pH, which resulted in the formation of monolayer after attaining a sustainable surface pressure. Langmuir films were transferred to silicon substrate, and atomic force microscopy images showed appropriate height profiles.

5.1 Introduction

The understanding of the molecular orientation distribution in organic thin films is not only of fundamental interest but also of practical importance for designing organic materials for optoelectronics and other device applications. Different kinds of organic materials have been extensively studied for understanding physical and chemical properties with regard to their molecular orientations [1–6].

Liquid crystals that have hydrophilic organic functional groups and hydrophobic alkyl chains are capable to form Langmuir monolayers at air–water interface [7–13]. This balance of hydrophillicity and hydrophobicity governs the stability of Langmuir films. Among LCs, bent-shaped liquid crystal molecules have attracted attention of both chemists and physicists. It is due to their extraordinary characteristics, including spontaneous supramolecular chirality, ferroelectricity and anti-ferroelectricity, electro-optic switching and exotic phases. The crucial prerequisite for achieving polar order and chirality in any of the materials is that the individual constituent molecule should possess a bent shape in the central core and form smectic layers in which the molecular planes are tilted, resulting in a spontaneously chiral architecture.

Efforts have been made to deposit LB films of rod-shaped liquid crystals in chapter 3, but it has been difficult to align bent-core molecules. In order to form their homogenous monolayer, researchers have used several methods to form composite films with long chain amphiphilic molecule and by mixing bent core molecules with 8CB [14, 15] but these mixed films exhibit different physicochemical properties. Few reports focused particularly on the interfacial behaviour of such molecules only at the air–water interface [16–21].

In this chapter, we have aligned pure monolayer of bent-core liquid crystal molecules with different end alkyl chains by varying pH of the subphase.

1 mg ml^{-1} solutions of **BC1** and **BC2** bent core liquid crystal in chloroform were obtained by ultra sonicating the mixtures for half an hour separately. 50 µl of each solution was spread drop wise on the aqueous surface using a Hamilton micro syringe held very close to the aqueous surface separately, Milli-Q filtered water (pH = 6.00) contained in the LB trough, and then the solvent was allowed to completely evaporate over a period of 15 minutes before compression of the monolayer at a constant sweeping @ 5 mm min^{-1} using derlin (polyactelylene) barriers. Then sub phase was replaced with 0.1mM solution of HCℓ in water to attain pH = 4 and 0.01 M solution of HCℓ in water to

attain pH=2 [27]. Again solutions of **BC1** and **BC2** in chloroform was spread at these pH values. pH measuring probe for KSV NIMA System (KN 0011) was attached through interface.

5.2 Π-A isotherms:

Surface pressure-area (Π-A) isotherms were plotted to study alignment of molecules at air-water interface [23]. Figure 5.1 shows the typical surface pressure profiles of bent core liquid crystalline molecule (**BC1**) as a function of area per molecule at three different sub phase pH levels. [Inset levels (**a**), (**b**), (**c**) represent hypothetical illustration to explain molecular orientation at different stages of compression.

At pH=6, compression of the monolayer @ 5mm min^{-1} for **BC1** molecule is initiated. The isotherm has a shoulder region within 65-45 A^{02}/molecule and surface pressure remains nearly at surface pressure value 0 mN m^{-1} asymptotically. We believe that the molecules lie flat on the surface even up to 45 A^{02}/molecule [inset level (a)] and they float on the water surface where as surroundings still remain in gaseous phase so the surface pressure does not increases from 0mN m^{-1} [24].

From the molecular structures we know that single molecule covers an area ~ 50.99 A^{02}. As a result of compression, molecular rearrangement has taken place among the molecules, and layers become thicker. As the area per molecule approaches 41 A^{02}/molecule, surface pressure starts increasing, thus molecules combine to form stacks [inset level (b)]. Limiting area for isotherm is obtained by extrapolating isotherm curve to zero surface pressure and the limiting area ($\mathbf{a_1}$) was attained at 40 A^{02}.

At pH=6, at – OOC group attached to phenyl rings in core will be negatively charge forming carboxylate ion (COO^-) , this negative charge will be delocalised at phenyl ring and both oxygen of carbonyl group. Hydroxyl group will also attain negative charge by deprotonation [25, 26]. On the other hand secondary amine ($–NH^+$) being weak base, it will accept proton from sub phase and attain positive charge on it. These charges produce partial dissociation of the core, which resulted in mixing at molecular scale. The charge interactions between the cores lead to the suppression of the phase separation and increase resistance to the compression [27, 28].

Hence, isotherm shifts toward lower molecular areas which have been resulted due to formation of molecular stacks on the sub phase.

At pH = 4 and 2, H_3O^+ and $C\ell^-$ ions are present at the interface. In this situation $-COO^-$ ion will pick up proton and form a molecule having net positive charge on secondary amine. It will make core as cation. Counter ions $C\ell^-$ present at interface, interact strongly with cation, chains being hydrophobic will be repelled upward from the sub phase [inset level (**c**)]. So this electrostatic interaction has resulted in the formation of new phase at the interface. It has modified the structure of the films. Secondary amines are weak bases, when carbon chains and core will get affinity from Si substrate then the $-NH^+$ will leave proton and monolayer will be transferred to substrate [27].

At pH=4, 2 we noticed that the surface pressure rose steeply for these molecules even at higher areas per molecule. Because central core of molecules to have good contact with the water surface due to presence of $C\ell^-$ ions, whereas the end chains are flexible and prone to leave it. This way, the molecules form monolayer at air-water interface. At pH=4, limiting area (**a_2**) was at 52.50 A^{02}/molecule where as pH=2, limiting area (**a_3**) was at 62.5 A^{02}/molecule. It shows that with decrease in pH, limiting area is increased. We infer that at lower compression, high surface pressure is achieved.

Figure 5.2 shows Π-A isotherm in case of bent core molecule **BC2** we notice that at pH=6, multilayer stacks are formed at air-water interface after passing through shoulder region (60-45 A^{02}/ molecule). Due to the affinity of core with water, molecule tends to align flat on its surface. Since **BC1** and **BC2** molecules have different length alkyl chains substituted at the ends, different inner angle of the central benzene ring of the core, it affects both configuration and stability of the molecule at the surface, as well as the way in which these molecules stack to form layers. At pH=4 and 2 for **BC2** molecules, surface pressure starts increasing at 60 A^{02}/ molecule. The well aligned monolayer is formed at air-water interface. Limiting areas A_1=39 A^{02}/ molecule, A_2= 57 A^{02}/ molecule and A_3= 60 A^{02}/ molecule are observed at pH=6, 4 and 2 respectively. It is seen that at pH=6, limiting area is less and as we decrease the sub phase pH limiting area moves to the higher values.

It is interesting to see that length of alkyl chains of **BC1** and **BC2** molecules are influencing monolayer formation at air-water interface. We revealed from isotherm data that the work of compression by barriers is dependent on alkyl chain lengths at edges of bent core liquid crystal molecules. **BC1** has smaller alkyl chain length as compared to **BC2**, hence **BC1** has smaller limiting area as compared to **BC2**, and less work is done by the barriers for aligning **BC2** molecules. Stability of molecules also depends upon length of alkyl chains. Molecules having longer alkyl chains will form a stable monolayer at

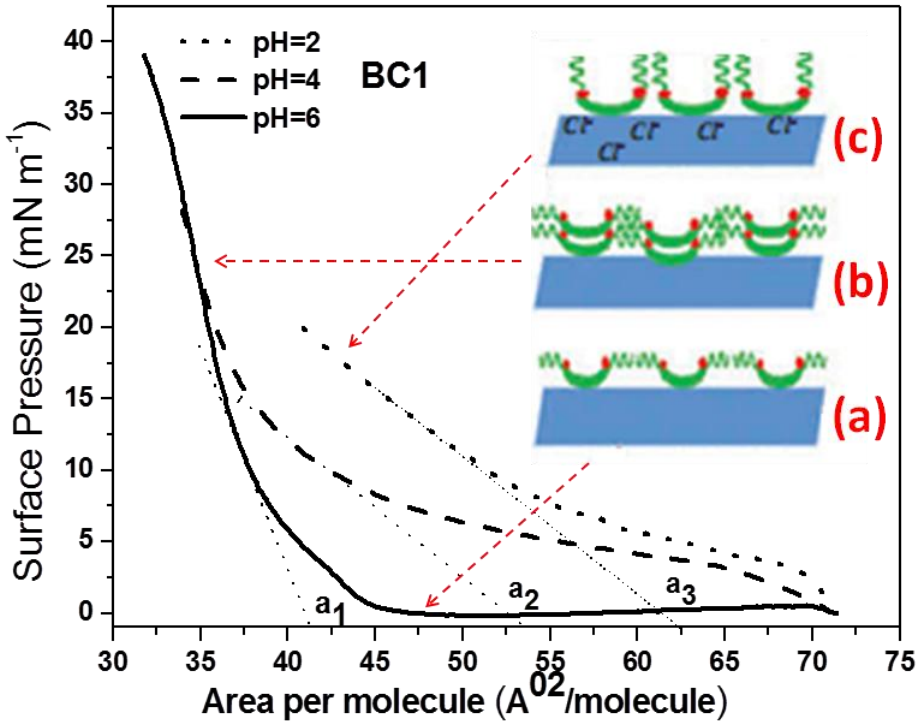

Figure 5.1 Compression isotherms of **BC1** molecules at three different sub phase pH = 6, 4 and 2 levels.

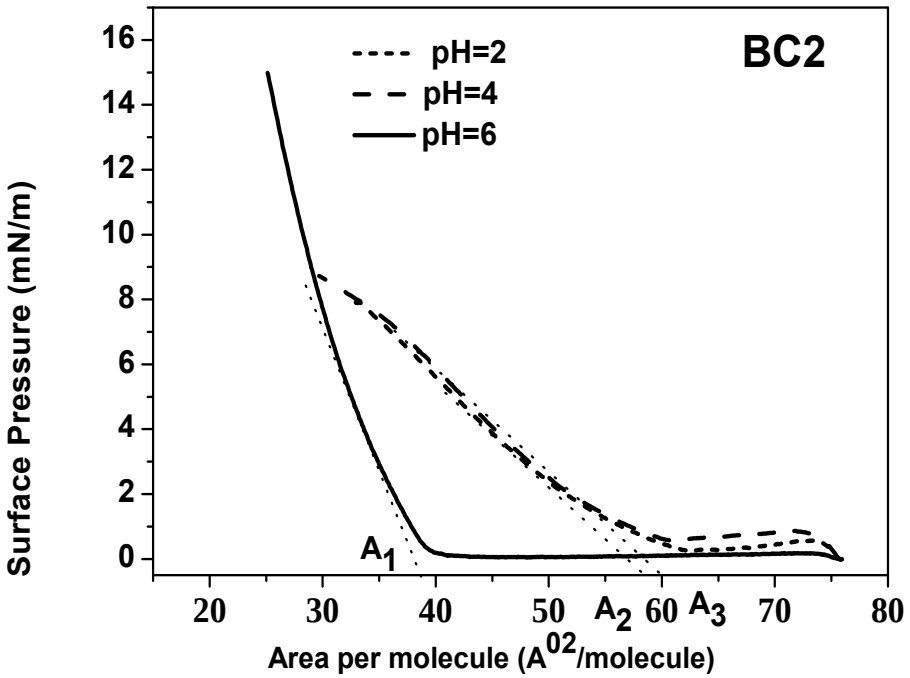

Figure 5.2: Compression isotherms of **BC2** molecules at three different sub phase pH = 6, 4 and 2 levels.

lower surface pressures as compared to smaller alkyl chain molecules, because the Van der Waals interactions between the chains is a major stabilizing factor. As we can see **BC1** has shorter alkyl chain lengths on edges, monolayers become stable to higher pressures as compared to **BC2** molecules [29, 30]. This isotherm data is supported with surface elasticity calculations and AFM topography results.

5.3 Surface pressure versus time plot and surface elasticity of Langmuir monolayer

The variation of surface pressure as a function of time at constant area is shown in figure 5.3 (a, b) for **BC1** and **BC2** molecules respectively. It measure the stability of monolayer when barriers are in compressed state, a nearly stable surface pressure with time is attained at constant area per molecule. The molecular area drop is negligibly small; it may be due to minimal reorganization of the monolayer under pressure over time (~ 1 hour) and due to the evaporation of the aqueous sub phase [31]. Films were transferred to the substrate at constant surface pressure 20 mN m^{-1} for **BC1** molecules and 8 mN m^{-1} for **BC2** molecules. The films were deposited at same surface pressure which ensures that topography will reveal information on account of sub phase pH, not due to barrier compression. During the deposition process number of molecules at air-water interface decreased as they are attached to silicon substrate and barriers automatically move closer to adjust this surface pressure. The deposition ratio was very close to unity on each substrate which indicates good transfer of molecules.

In order to understand the nature of phase transformation behaviour, we attempt to evaluate the surface elasticity (E_o) of the Langmuir monolayer [32-34] which is given by:

$$\mathbf{E_o} = -A_m \frac{d\pi}{dA_m}$$

where Π is the surface pressure of the monolayer and A_m is the area per molecule in the monolayer. Surface elasticity (E_o) is the representing a rheological quantity related to the monolayer rigidity and to its capability to store elastic energy. The compression of the monolayer is performed at a sufficiently low rate to ensure that the system is always in a stationary state and possible relaxation processes in the monolayer can be neglected.

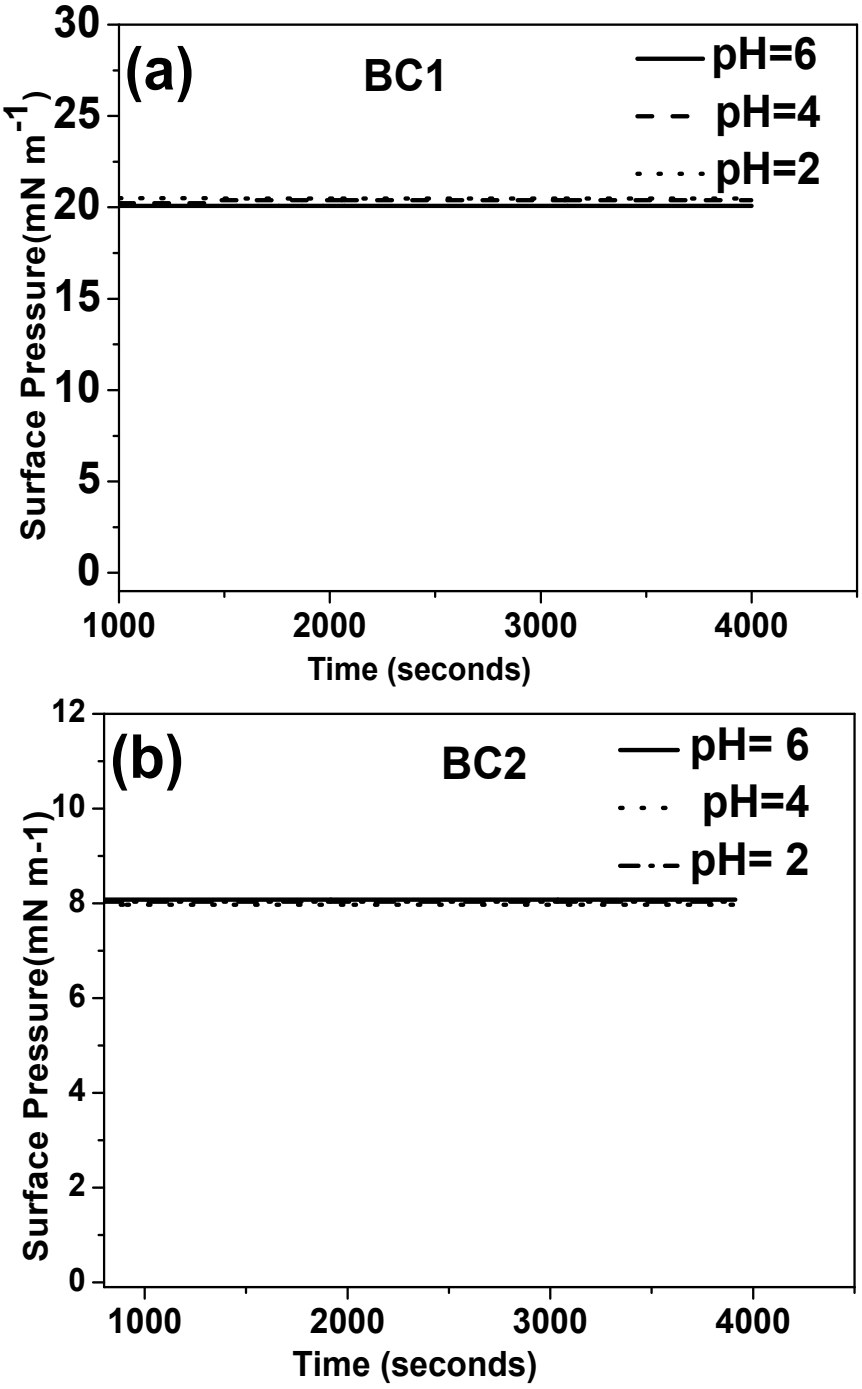

Figure 5.3: Surface pressure as a function of time at constant area (a) shows that **BC1** forms a stabilised layer at air–water interface at 20 m Nm^{-1}.(b) **BC2** molecule has ESP nearly at 8 m Nm^{-1}.

The variation of surface elasticity E_o with A_m for **BC1** and **BC2** are shown in figure 5.4 (a, b) respectively. The minima in the surface elasticity plot represent coexistences of different phases in the monolayer. Elasticity increases with formation of new phase and reaches a maximum at the maximum packing density in the new phase. Generally this new phase is condensed phase having well patterned monolayer at air-water interface. The E_o maxima in the condensed state for sub phase pH 6 for **BC1** molecule was at 33.47 A^{02} and when sub phase pH was reduced to 4, 2 maxima peak was attained at 41.89 A^{02} and 59.46 A^{02} respectively. Thus peak of E_o represent formation of condensed phase, at lower value of pH condensed monolayer was formed.

Similarly, surface elasticity for **BC2** molecule is shown in Figure 5.4 (b). E_o maxima for pH= 6, 4, 2 are attained at 31.99 A^{02}, 60.30 A^{02}, 73.05 A^{02} respectively. We infer that on lowering the sub phase pH monolayers are formed when barriers were compressed to lesser extent.

5.4 Imaging with AFM

Atomic force microscopy (AFM) (Solver-NEXT NT-MDT; Zelenograd, Moscow, Russia) was used for topographical investigations of the thin films. AFM images were taken in non-contact mode (scan rate 1 Hz). Silicon nitride (SiN) probe of tip curvature radius 2 nm was attached to a cantilever (resonance frequency; 87-230 kHz, typical force constant 5.1nN m^{-1}). The topography data were sampled in a grid of 512 × 512 points or 1024 ×1024 points. The imaging was carried out under ambient laboratory conditions. Initially properly cleaned silicon substrate was scanned under AFM and root mean square roughness < 1nm was observed. It ensured smoothness of the silicon and its sustainability for monolayer deposition.

LB films were prepared by vertical dipping into the sub phase at a constant surface pressure. The Si substrate was first immersed and then extracted from the sub phase, the transfer rate was 5 mm min^{-1} for all pH levels. This is automatically done by the deposition KSV NIMA-LB software. Transfer ratio was close to 1.0 for all depositions and then films were dried in vacuum desicators before imaging. AFM images were processed with NOVA P9 Software (Image Analysis 2.1.0.800) which was used also to determine 3-D view and height profiles.

At pH = 6 with compression of barrier, area per molecule decreases and the structure

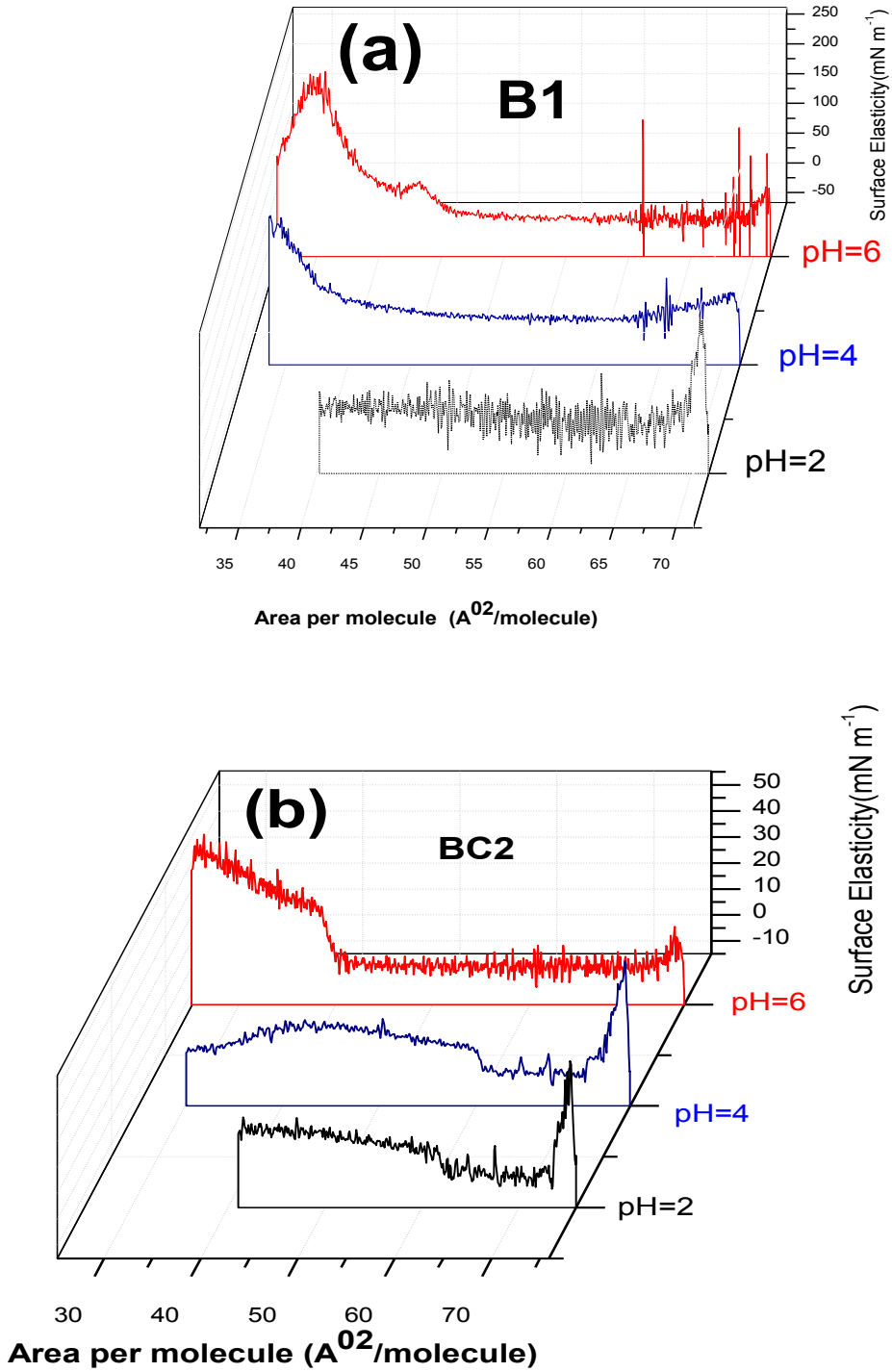

Figure 5.4: Surface elasticity profiles as a function of area per molecule (a and b) for **BC1** and **BC2** molecules respectively.

become more compact. As inferred from isotherm data, stable surface pressure of ($20 mNm^{-1}$) was due to 3-D network formed by molecular stacks, on the same track AFM show bright images, suggesting an overlapping of molecules [21, 35]. It forms a granular structure having height about 2-16 nm as shown in figure 5.5. Figure 5.5(a) represent $10\times10\ \mu m^2$ image of **BC1** molecule deposited at $20 mNm^{-1}$, a 3D image and height profile also indicate formation of layer pattern on Si substrate. Figure 5.5 (b) elaborate topography at $5\times5\ \mu m^2$, 3-D view and height profile indicate that molecules are showing height in the range of 2-16 nm, which is quite larger than size of bent core molecule (4.1nm). It confirms nano-metric molecules agglomerate in a layering pattern on the substrate with non uniform height varying in 2-16 nm.

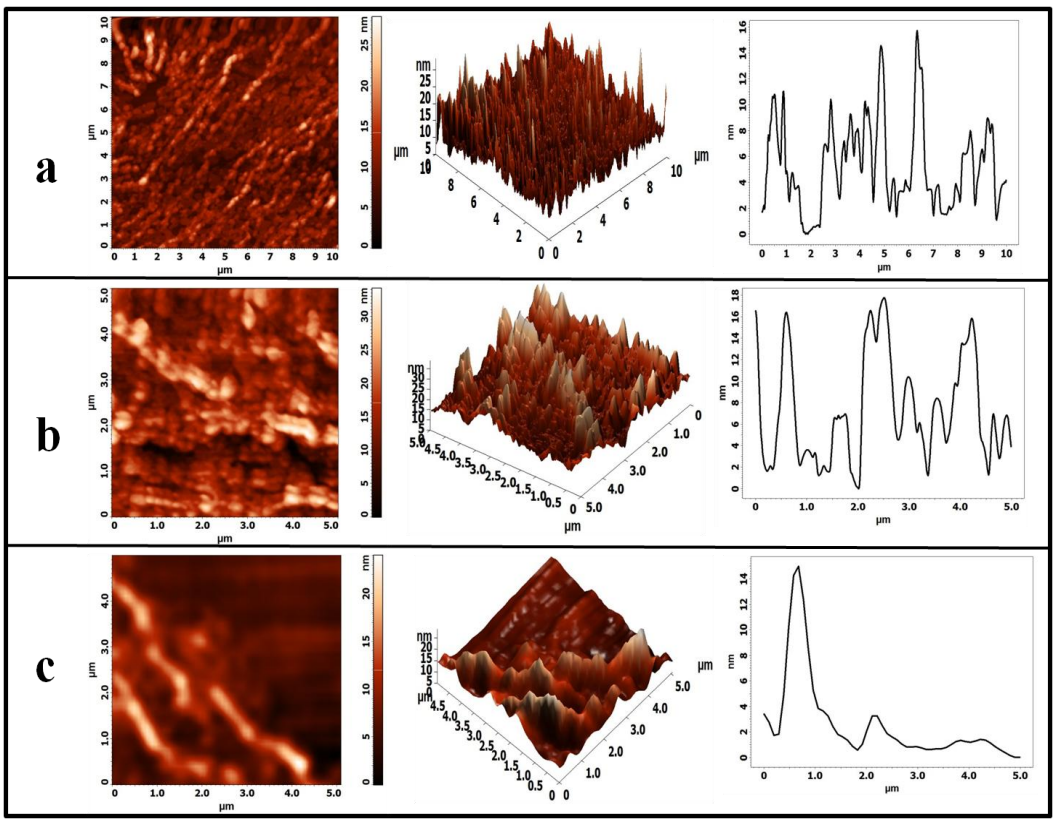

Figure 5.5: AFM images of BC1 molecule deposited at 20 mN m^{-1} having subphase pH = 6. (a) $10 \times 10\text{-}\mu m^2$ image along with its 3D view and height profile. (b) An image taken at scale of $5 \times 5\ \mu m^2$. (c) An image taken at the edge of deposited film. 3D view and height profile show distinct boundary between deposited film and substrate.

Figure 5.5(c) is particular image scanned at edge of deposited film. The 5×5 μm^2 is consisting of edge film having height profile 10-16 nm and nearly 0 nm at non-deposited region. Thus, LB layers deposited shows layer pattern [36-39].

As we reduce pH of sub phase to 4. Figure 5.6(a) shows AFM image at bent core molecule deposited at 20mN/m with sub phase pH = 4 and 5.6 (b) shows AFM image at same surface pressure but pH was reduced to 2.

In the case of deposited monolayer LB-films at pH=4 a multilayer pattern is again obtained having height about 9 nm, which is less than topographical height of pH=6 film. It infers that presence of counter ions has reduced the extent of stacking molecules at the interface.

At pH = 2, images are showing a homogeneous and nearly mono modal grain size distribution at large micrometric length scale which agrees with the molecular dimensions of the bent-core compound (4.1 nm).

So AFM images of bent core Langmuir–Blodgett (LB) films indicate that at low pH, organized monolayer of bent core molecule has been formed at the air/aqueous and air/solid interface rather than a cluster of molecules. Figure 5.7(a) shows image of **BC2** molecule deposited at 8mN/m having sub phase pH=6.

It shows again a clustering pattern of molecules having height about (2-14) nm. A similar trend to **BC1** molecule is observed, as we reduced the sub phase pH=4, height of deposited film decreased to 8nm as shown in figure 5.7(b).

At pH = 2 monolayer of bent core molecule is obtained having height nearly equal to 4.9 nm as shown in figure 5.7(c), which is equal to molecular dimensions of bent core molecules **BC2** (5.1nm). Hence again pH of sub phase has provided better alignment for bent core molecule.

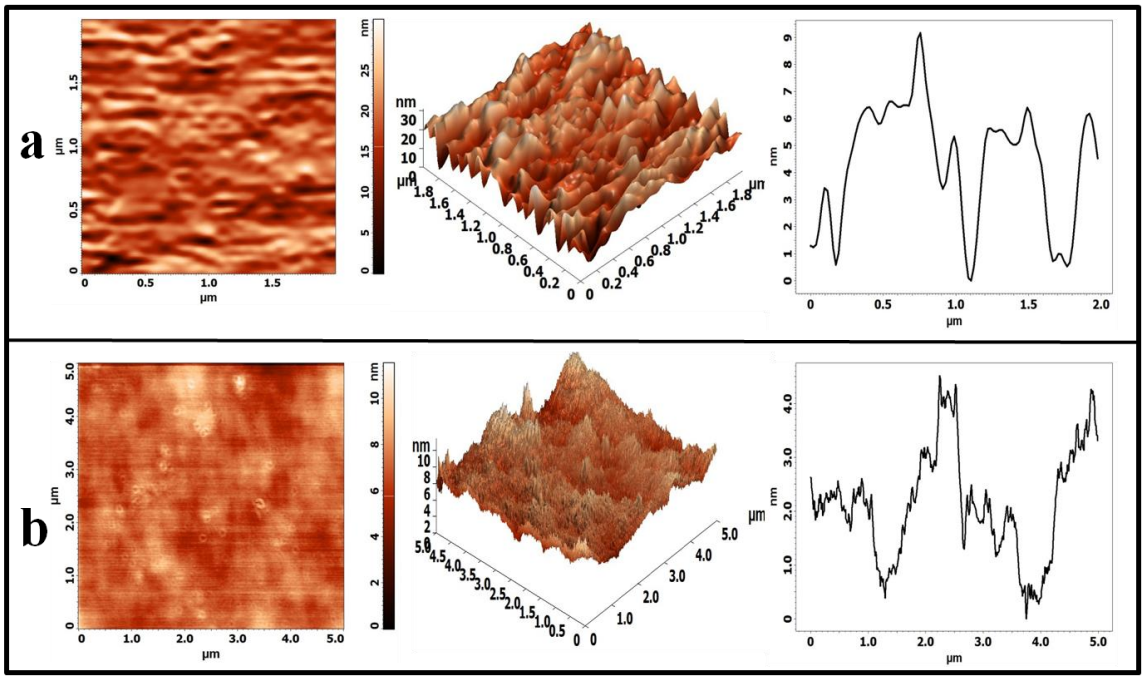

Figure 5.6: AFM images show topography of **BC1** molecule deposited at 20 mN m^{-1}. (a) 2 × 2-μm^2 image of **BC1** at sub phase pH = 4 along with 3D profile and height profile. (b) 5 × 5-μm^2 image of **BC1** at sub phase pH = 6 along with 3D profile and height profile.

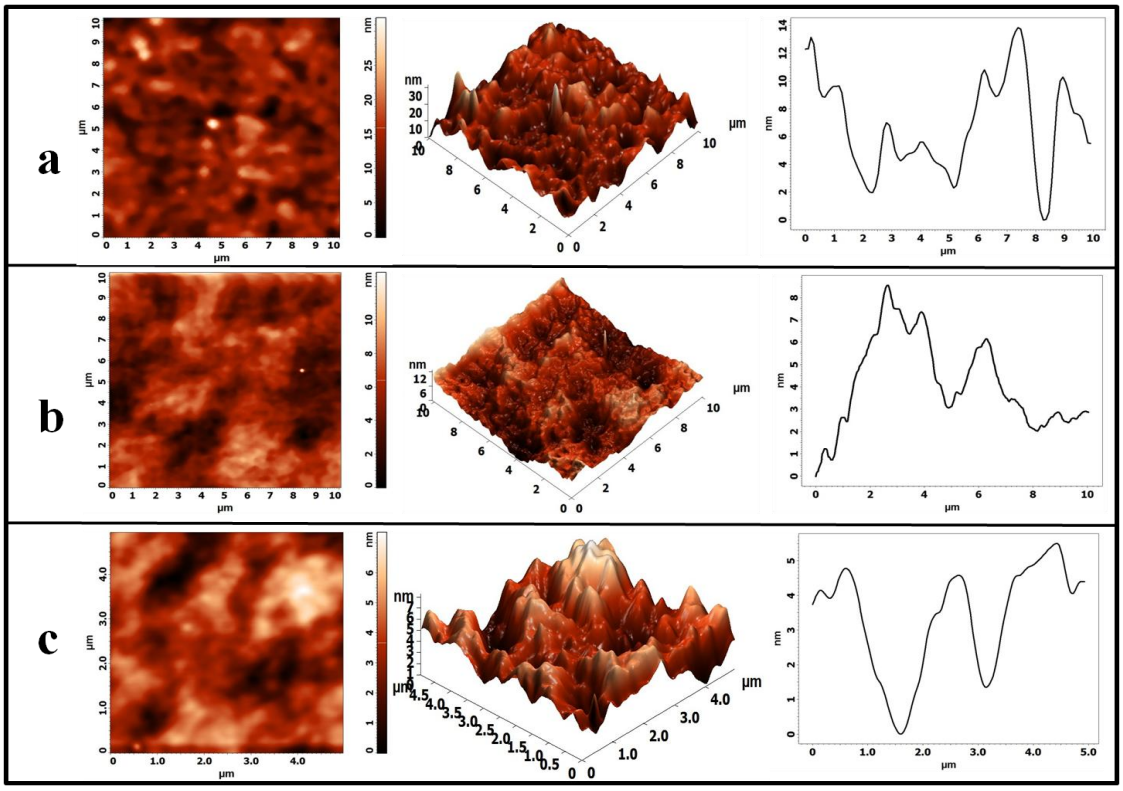

Figure 5.7: AFM image of **BC2** molecules deposited at three different sub phase pH, and deposition surface pressure in all cases was 8 m Nm^{-1}. (a) A 10 × 10-μm^2 image along with its 3D view and height profile of **BC2** molecule deposited at pH = 6. (b) A 10 × 10-μm^2 image along with its 3D view and height profile at pH = 4. (c) A 5 × 5-μm^2 image taken at pH = 2.

5.5 Conclusions

It is inferred that pH plays a vital role for orientation and ordering of bent-core molecules. Pattern of limiting area in isotherms confirmed the formation of monolayer with a decrease in pH. The successful matching of AFM data with a corresponding molecular model also provided information about packing of bent-core molecule at air–water interface. Thus, LB technique has provided new insight into monolayer formation of bent-core molecule. It provides new innovations in research and technology with a form of mysterious soft matter state.

References:

1 D Liu, D J Broer . Liquid Crystal Polymer Networks: Preparation, Properties, and Applications of Films with Patterned Molecular Alignment. Langmuir. 2014, **30 (45)**, 13499.

2 A Nayak, K A Suresh. Conductivity of Langmuir-Blodgett films of a disk-shaped liquid-crystalline molecule–DNA complex studied by current-sensing atomic force microscopy. Phys. Rev. E. 2008, **78**, 021606(1).

3 J K Basu, M K Sanyal. Ordering and growth of Langmuir–Blodgett &films: X-ray scattering studies. Phys. Rep. 2002, **363**,1

4 L T Cheng, W Tam, S H Stevenson, G R Meredith, G Rikken, S R Marder. Experimental Investigations of Organic Molecular Nonlinear Optical Polarizabilities. 1. Methods and Results on Benzene and Stilbene Derivatives. J. Phys. Chem.1991, **95**, 10631.

5 T F Heinz, H W K Tom, Y R Shen. Determination of molecular orientation of monolayer adsorbates by optical second-harmonic generation. Phys. Rev. A.1983, **28(3)**, 1883.

6 A Jakli, D Kruerke , G G Nair. Liquid crystal fibers of bent-core molecules. Phys. Rev. E. 2003, **67**, 051702(1).

7 C M Knobler. Langmuir monolayers and Liquid Crystals. Mol. Cryst. Liq. Cryst. 2001, **364**, 133.

8 M C Friedenberg, G G Fuller, C W Frank, C R Robertson. Formation of Bilayer Disks and Two-Dimensional Foams on a Collapsing/Expanding Liquid-Crystal Monolayer. Langmuir.1994, **10**, 1251.

9 M N G Mul de, J A Mann, Jr. Multilayer Formation in Thin Films of Thermotropic Liquid Crystals at the Air-Water Interface. Langmuir.1994, **10**, 2311.

10 M N G Mul de, J A Mann, Jr. Determination of the Thickness and Optical Properties of a Langmuir Film from the Domain Morphology by Brewster Angle Microscopy. Langmuir.1998, **14**, 2455.

11 R Kaur, K K Raina. Influence of single-wall carbon nanotubes on Langmuir–Blodgett films of ferroelectric liquid crystals as studied by atomic force microscopy. Liq. Cryst.2014, **41(8)**, 1065.

12 Q Xue, K Yang, C Xiao, Q Zhang. Direct observation of 2-D phase transitions of Chiral liquid crystals at the air/water interface. Thin Solid Films.1999, **347**, 63.

13 K S Krishnamurthy, S S Katti. Monolayer behaviour of a nematogenic phenyl benzoate at the air-water interface. Liq. Cryst.1989, **6(3)**, 281.

14 W Iglesias, T J Smith, P B Basnet, S R Stefanovic, C Tschierske, D J Lacks, A J Akli, E K Mann. Alignment by Langmuir/Schaefer monolayers of bent-core liquid crystals. Soft Matter. 2011, **7**, 9043.

15 R Kaur, G K Bhullar, K K Raina. Behaviour of an ultrathin ferroelectric liquid crystal Langmuir–Blodgett film at an air–water and air–solid interface. Liq. Cryst.2012, **39(11)**, 1375.

16 L Zou, J Wang, V J Beleva, E E Kooijman, S V Primak, J Risse, W Weissflog, A Jakli, E K Mann. Langmuir Monolayers of Bent-Core Molecules, Langmuir. 2004, **20**, 2772.

17 J Wang, L Zou, A Jakli, W Weissflog, E K Mann. Anisotropy in Langmuir Layers of a Bent-Core Liquid Crystal. Langmuir.2006, **22**, 3198.

18 T Yamamoto, S Oguchi, T Manaka, M Iwamoto. Measurement of interfacial dielectric polarization for the investigation of the orientational structure of monolayers comprised of banana-shaped molecules at an air–water interface. Thin Solid Films. 2006, **499**, 242.

19 N Duff, L Wang, E K Mann, D J Lacks. Molecular Dynamics Investigation of Bent-Core Molecules on a Water Surface Langmuir. 2006, **22**, 9082.

20 N Duff, E K Mann, D J Lacks. Molecular Dynamics Investigation of the Effects of a Water Surface on the Aggregation of Bent-Core Molecules. Langmuir. 2008, **24**, 4456.

21 I Giner, I Gasc, J Vergara, M C Lopez, M B Ros, F M Royo. Molecular Arrangement in Langmuir and Langmuir-Blodgett Films of a Mesogenic Bent-Core Carboxylic Acid. Langmuir.2009, **25(20)**, 12332.

22 L Dziri, S Boussaad, N Tao, R M Leblanc. Effect of pH on acetylcholinesterase Langmuir and Langmuir–Blodgett films studied by surface potential and atomic force microscopy. Thin Solid Films. 1998, **56,** 327**.**

23 M C Petty, Langmuir-Blodgett films: An Introduction, Cambridge University Press, 1996.

24 L. Zhao, C Feng, X Pang, J Jung, M C Stefan, P Sista, R Han, N Fang, Z Lin. Self-assembly of a conjugated triblock copolymer at the air–water interface Soft Matter. 2013, **9**, 8050.

25 W Wang, R Y Park, A Travesset, D Vaknin. Ion-Specific Induced Charges at Aqueous Soft Interfaces. Phys. Rev. Lett. 2011, **106**, 056102(1).

26 A Aroti , E Leontidis , E Maltseva, G Brezesinski. Effects of Hofmeister Anions on DPPC Langmuir Monolayers at the Air-Water Interface. J. Phys. Chem. B. 2004, **108**, 15238.

27 T S Harish, P Viswanath. Effect of cations on condensation of a mesogenic amphiphilic molecule at the air–aqueous electrolyte interface. Phys.Chem.Chem.Phys. 2014, **16**, 1276.

28 A M Brzozowska1, F Mugele, M H Duits. Stability and interactions in mixed monolayers of fatty acid derivatives on Artificial Sea Water. Coll. Surf. A: Physicochem. Eng. Aspects. 2013, **433**, 200.

29 L T Nguyen, A Ardana, E J Vorenkamp, G Brinke, A J Schouten. Chain length dependence of the helix orientation in Langmuir–Blodgett monolayers of a-helical diblock copolypeptides. Soft Matter.2010, **6**, 2774.

30 K D Comeau, M V Meli. Effect of Alkanethiol Chain Length on Gold Nanoparticle Monolayers at the Air-Water Interface. Langmuir.2012, **28**, 377.

31 R C Chambers, J O A Elizabeth, D McAdams, E J Haydenband, D J A Brown. Creating monolayers and thin films of a novel bis(alkyl) substituted asymmetrical polyoxotungstate, $\{[CH_3(CH_2)_{11}Si]_2OSiW_{11}O_{39}\}^{4-}$ using the Langmuir–Blodgett technique. Chem. Commun.2003, **15**, 2456.

32 H Hilles, A Maestro, F Monroy, Ortega F, R G Rubio, M G Velarde. Polymer monolayers with a small viscoelastic linear regime: Equilibrium and rheology of poly(octadecyl acrylate) and poly(vinyl stearate). J. Chem. Phys. 2007, **126**, 124904 (1).

33 T Verwijlen, L Imperiali, J Vermant. Separating viscoelastic and compressibility contributions in pressure-area isotherm measurements. Adv. Coll. Interf. Sci. 2014, **206**,428.

34 G L Caballero, A M Molina, A Y S Trevino, M A Rodrıguez-Valverde, M A C Vılchez, J M Valderrama. Using AFM to probe the complexation of DNA with anionic lipids mediated by Ca^{2+}: the role of surface pressure Soft Matter. 2014, **10,** 2805.

35 S Kundu, A Datta, S Hazra. Manipulating headgroups in Langmuir–Blodgett films through subphase pH variation. Chem.Phys. Lett. 2005, **405**, 282.

36 T J Smith, W Iglesias, S R Stefanovic, E K Mann, C Tschierske, A Jakli, D J Lacks. Effects of Tether Length on the Behavior of Amphiphilic Bent-Core Molecules at Water Surfaces. J. Phys. Chem. B, 2011, **115**, 12809.

37 T J Joncheray, K M Denoncourt, C Mathieu, M A R Meier, U S Schubert, R S Duran. Langmuir and Langmuir-Blodgett Films of Poly(ethylene oxide)-b-Poly(E-caprolactone) Star-Shaped Block Copolymers. Langmuir.2006, **22**, 9264.

38 S Reuter, E Amado, K Busse, M Kraska, B Stühn, C Tschierske, J Kressler. Formation of 2D spherulites in Langmuir films of amphiphilic T-shaped liquid crystals. J. Colloid Interface Sci. 2012, **372**, 192.

39 T Schmatko, P Muller, M Maaloum. Surface charge effects on the 2D conformation of supercoiled DNA. Soft Matter.2014, **10**, 2520.

Chapter 6

CONCLUSIONS AND FUTURE SCOPE OF THE WORK

The thesis presents systematic experimental method for the formation of Langmuir Blodgett films of liquid crystals and their composite systems. Monolayers and multilayers are transferred to solid substrate by Y-type deposition (Langmuir Blodgett Technique).These nanometric films have many applications in sensors and electro-optic devices. Following inferences are drawn:

- FLC molecules posses proper balance between hydrophilic (*CH-Cl, –OOC, –CN, C-NH) and hydrophobic (alkyl chains) groups. Average Length of FLC molecules is ≈ 27.836 Å. FLC molecules form stable monolayer at air-water interface. Orientation and ordering of the liquid crystal monolayer was attained at constant compression of barriers. Negligible hysteresis was noticed during the compression and expansion cycles of the isotherm which was due to chain entanglement and molecular reorganisations. FLC monolayers as well multilayers were transferred to solid substrate by Y-type (centro-symmetric) manner at constant surface pressure 5 mN m^{-1}.

  Low Angle XRD profile of multilayers showed an intense peak at $2\theta = 3.2^{\circ}$, corresponding to the smectic layer ordering of liquid crystal molecules with a layer spacing of ~27.52 Å. All the functional groups present in the FLC film were analysed by FTIR spectrum. Monolayer of FLC was scanned in non-contact mode. It showed elongated ferroelectric liquid crystal domains, with average height about 2.5 nm.

- Dispersion of SWCNTs in FLC has given significant results because they possess large surface area and π–π surface electrons that result in the strong electrostatic interactions between SWCNTs and the surrounding host medium (FLC). The interaction between nanotubes and LC molecules in the monolayer was increased during barrier compression, resulting in increased surface pressure in isotherm plots. At low wt% mixing, it is clear from low angle XRD profile that doping has not altered layer structure of host FLC. FTIR spectra of LB films composite system confirmed that transfers of FLC–SWCNTs composite were done successfully. Under non-contact mode AFM imaging films of nanotubes appears

to be consisting of a network having interconnected bundles of nanotubes. In LB films of FLC-SWCNTs composite systems, complex pattern of both globular as well as tubular topography was observed. These investigations have opened up vistas for understanding the switching and other electrical properties of FLC–SWCNTs thin films.

- Langmuir–Blodgett films of ferroelectric liquid crystal doped with low concentration of functionalized ZnO: Aℓ (AZO) and Ag nano particles were deposited on silicon and glass substrate by using Y-type deposition. Interactions between nano-particles and FLC molecules resulted in phase changes during compression. FTIR spectra confirms molecular interaction in composite systems Translation ordering of FLC was not disturbed as peak of smectic C phase remain unaltered in low angle XRD profile. AFM images confirmed domain structure of FLC as well globular network of nano-particles doped in FLC.

- Monolayers of Bent core molecules were successfully deposited by varying pH of the subphase. Sub phase was prepared at three different pH levels = 6, 4, 2. With reduction of pH counter ions present at air-water help in alignment and ordering of bent core molecules. Length of alkyl chains has their influence on monolayer formation. **BC1** has smaller alkyl chain length as compared to **BC2**. **BC1** has smaller limiting area; hence more work of compression was done in this case. AFM images deposited at three different pH levels indicate decrease in height profile with reduction of pH of sub phase. It provides new innovations in research and technology with a form of mysterious soft matter state.

6.1 Future Scope of the Work

- FLC formed stable monolayer at interface. We have studied isotherm and hysteresis plots. As FLCs have permanent dipole moment, Surface potential (ΔV) of ordered monolayer can be calculated by attaching surface potentiometer at interface. Dipole moment, $\mu_{\perp}$ can be calculated from the Helmholtz equation using the measured ΔV. This will give complete study of molecular ordering and orientation at air-water interface.

- All isotherms are measured at constant compression speed of barriers. However studies can be extended to measure isotherms at oscillating barrier mode. Viscoelastic parameter of monolayer can be measured at oscillating barrier method. This will lead to calculation of elastic and viscous modulus of monolayers.